Global primary productivity and the role of climate modes of variability

André David Belo do Couto

A thesis submitted in fulfilment
of the requirements for the degree of
Doctor of Philosophy (Ph.D.)

Department of Environment and Geography
Faculty of Science
Macquarie University
Sydney
Australia

June 2011

CONTENTS

ABSTRACT

Phytoplankton are a unique group of organisms, mostly due to their exclusive capacity to photosynthesise inorganic matter into highly energetic organic compounds. Consequently phytoplankton growth, i.e., primary productivity, fuels almost all life in the global ocean and plays a crucial role in biogeochemical cycles and climate processes. Although it is commonly known that phytoplankton primary productivity is highly variable at intra-annual scales, inter-annual patterns of variability have only relatively recently been observed with the advent of remote sensing technology. Satellite instruments detect and estimate chlorophyll, a molecule present in all phytoplankton, and primary productivity rates, at a global scale. Here, we use remote sensing products to assess net primary productivity and surface chlorophyll-*a* patterns of variability from intra- to multi-annual, and global to regional scales, and evaluate its physical forcing mechanisms. We aim to assess the connections between large-scale climate variability and inter- and multi-annual phytoplankton patterns of variability via empirical analysis of satellite derived Chl and various geophysical parameters. The main methodology utilised to this end is the Empirical Orthogonal Function (EOF) for detecting standing signals and its extended form to isolate propagating features. Our findings include a much higher percentage of NPP variability at seasonal scales (~90%) than previously acknowledged, an anomalous change of 90 Pg.C (Pg = 10^{15}g) in the last decade coupled to the classic El Niño – Southern Oscillation (ENSO) regional climate phenomenon, and an extra 18 Pg.C fixed in the ocean which can be attributed to the influence of the past decade's trend found in a controversial second main mode of variability. Further, we use extended EOF (EEOF) to isolate and analyse propagating features of surface chlorophyll-*a* across the global ocean and link them to regional climate modes of

variability. We then focus on the Tropical and South Pacific regions, characterizing the seasonal atmosphere and ocean dynamics and isolating the regional propagating inter-annual features. Finally, we assess the influence of the East Australian Current on regional remotely sensed chlorophyll, and investigate the role of large-scale regional climate modes of variability on chlorophyll patterns.

DECLARATION

I certify that the work in this thesis entitled "Climate variability modes influence on global ocean phytoplankton variability from satellite sensors" has not previously been submitted for a degree nor has it been submitted as part of requirements for a degree to any other university or institution other than Macquarie University.

I also certify that the thesis is an original piece of research and it has been written by me. Any help and assistance that I have received in my research work and the preparation of the thesis itself have been appropriately acknowledged.

This thesis differs from traditional thesis by including, in their original form, a series of co-authored journal articles in Chapters 3 to 8. It is noted here that the candidate's contribution to each of these papers is outlined in the Chapter Overview preceding each of the inserted manuscripts.

André David Belo do Couto

Student N#41 167 988

AKNOWLEDGEMENTS

I would like to thank a bunch (!) to my first principal supervisor Associate Professor Neil J. Holbrook for providing me the opportunity to embark in this project, also for his continued advice and support throughout three years and half +, despite his early relocation (in the lifetime of this project) to another state. The constant scientific support and input were crucial.

Also I would like thank Angela M. Maharaj, for carrying out the heavy duty of being my principal supervisor- the second. I must say that for a overseas Ph.D., it is essential to have the support of one that grew up at MQ University study rooms, and know all the tricks to go around the 'icebergs' that might sink any project, further knowledge of good English is essential.

Thank you Kevin Cheung, for being my third main supervisor, and thank you to HDRO and MQRes, MQ international, PGRF and the Department, students and staff.

To my all friends that *I* had the chance to feel alive both in Sydney and in Hobart, with, without them surviving through this adventure wouldn't have been possible. A spatial thanks to my friends Neil, Angela, Mauro, Miguel, Zygy & Mariana, Jorge Ramos, Ryan & Siri & $_{baby}$J, Chico, Pip, Clare Brooker, Eric, Paul James, Selma Justus Kinthiia, Jo Hoyle, Suzanne, Michael Gotsbacher, Lilia Margarita Flores Mateus, Eugenia di Fiori, Sydney, Hobart, Ensenada and Vezigrad and BD, who in some way helped me to solve the never ending list of riddles that frightened me along this work. And, for moments we spent together a special thanks to the WildChick.

and the most important THANK YOU to my family,
Obrigado pelo vosso apoio, contacto e exclusiva visita!!!
vó Julia', sempre que olho o céu sei que las estás :-)

CHAPTER 1

INTRODUCTION

Phytoplankton is the group of oceanic drifting microscopic organisms, capable of combining incoming solar radiation and inorganic compounds to form organic molecules, in a process called photosynthesis. This restricted group of plankton uses carbon dioxide (CO_2) and water (H_2O) molecules with sunlight, to produce three-carbon sugars, while releasing oxygen (O_2). These three carbon sugars are later on combined to form sucrose and starch, and fuel most of the oceanic living organisms. This process of incorporation of inorganic carbon onto organic compounds is known as primary productivity (PP). If we subtract phytoplankton respiration processes from this rate we get the net PP (NPP) rate, which is the rate of fixed carbon that is available to fuel the web food of most oceanic environments.

These organisms are, not only, the main food source for most of the oceanic biomes, but also play a significant role in the carbon (Figure 1) and oxygen cycles, thus having , critical implications on climate processes [*Murtugudde et al.*, 2002]. Phytoplankton, and its NPP play a crucial role in a natural mechanism known as the oceanic biological pump. As these autotrophic organisms fix CO_2, the carbon molecule is carried throughout the food web and eventually sinks. A s a result, carbon is sequestrated temporarily or permanently into the deep ocean. This subject has stimulated much scientific interest , as the biological pump is one of the natural mechanisms to sink atmospheric CO_2, one of the leading greenhouse gases that contributes to anthropogenic induced climate change [*Sabine et al.*, 2004]. NPP variability, recent trends and future impacts on the carbon cycle are thus a subject of much interest [*Arrigo*, 2007; *Riebesell et al.*, 2007].

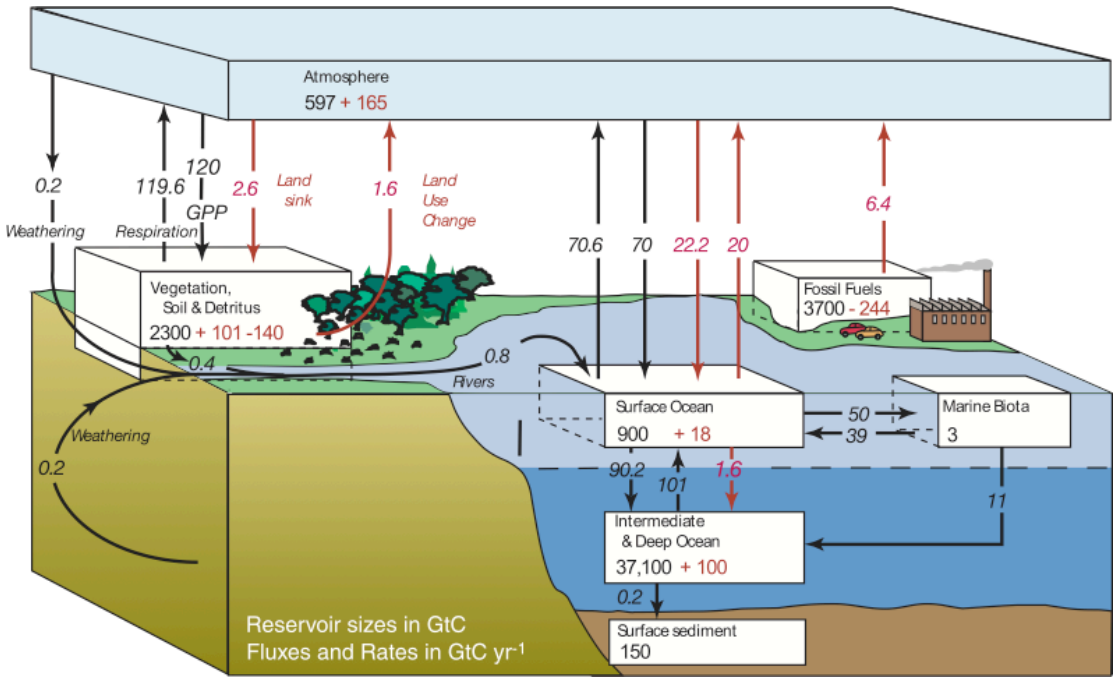

Figure 1. Global carbon cycle showing the natural (pre-industrial) main reservoirs and fluxes in black, and the anthropogenic ones in red [*IPCC*, 2007].

Each year the gross NPP is estimated to be close to 50 petagrams of carbon [*Field et al.*, 1998] (Pg.C, where 1 Pg is 10^{15} g). However, phytoplankton and its NPP, is limited by nutrient availability, such as nitrogen and iron concentration [*Behrenfeld et al.*, 2006], and constrained to live in the well-lit surface layer of the ocean. Consequently, phytoplankton growth is regulated directly by the abundance of these two factors, which together with loss processes (such as grazing and advection) regulate its seasonal cycle. In fact, roughly 60% of phytoplankton global variability follows the seasonal pattern [*Yoder and Kennelly*, 2003]. Global phytoplankton production depends on seasonal nutrient concentration within the euphotic depth, which vary with stratification and incident sunlight irradiance, at different latitudes [*A Longhurst*, 1995; *A R Longhurst*, 2007]. At tropical and subtropical latitudes, wind-driven mixing forces destratification bringing deep nutrient-rich waters into the euphotic depth (where sunlight irradiance intensity is enough for photosynthesis)

stimulating NPP during winter. However, whilst in winter nutrients at the surface layer are being consumed rapidly until exhaustion and the upper trophic level organisms are overwhelmed with the increase of autotrophs, the summer heat causes a strong stratification, avoiding vertical mixing, and preventing nutrient-rich waters to surface, which results in a low NPP rate. In contrast, at higher latitudes where a strong and deep mixing occurs, an intensive sunlight period during summer stimulates great NPP, whilst long periods with very low or no sunlight photosynthetic irradiance disable phytoplankton growth. At midlatitudes, winter minimum of sunlight irradiance together with strong summer stratification limit seasonal photosynthetic rates, consequently phytoplankton abundance and its NPP. Hence, seasonal changes in physical forcings and biological responses lead to seasonal NPP spatial and temporal variability patterns, which differ depending on latitude and other regional ocean characteristics.

Within interannual time scales the mechanism that induces most global NPP variability is the El Niño – Southern Oscillation (ENSO) [*Francisco P. Chavez et al.*, 2011]. ENSO is not only a great stimulator for global NPP variability but is also the strongest source of global interseasonal ocean variability and a dominant mode on climate variability [*Deser et al.*, 2010]. ENSO phase of El Niño (meaning the child in Spanish, as the phase switch occurs close to Christmas) is known to produce warm sea surface temperature (SST) anomalies in the equatorial and eastern Pacific within a period of 3 to 7 years [*Amador et al.*, 2006]. Between these events instead of warmth, a cool signature is observed at the surface, which is identified as the La Niña phase. The eastern equatorial Pacific cool surface signature is maintained by isopycnal tilting and upwelling driven by trade winds, and spreads westward along the equator with the help of the equatorial upwelling mechanism. This cool region goes by the name of

the equatorial Pacific cold tongue (or just 'cold tongue'). Trade winds advect the equatorial warm surface waters to the western Pacific region forming the western Pacific warm pool (WPWP), which is a planetary heat reservoir. The thermocline, a sharp change in temperature with depth indicating the interface of the ocean surface layer and the deep ocean, is then deeper from east to west. Hence deep nutrient rich waters are closer to the surface in the eastern region, and far from the euphotic layer at the western region. Atmospherically, a cool dry high-pressure air mass is observed in the eastern equatorial Pacific cool SST region, whilst a low sea level pressure (SLP), characterised by a warm and moist rising air mass, occurs in the western region above the WPWP. An El Niño event first starts to develop with strong westerly winds in the western Pacific, and from the WPWP a series of Kelvin waves propagate eastward along the equator, deepening the thermocline away from the euphotic layer in the eastern region. As a result the zonal SST along the equator is more uniform as is also the mix layer depth, (the low density surface layer of the ocean) thus ceasing the eastern isopycnal tilting and upwelling, and hence, also ceasing the emerging of nutrient-rich waters to the euphotic depth. During the La Niña phase, the cold tongue region is overwhelmed with nutrients from the emerging isopycnal, whilst the WPWP waters are poor in nutrient concentration. Hence, a PP enhancement occurs in the cold tongue, and low values of NPP and variability happen in the WPWP region. During the El Niño phase, eastern nutrient-rich upwelling water mechanism ceases, and phytoplankton abundance can be reduced by as much as 80% [*F. P. Chavez et al.*, 1999], while in the western Pacific PP increases [*Dandonneau et al.*, 2004]. These phytoplankton changes occur not only in the PP rates, but also in the composition and size structure of the organisms which affects the entire ecosystem. During La Niña phase conditions, a diatom-dominated coastal upwelling ecosystem dominates eastern

Pacific margins and the open ocean ecosystem is maintained for hundreds of kilometres from shore. During an El Niño phase, the open ocean ecosystem moves inshore, replacing the vast high productivity waters with a very narrow high-PP coastal zone [*Dandonneau et al.*, 2004; *Pennington et al.*, 2006].

Changes occurring on NPP variability in periods of a decade or longer are scarce in literature, mainly due to data resources. The few studies that exist suggest that decadal changes in NPP are linked with the Pacific Decadal Oscillation (PDO) [*Francisco P. Chavez et al.*, 2011; *Francisco P. Chavez et al.*, 2003]. PDO is a decadal periodic climate phenomenon, which includes ENSO [*Mantua et al.*, 1997] Abeit with a stronger influence at higher latitudes and weaker in the tropics. PDO also exhibits a different spatial character and has a very strong North Pacific signature.

Another strong signal multiannual cycle closely related to ENSO, now identified as the non-linear phase of ENSO [*Takahashi et al.*, 2011], is the relatively recently identified El-Niño Modoki (EM). EM is also described as a Tropical Pacific decadal cycle climate phenomenon [*Ashok et al.*, 2007]. As its name indicates, EM as a similar signature as ENSO (on SST and SLP pattern), but , different (as modoki in Japanese means 'similar but different'). El Niño phase of EM is characterized by an anomalous SST warming in the central Tropical Pacific flanked by cool patterns in the eastern and western region.

Nevertheless, the influence of both PDO and EM on global productivity patterns is either still unclear in literature (PDO), or non-existent (EM). In both cases the quality and quantity of its influence on NPP is still to be determined [*Francisco P. Chavez et al.*, 2011]. Long-term trends of NPP on other hand are still being discussed quite actively [*Boyce et al.*, 2010; *McQuatters-Gollop et al.*, 2011; *Rykaczewski and Dunne*, 2011]. As PP datasets are currently being upgraded with new remote sensing

technologies, existing long-term *in situ* observations of PP are insufficient to represent the world ocean in its total coverage. The use of remote sensing observations is now being considered to evaluate such patterns as these observations are becoming decadal.

Observations of phytoplankton are spatially very sparse due to the inherent costs of *in situ* observations throughout the vast global ocean [*Morel and Berthon*, 1989]. Since the 1970's, remote sensors placed on satellite platforms have enabled the observation of ocean colour, which is closely related to the amount of surface chlorophyll-*a* (Chl) biomass [*O'Reilly et al.*, 2000], a molecule existent in all phytoplankton organisms crucial to the photosynthetic process [*Raven et al.*, 2005]. To extrapolate Chl biomass quantity to phytoplankton growth rate throughout the water column, several authors have developed particular algorithms with a broad range of approaches [*Carr et al.*, 2006], which significantly capture the signal [*Friedrichs et al.*, 2009]. Satellite derived data is mainly used since it allows the estimate of phytoplankton biomass indicators from global to regional scales at a relatively high frequency sampling. Methods used within this work are described in the following chapter.

This project was motivated by the increasing awareness of the importance of the inter- to multi-annual longer-term trends of the ocean biological patterns, and the mechanisms that underpin such patterns. Here we aim to assess the connections between large-scale climate, natural and/or anthropogenic, variability and inter- and multi-annual phytoplankton patterns of variability via empirical analysis of satellite derived Chl and various geophysical parameters. This study makes new contributions to the contemporary knowledge of biogeochemical cycles, in particular to the carbon

cycle, with direct implications for carbon storage and transition between the atmosphere and ocean, in relation to the interface dynamics. Furthermore, this work extends the predictability skills of ocean biological variability in a changing world. The specific objectives of this thesis are:

i. Isolate standing and propagating inter-annual global patterns of NPP and investigate their relationship to major climate modes of variability;

ii. Assess the Southern Hemisphere seasonal and inter-annual Chl variability main patterns;

iii. Determine the phytoplankton seasonal cycle and relate it with forcing variables, identifying the major mechanisms which explain most of its variability, in the Tropical and South Pacific.

iv. Identify and quantify the major mechanisms and forcing variables which explain propagating features of inter-annual NPP variability in the Tropical and South Pacific.

v. Examine the East Australian Current region as a case study of phytoplankton variability and the role of regional climate modes of variability from seasonal to multi-annual timescale.

The thesis is organized as follows. Chapter 2 covers data and methodology before results are presented in the next 6 chapters. Note that an independent literature review is not provided, as this project is highly interdisciplinary. Instead, a review of the related literature is provided in each chapter manuscript as it relates to the specific thesis objective being addressed. For the results, we first embark on a global approach (chapter 3 and 4), focusing on increasingly more limited regions in the subsequent chapters. Chapter 5 focuses on Southern Hemisphere Chl variability patterns, whilst 6

and 7 are dedicated to the Tropical and South Pacific seasonal and inter-annual phytoplankton characterization. Finally, chapter 8 is further limited to the more regional East Australian Current area. With the exception of chapters 4 and 5, chapters are written and divided into fully drafted papers to be submitted to peer reviewed journals. Chapter 4 is an accepted peer-reviewed proceedings paper at the Global Conference on Global Warming 2011 (GCGW-11) to be held at Lisbon, Portugal, between 11 and 14 of July 2011. Chapter 5 is a peer-reviewed proceedings paper from the 2009 9th International conference on Southern Hemisphere Meteorology and Oceanography (ICSHMO), held in Melbourne, Australia. Finally chapter 9 provides a discussion of the thesis, suggestions for further work and some concluding remarks.

References

Amador, J. A., E. J. Alfaro, O. G. Lizano, and V. O. Magaña (2006), Atmospheric forcing of the eastern tropical Pacific: A review, *Progress In Oceanography*, *69*(2-4), 101-142.

Arrigo, K. R. (2007), Carbon cycle: Marine manipulations, *Nature*, *450*(7169), 491-492.

Ashok, K., S. K. Behera, S. A. Rao, H. Weng, and T. Yamagata (2007), El Niño Modoki and its possible teleconnection, *Journal of Geophysical Research C: Oceans*, *112*(11).

Behrenfeld, M. J., K. Worthington, R. M. Sherrell, F. P. Chavez, P. Strutton, M. McPhaden, and D. M. Shea (2006), Controls on tropical Pacific Ocean productivity revealed through nutrient stress diagnostics, *Nature*, *442*(7106), 1025-1028.

Boyce, D. G., M. R. Lewis, and B. Worm (2010), Global phytoplankton decline over the past century, *Nature*, *466*(7306), 591-596.

Carr, M. E., et al. (2006), A comparison of global estimates of marine primary production from ocean color, *Deep-Sea Research Part II: Topical Studies in Oceanography*, *53*(5-7), 741-770.

Chavez, F. P., M. Messié, and J. T. Pennington (2011), Marine Primary Production in Relation to Climate Variability and Change, *Annual Review of Marine Science*, *3*(1), 227-260.

Chavez, F. P., J. Ryan, S. E. Lluch-Cota, and M. Ñiquen C. (2003), From Anchovies to Sardines and Back: Multidecadal Change in the Pacific Ocean, *Science*, *299*(5604), 217-221.

Chavez, F. P., P. G. Strutton, G. E. Friederich, R. A. Feely, G. C. Feldman, D. G. Foley, and M. J. McPhaden (1999), Biological and chemical response of the equatorial Pacific Ocean to the 1997-98 El Nino, *Science*, *286*(5447), 2126-2131.

Dandonneau, Y., P.-Y. Deschamps, J.-M. Nicolas, H. Loisel, J. Blanchot, Y. Montel, F. Thieuleux, and G. Bécu (2004), Seasonal and interannual variability of ocean color and composition of phytoplankton communities in the North Atlantic, equatorial Pacific and South Pacific, *Deep Sea Research Part II: Topical Studies in Oceanography*, *51*(1-3), 303-318.

Deser, C., M. A. Alexander, S.-P. Xie, and A. S. Phillips (2010), Sea Surface Temperature Variability: Patterns and Mechanisms, *Annual Review of Marine Science*, *2*(1), 115-143.

Field, C. B., M. J. Behrenfeld, J. T. Randerson, and P. Falkowski (1998), Primary production of the biosphere: Integrating terrestrial and oceanic components, *Science*, *281*(5374), 237-240.

Friedrichs, M. A. M., et al. (2009), Assessing the uncertainties of model estimates of primary productivity in the tropical Pacific Ocean, *Journal of Marine Systems*, *76*(1-2), 20.

IPCC (2007), Climate change 2007: The physical science basis. Contribution of working group I to the fourth assessment report of the intergovernmental panel on climate change (IPCC)*Rep.*, 996 pp, Cambridge University Press, Cambridge, United Kingdom, New York, NY, USA.

Longhurst, A. (1995), Seasonal cycles of pelagic production and consumption, *Progress In Oceanography*, *36*(2), 77-167.

Longhurst, A. R. (2007), in *Ecological Geography of the Sea*, edited, p. 542, Academic Press, Burlington.

Mantua, N. J., S. R. Hare, Y. Zhang, J. M. Wallace, and R. C. Francis (1997), A Pacific Interdecadal Climate Oscillation with Impacts on Salmon Production, *Bulletin of the American Meteorological Society*, *78*(6), 1069-1079.

McQuatters-Gollop, A., et al. (2011), Is there a decline in marine phytoplankton?, *Nature*, *472*(7342), E6-E7.

Morel, A., and J. F. Berthon (1989), Surface pigments, algal biomass profiles, and potential production of the euphotic layer: relationships reinvestigated in view of remote-sensing applications, *Limnology & Oceanography*, *34*(8), 1545-1562.

Murtugudde, R., J. Beauchamp, C. R. McClain, M. Lewis, and A. J. Busalacchi (2002), Effects of penetrative radiation of the upper tropical ocean circulation, *Journal of Climate*, *15*(5), 470-486.

O'Reilly, J. E., et al. (2000), Ocean color chlorophyll a algorithms for SeaWiFS, OC2, and OC4: Version 4. In: SeaWiFS Postlaunch Technical Report Series, in *SeaWiFS Postlaunch Calibration and Validation Analyses, Part 3*, edited by S. B. Hooker and

E. R. Firestone, pp. 9-23, NASA, Goddard Space Flight Center, Greenbelt Maryland.

Pennington, J. T., K. L. Mahoney, V. S. Kuwahara, D. D. Kolber, R. Calienes, and F. P. Chavez (2006), Primary production in the eastern tropical Pacific: A review, *Progress in Oceanography*, *69*(2-4), 285-317.

Raven, P. H., R. F. Evert, and S. E. Eichhorn (2005), Photosynthesis, Light, and Life, in *Biology of Plants*, edited, pp. 119–127, Freeman, W. H. .

Riebesell, U., et al. (2007), Enhanced biological carbon consumption in a high CO2 ocean, *Nature*, *450*(7169), 545-548.

Rykaczewski, R. R., and J. P. Dunne (2011), A measured look at ocean chlorophyll trends, *Nature*, *472*(7342), E5-E6.

Sabine, C. L., et al. (2004), The Oceanic Sink for Anthropogenic CO2, *Science*, *305*(5682), 367-371.

Takahashi, K., A. Montecinos, K. Goubanova, and B. Dewitte (2011), ENSO regimes: Reinterpreting the canonical and Modoki El Niño, *Geophys. Res. Lett.*, *38*(10), L10704.

Yoder, J. A., and M. A. Kennelly (2003), Seasonal and ENSO variability in global ocean phytoplankton chlorophyll derived from 4 years of SeaWiFS measurements, *Global Biogeochemical Cycles*, *17*(4), 23-21.

CHAPTER 2

DATA AND METHODS

The main methodologies used throughout this thesis are reported here. The first part covers the description of the data, data preparation process and description of the methodology to achieve climatological and inter-annual patterns from the original data (Section 2.1). Section 2.2 describes how relationships between different variables were analysed. This is followed by an explanation of the regression method, the empirical orthogonal function (EOF) and the extended version of the EOF mathematical tool used here, and, finally, the North *et al*. [1982] modal independency test (Section 2.6). This chapter is finalised with a brief discussion.

2.1. Data

Several data sets, representing either atmospheric or oceanographic fields, were used throughout this project. Please note that each chapter has a detailed description of the specific datasets used. Throughout this project we used the remotely sensed chlorophyll-*a* concentration (Chl) and calculated net primary productivity (NPP) estimates as a large-scale phytoplankton indicator. Even though these estimates are close to known empiric values, a bias is inherent and quite difficult to determine due to the wide coverage of the data in both, time and space dimensions. Nevertheless, data providers include in their data processing routines, calibration and validation methods to improve data quality. We also chose to use this data as it is commonly used inthe literature , as these are the only available datasets that allow perusing the proposed objectives in this project mainly due to their unique capability of monitoring

phytoplankton related patterns at a near-global scale. Remote sensed Chl and NPP estimaes are further discussed in the following section.

Throughout this project these data are compared to several regional climate signal indicators. These climate indicators (or indices) are often used to monitor a specific regional climate mechanism such as El Niño – Southern Oscillation (ENSO) [*Behrenfeld et al.*, 2006]. Climate indices are calculated using a time series of observations of one or more environmental characteristics such as sea surface temperature (SST) or sea level pressure (SLP). Note that each chapter contains a description of the climate index/indices on the chapter data section (if any used). Here we will describe briefly the ones that are most used and revealed a greater importance throughout this thesis, which are: the multivariate ENSO index (MEI), and the improved El-Niño modoki index (IEMI).

2.1.1. Estimating Chl and NPP form remote sensing

In this section we discuss how Chl and NPP (natural indicators of phytoplankton biomass) are measured from satellite platforms from outer space, and, how accurate these measurements are. Please note that, we use the acronym Chl to indicate chlorophyll-*a* estimates.

As previously discussed, phytoplankton has a molecule (chlorophyll) in their cells which grantsthese organisms the capacity to photosynthesise. This molecule absorbs light photons, and, in a chain of cellular reactions, the sunlight energy is eventually transferred to other organic compounds and stored. However, depending on the type of chlorophyll molecule, the type of light absorbed varies. As virtually all phytoplankton have the type Chl in their system, ideally when observing the

concentration of this specific molecule in a water body, one can estimate the quantity of phytoplankton biomass in it. In other words, the greener the water body, the more phytoplankton it contains. This is possible since Chl has a unique absorption light spectrum with two main peaks, one in the red wavelength of the visible part of the electromagnetic spectrum (~450 nm) and other at the blue (~650 nm), thus emitting mainly green wavelengths. Hence, Ocean Colour sensors on outer space platforms record the ocean emitting radiation on several visible wavelengths. SeaWiFS for example, recorded 8 different wavelengths in the visible domain of the electromagnetic spectrum [*O'Reilly et al.*, 2000]. Ocean Colour remote sensed values, need visible radiation available, thus values are only recorded during daytime. Hence, satellite platforms where these sensors are installed have sun-synchronous orbits. Nevertheless, situations of total darkness occur and radiation values are not recorded, such as the polar-regions during the winter periods. Thus all data derived from Ocean Colour sensors have a near global coverage.

Several algorithms exist that estimate chlorophyll-*a* concentrations using information from visible radiation measurements. Throughout this project we use chlorophyll-*a* values that were estimated by the current default algorithm for SeaWiFS data, the OC4v6 [*O'Reilly et al.*, 2000]. The OC4v6 is as follows, $Chl = 10^{\alpha}$, where $\alpha = a0 + a1X + a2X^2 + a3X^3 + a4X^4$, and $a0$ is 0.3272, $a1$ is -2.9940, $a2$ is 2.7218, $a3$ is -1.2259, $a4$ is -0.5683, $X = \log10(Rrs1/Rrs2)$, where $Rrs1$ is the radiation of the blue band with highest value from the radiations measured by the SeaWiFS sensor within the blue band, i.e., 443 > 489 > 510 nm, and $Rrs2$ is the green radiation value, i.e., 555 nm measurement from the sensor. These remote sensing driven Chl estimates have a strong linearity when compared with *in situ* measurements ($r^2 = 0.83$), to the best linear fit curve with an offset of 0.00, and slope

of 1.00) [http://oceancolor.gsfc. nasa.gov/REPROCESSING/R2009/ocv6/ocval_swf. png].

Chl values are not free of errors. Further, although a validation process is carried out by the data providers, an error from these data are certainly very difficult to assess due to the large coverage (in space and frequency). As satellites may sample a vast area in the ocean in a few seconds, it would take months to cover such an area doing *in situ* ship measurements, with high costs.

Additionally Chl estimates may be influenced by the presence of other coloured (or chromophoric) dissolved organic matter (CDOM). CDOM, or yellow substance, are a group of organic, dissolved substances, consisting of humic and fulvic acids originated for example from the degradation of phytoplankton cells and other organic particles, or they may be advected from a distant source by, for example, rivers [*Sathyendranath*, 2000]. CDOM is typically found in coastal regions or lakes, the so-called case 2 waters, as opposed to the open ocean (case 1 waters). Case 1 waters, by definition, are those in which phytoplankton is the principal agent responsible for variations in the optical properties of the water. Whilst, in case 2 waters other agents, such as CDOM, but also inorganic suspended material have a strong contribution. But given that Case 1 waters are considered to encompass over 90% of the world oceans [*Sathyendranath*, 2000], and data used throughout this work only uses Case 1 waters for Chl estimates [*O'Reilly et al.*, 2000], a CDOM influence assessment was not considered necessary for this study.

Even though Chl values are directly linked with phytoplankton biomass, the estimated phytoplankton growth (or productivity) from satellite derived fields is quite complex [*Behrenfeld and Falkowski*, 1997a], and the algorithms developed to date give low bias estimates [*Carr et al.*, 2006]. The main problem arises from the

uncertainty of the primary productivity vertical profile. As the vertical satellite point of view does not identify the depth where ocean colour emitted radiation is defined from. Further, the several algorithms that assume a defined vertical profile lack information on the different PP rate depending on the multivariate species of plankton that are within a certain region. Nevertheless, from several algorithms that try to estimate such rates, some achieve a reasonable estimation when comparing to the available *in situ* measurements [*Friedrichs et al.*, 2009].

Algorithms used in this project to calculate PP/NPP were the commonly used Vertically Generalized Production Model (VGPM) [*Behrenfeld and Falkowski*, 1997b] and the Eppley [*Eppley et al.*, 1985]. Since the Eppley model calculates NPP as a direct function of Chl only, it assumes that NPP is solely dependent on biomass, ignoring environmental conditions. The VGPM, however, takes into account several environmental characteristics, including the daily photoperiod, sea surface daily photosynthetically active radiation, and, the euphotic depth, as well as the remote estimates of Chl concentrations. Both provide a good estimate of the global NPP variability amongst other PP algorithms (r = ~0.8) [*Carr et al.*, 2006], but with greater uncertainty when compared with Tropical Pacific *in situ* observations (r = ~0.6) [*Friedrichs et al.*, 2009].

Chl and VGPM NPP datasets used in this work were obtained from the Oregon State University Ocean Productivity site [http://www.science.oregonstate.edu/ocean .productivity/]. Both datasets are composed by satellite driven global observations in a spatial grid of ~1/6º of spatial resolution. Chl /NPP global estimates used here are monthly composites starting in October 1997 to December 2007 SeaWiFS derived dataset, and in Chapter 7, MODIS derived data was added to this so a longer record would be achieved. SST data was obtained with the same temporal resolution and

length. SST is used as a proxy for the physical environmental conditions throughout the project.

2.1.2. Multivariate ENSO index (MEI)

MEI is often used to monitor and describe ENSO variability [e.g. *Behrenfeld et al.*, 2006]. This climate index is the most comprehensive index for basin-scale climate investigations, taking into account six observed atmosphere and ocean physical variables across the tropical Pacific. (sea level pressure, zonal and meridional surface wind components, sea surface temperature, surface air temperature and total cloudiness fraction of the sky). The main principal component of these combined is calculated as in Wolter [1993]. Here we obtain this index from the U.S. National Oceanic and Atmospheric Administration webpage (http://cdc.noaa.gov/people/Klaus.wolter/MEI).

2.1.3. Improved El-Niño modoki index (IEMI)

Developed by *Ashok et al.* [2007] and improved by *Li et al.* [2010], the IEMI is calculated using remotely sensed SST measurements. This index is calculated as follows: $IEMI = 3.0T_{a,A} - 2.0T_{a,B} - 1.0T_{a,C}$, where A, B and C represent the area averaged T_a over each of the boxes *A* (165ºE – 140ºW, 10ºS – 10ºN), *B* (110º – 70ºW, 15ºS – 5ºN), and *C* (125 – 145ºE, 10ºS – 20ºN) respectively (Figure 1).

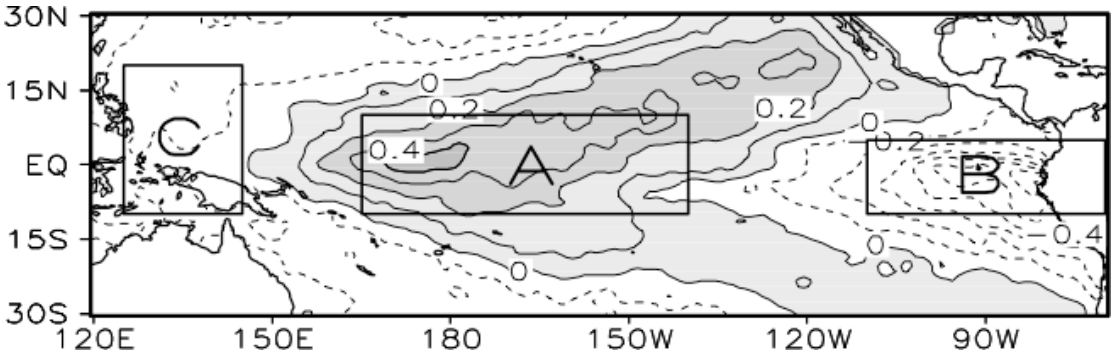

Figure 1. The spatial pattern (units: ◦C) of the second main mode of variability in the tropical Pacific SSTAs during 1979– 2008 identified as the EM SSTA signature yielded by an EOF analysis. Also showing the considered areas (boxes A, B and C) used to calculate the IEMI [Adapted from *Li et al.*, 2010].

2.2. Methods

2.2.1. Computing anomalies for chlorophyll and primary productivity

Commonly, phytoplankton observations are statistically described with log-distributed abundance populations [*Ahrens and Peters*, 1991; *Tett*, 1973] since the majority of the species in open ocean waters have an exponential growth rate [*Eppley*, 1972]. Hence, phytoplankton related observations are commonly analysed with a log normal model [*Campbell*, 1995; *Gladan et al.*, 2009; *Kahru et al.*, 2010] to stabilize the variance and to reduce the skewness of the non-normally distributed original data.

In our analysis, we obtain the inter-annual Chl and PP anomaly value (A), i.e., the amount by which the value of the observation that is considered to be different from the normally observed value, by calculating the mean (climatological) value (C) and subtracting it from the original value (O), $C = \overline{\log_{10}\left(O_{(x,y)}\right)_{(tm)}}$ and $A_{(x,y,t)} = O_{(x,y,t)} - 10^{C}$, where x is the longitudinal parameter, y the latitudinal parameter

and t denotes time, thus, $C_{(x,y,tm)}$ is the average of the log-distributed $O_{(x,y)}$ for a specific location and month of the year (tm).

2.2.2. Correlation and significance coefficients

To evaluate the relationship between two different patterns, either temporally or spatially distributed, we calculate the coefficient of correlation (r) between them. This is done by computing $r = \mathrm{cov}(X,Y)/\sigma_X\sigma_Y$. Further, the significance of such relationships is assessed by calculating if the probability of the different observed means, of each variable, can be explained by the process of random sampling (p). Throughout this work, however, we calculate p following *two* different approaches depending on the number of samples (n). The t-statistic criterion is used specifically in chapter 5 when intra-annual variability is assessed with a monthly sample rate, i.e., n = 12, following $\mathrm{p} = \overline{X} - \overline{Y}/(\sigma_Y/\sqrt{n-2})$, where $\overline{X}$ and $\overline{Y}$ are the population means. For other correlation significance tests, we replace the formula argument n-2 with $n \times \Delta_t \div \tau_n$, where Δ_t is the time interval sampled and τ_n is the integral time scale determining the time period required to gain a new "degree of freedom" as outlined by Davis [1976]. This reduces the effective number of degrees of freedom providing a more robust level of confidence to account for auto-covariance in geophysical datasets.

2.2.3. Regression analysis

The regression analysis is a widely used technique in geophysical sciences to model and analyse the relationship of dependent variables [*Cimatoribus et al.*, 2011; *Cunningham et al.*, 2011]. In chapter 5, we use this technique to assess the predictability of Chl in the Tropical and South Pacific using other geo-fields, such as

sea surface temperature and wind speed, where a regression analysis is defined as follows: $A\ (x,y,t) = a\ (x,y) \times B\ (x,y,t) + b\ (x,y) \times C\ (x,y,t)$, where variable A is estimated from variables B and C, x and y represent longitude and latitude, and, a and b the regression coefficients [*Strutz*, 2010].

2.2.4. Empirical Orthogonal Function (EOF)

First introduced by Lorenz [1956], the empirical orthogonal function (EOF) technique, also known as principal component analysis (PCA), is frequently used [*Chu*, 2011; *Yu and Kim*, 2011] to explain the observed variability by isolated modes. This technique decomposes datasets by identifying the pattern that best explains the data variability, followed by successive orthogonal best fits [*Bjornsson and Venegas*, 1997]. In this study, we use this technique to isolate patterns of inter-annual variability. The patterns in the main modes of variability usually allow for the identification of the mechanisms that drive them, hence, enabling the identification of such forcing.

In this study, we calculated the EOF modes by computing the covariance matrix of the pre-shaped data into space × time and solving the eigenvalue problem [*Bjornsson and Venegas*, 1997]. After calculating the anomaly values (A), data is put into a matrix shape (space × time) and its covariance matrix is calculated, $R = F^t \times F$, where F is our two dimensional matrix and t stands for transposing. This is followed by solving the eigen problem, $R \times C = C \times \Lambda$, where Λ is a matrix containing the eigenvalues λ_i of R, and C contains the eigenvectors c_i of each eigenvalue. The eigenvalues represent the amount of variability that each eigenvector pattern represents of the anomaly variability.

Note that we do not normalise the data i.e., divide the value $A_{(x,y,t)}$ by $\sigma_{(x,y),}$ prior to computing the EOF. Although this is a common procedure when calculating EOF, values obtained are dimensionless if normalised. This limits the capacity to quantify the amount of variance that each mode represents in real units.

2.2.5. Extended EOF (EEOF)

The EOF tool can only explain standing oscillation variability, and does not account for propagating features [*Bjornsson and Venegas*, 1997]. In chapters 4 and 6, the extended variation of the EOF is applied, targeting large-scale propagating features that might occur within phytoplankton variability.

To calculate the extended EOF (EEOF), one has to prearrange the dataset before computing the EOF by concatenating the field by a predefined time lag [*Venegas*, 2001]. Prior to the calculus of the anomaly values and a reshape of the data into space × time, a time lag (L) is predefined. L represents the cycle of the period of events that the analysis will focus on. This is followed by re-arranging and concatenating the data in to the form as follows:

$$F = \begin{bmatrix} F_1(1) & F_1(2) & \cdots & F_1(N-L) \\ F_2(1) & F_2(2) & \cdots & F_2(N-L) \\ \cdots & \cdots & \cdots & \cdots \\ F_M(1) & F_M(2) & \cdots & F_M(N-L) \\ F_1(2) & F_1(3) & \cdots & F_1(N-L+1) \\ F_2(2) & F_2(3) & \cdots & F_2(N-L+1) \\ \cdots & \cdots & \cdots & \cdots \\ F_M(2) & F_M(3) & \cdots & F_M(N-L+1) \\ \cdots & \cdots & \cdots & \cdots \\ \cdots & \cdots & \cdots & \cdots \\ F_1(L+1) & F_1(L+2) & \cdots & F_1(N) \\ F_2(L+1) & F_2(L+2) & \cdots & F_2(N) \\ \cdots & \cdots & \cdots & \cdots \\ F_M(L+1) & F_M(L+2) & \cdots & F_M(N) \end{bmatrix}$$

Data matrix F has dimensions M (L + 1) × N - L, where M represents locations, and N time increments.

2.2.6. North et al, [1982] test

Several tests exist to determine if the yielded EOF or EEOF modes are significant and independent from each other. Throughout this work we use the modal independency test, following the North *et al.* criterion [1982], which determines the modal independency from other modes by calculating the eigenvalue standard error interval for each screened mode. Modal independency is calculated as follows [*North et al.*, 1982]: $\delta_{\lambda_i} = \lambda_i \times (2/n)^{1/2}$, where λ_i is the eigenvalue, and n is the sampling number.

2.3. Discussion

In this chapter we present to the reader the main datasets and methodologies used throughout this work.

The most accurate phytoplankton biomass observations are time-space limited in a global frame (*in situ* observations). As remote sensing Chl dataset is composed of large-scale observations, with a relatively high frequency sampling rate, these enable the assessment of the influence of climate mechanisms on large-scale Chl variability patterns more adequately. Hence, we have chosen to use remotely sensed Chl as an indicator of phytoplankton biomass variability patterns as we find it to be the most suitable record available to pursue our proposed objectives. On the other hand, climatological studies often require a record of long-term coverage that remote sensing Ocean Colour observations cannot provide. Commonly, climate variability takes 30 years of observations to verify such mechanisms [*IPCC*, 2007]. The available remote sensing Chl observations only allow a 14-year period of continuous near global coverage observations. Nevertheless, Chl data for more than a decade is enough to identify interannual phytoplankton variability patterns induced by climate dynamics.

The methods described here allow for the calculus of ocean productivity from Chl observations (section 2.2.1), to isolate main and significant modes of variability (2.2.4), taking into account standing (EOF) or propagating (EEOF, section 2.2.5) features, to detect modal significance (section 2.2.6), to qualify and calculate the significance of the relationship between these modes and climate variability (section 2.2.2) and, finally, to forecast phytoplankton variability future scenarios (section 2.2.3). These tools allow us to address the key objectives of this project (described in the previous chapter), and its results are described in the following 6 chapters.

2.4. References

Ahrens, M. A., and R. H. Peters (1991), Patterns and Limitations in Limnoplankton Size Spectra, *Canadian Journal of Fisheries and Aquatic Sciences*, *48*(10), 1967-1978.

Ashok, K., S. K. Behera, S. A. Rao, H. Weng, and T. Yamagata (2007), El Niño Modoki and its possible teleconnection, *Journal of Geophysical Research C: Oceans*, *112*(11).

Behrenfeld, M. J., and P. G. Falkowski (1997a), A consumer's guide to phytoplankton primary productivity models, *Limnology and Oceanography*, *42*(7), 1479-1491.

Behrenfeld, M. J., and P. G. Falkowski (1997b), Photosynthetic rates derived from satellite-based chlorophyll concentration, *Limnology and Oceanography*, *42*(1), 1-20.

Behrenfeld, M. J., R. T. O'Malley, D. A. Siegel, C. R. McClain, J. L. Sarmiento, G. C. Feldman, A. J. Milligan, P. G. Falkowski, R. M. Letelier, and E. S. Boss (2006), Climate-driven trends in contemporary ocean productivity, *Nature*, *444*(7120), 752-755.

Bjornsson, H., and S. A. Venegas (1997), A manual for EOF and SVD analyses of climate data*Rep.*, 52 pp, McGill University, Montréal, Québec.

Campbell, J. W. (1995), The lognormal distribution as a model for bio-optical variability in the sea, *J. Geophys. Res.*, *100*(C7), 13237-13254.

Carr, M. E., et al. (2006), A comparison of global estimates of marine primary production from ocean color, *Deep-Sea Research Part II: Topical Studies in Oceanography*, *53*(5-7), 741-770.

Chu, P. (2011), Global upper ocean heat content and climate variability, *Ocean Dynamics*, 1-16.

Cimatoribus, A. A., S. S. Drijfhout, and H. A. Dijkstra (2011), A global hybrid coupled model based on atmosphere-SST feedbacks, *Climate Dynamics*, 1-16.

Cunningham, A., I. D. Carrie, and R. E. Korb (2011), Two-component modeling of the optical properties of a diatom bloom in the Southern Ocean, *Remote Sensing of Environment*, *115*(6), 1434-1442.

Davis, R. E. (1976), Predictability of Sea Surface Temperature and Sea Level Pressure Anomalies over the North Pacific Ocean, *Journal of Physical Oceanography*, *6*(3), 249-266.

Eppley, R. W. (1972), Temperature and phytoplankton growth in the sea, *Fishery Bulletin*, *70*, 1063-1085.

Eppley, R. W., E. Stewart, M. R. Abbott, and H. U. (1985), Estimating ocean primary production from satellite chlorophyll. Introduction to regional diffrences and statistics for the Southern California Bight, *Journal of Plankton Research*, *7*(1), 14.

Friedrichs, M. A. M., et al. (2009), Assessing the uncertainties of model estimates of primary productivity in the tropical Pacific Ocean, *Journal of Marine Systems*, *76*(1-2), 20.

Gladan, Ž. N., I. Marasović, B. Grbec, S. Skejić, M. Bužančić, G. Kušpilić, S. Matijević, and F. Matić (2009), *Inter-decadal Variability in Phytoplankton Community in the Middle Adriatic (Kaštela Bay) in Relation to the North Atlantic Oscillation*, 8 pp., Springer, Heidelberg, ALLEMAGNE.

IPCC (2007), Climate change 2007: The physical science basis. Contribution of working group I to the fourth assessment report of the intergovernmental panel on climate change (IPCC)*Rep.*, 996 pp, Cambridge University Press, Cambridge, United Kingdom, New York, NY, USA.

Kahru, M., S. T. Gille, R. Murtugudde, P. G. Strutton, M. Manzano-Sarabia, H. Wang, and B. G. Mitchell (2010), Global correlations between winds and ocean chlorophyll, *J. Geophys. Res.*, *115*(C12), C12040.

Li, G., B. Ren, C. Yang, and J. Zheng (2010), Indices of El Niño and El Niño Modoki: An improved El Niño Modoki index, *Advances in Atmospheric Sciences*, *27*(5), 1210-1220.

Lorenz, E. N. (1956), Empirical orthogonal functions and statistical weather prediction*Rep.*, 49 pp, Department of Meteorology, Massachusetts Institute of Technology.

North, G. R., T. L. Bell, R. F. Cahalan, and F. J. Moeng (1982), Sampling Errors in the Estimation of Empirical Orthogonal Functions, *Monthly Weather Review*, *110*(7), 699-706.

O'Reilly, J. E., et al. (2000), Ocean color chlorophyll a algorithms for SeaWiFS, OC2, and OC4: Version 4. In: SeaWiFS Postlaunch Technical Report Series, in *SeaWiFS Postlaunch Calibration and Validation Analyses, Part 3*, edited by S. B. Hooker and E. R. Firestone, pp. 9-23, NASA, Goddard Space Flight Center, Greenbelt Maryland.

Sathyendranath, S. (Ed.) (2000), *Remote Sensing of Ocean Colour in Coastal, and Other Optically-Complex, Waters*, Dartmouth, Canada.

Strutz, T. (2010), *Data Fitting and Uncertainty: A practical introduction to weighted least squares and beyond*, Vieweg andTeubner, Wiesbaden.

Tett, P. (1973), The use of log-normal statistics to describe phytoplankton populations from the Firth of Lorne area, *Journal of Experimental Marine Biology and Ecology*, *11*(2), 121-136.

Venegas, S. A. (2001), Statistical methods for signal detection in climate*Rep.*, Danish Centre for Earth System Science, Niels Bohr Institute for Astronomy, Physics and Geophysics, University of Copenhagen, Denmark.

Wolter, K., and M. S. Timlin (1993), Monitoring ENSO in COADS with a seasonally adjusted principal component index., paper presented at Proc. of the 17th Climate Diagnostics Workshop, Norman, OK, NOAA/NMC/CAC, NSSL, Oklahoma Clim. Survey, CIMMS and the School of Meteor., Univ. of Oklahoma.

Yu, J.-Y., and S. T. Kim (2011), Relationships between Extratropical Sea Level Pressure Variations and the Central Pacific and Eastern Pacific Types of ENSO, *Journal of Climate*, *24*(3), 708-720.

CHAPTER 3

Global patterns of inter-annual net primary productivity

3.1 CHAPTER OVERVIEW

This chapter investigates the two main patterns of global inter-annual NPP variability and their connection with regional climate modes. To this end, we use the empirical orthogonal function tool on global NPP vertically generalized production model estimates to isolate the patterns that explain more variability. We qualitatively evaluate the relationship between the yielded modal time series and various climate indices in order to assess the atmosphere and ocean physical characteristics associated with these two modes. This chapter covers the first objective of this thesis.

The main text of this section is a fully drafted paper entitled 'Mechanisms that drive inter-annual global net primary productivity from satellite data using empirical orthogonal functions', intended for submission to the Journal *Nature Geoscience*, co-authored by A. B. Couto, A. M. Maharaj and N. J. Holbrook.

Candidate's contribution to this paper

In this paper, I obtained the dataset, wrote the scripts and performed all the data analysis. I also produced the figures and drafted the manuscript, which was then evaluated by both co-authors. However, discussion and input from both co-authors was attained regularly, mainly during the writing process.

Global net primary productivity: ENSO mechanisms

André B. Couto

Department of Environment and Geography, Macquarie University, Sydney, New South Wales, Australia

Angela M. Maharaj

Department of Environment and Geography, Macquarie University, Sydney, New South Wales, Australia

Neil J. Holbrook

School of Geography, University of Tasmania, Hobart, Tasmania, Australia

For submission to *Nature*

Summary

Recently discussions regarding global oceanic productivity temporal trends have been raised and no consensus is yet established [1-3]. This is mainly due to the restrictions imposed by observations available and methods used to analyse them. The recent trends of the environmental conditions are a global concerning issue. Questions such as whether these trends are part of natural climate variability or if they are forced by anthropogenic activity? And the impacts that these will have? Are still to answer. Climate variability is the result of the interactions of a complex system, where the ocean plays one of the main roles. The main food source of most oceanic ecosystems is the drifting phytoplankton. These microscopic organisms, which use solar energy to

fix inorganic elements such as CO_2 in a process named photosynthesis, are the main primary producers in the ocean [4]. Net primary productivity (NPP) rates are mainly regulated by phytoplankton growth, which is essentially determined by sunlight and nutrient availability [5], against loss processes (such as grazing). The two growing limiting variables are fundamentally related to climatic variability, mainly through atmosphere and ocean dynamics. Although we found that intra-annual patterns of climate variability dominate the spatial and temporal variance in NPP, significant inter-annual variability is also observed. El Niño – Southern Oscillation (ENSO) dynamics has been identified as the main driver for oceanic NPP inter-annual variability [6], and, past decadal trends have been established as a possible connection with the Pacific Decadal Oscillation [7]. However, here we uncover and isolate two independent modes of NPP in the un-seasonal inter-annual variability that explained ±172 Pg C in a decade. The leading mode is identified as representative of the direct impact of ENSO on NPP (explaining ±90 Pg C of inter-annual NPP from the end of 1997 to December 2007), but the second mode is identified as the direct impact of El–Niño Modoki decadal variability, which explains ± 64 Pg C in the same time frame, and is fuelled to ±82 Pg C with a decadal trend, possibly linked to anthropogenic climate change and global ocean warming.

Main

Forty percent of the Earth's primary productivity, which is the rate of fixed atmospheric carbon onto organic compounds, is done by the oceanic drifting phytoplankton [5]. The net primary productivity (NPP) is the base of most oceanic biomes in the food chain, playing a critical role in climate processes [8] and biogeochemical cycles [9]. NPP is clearly critical for earth system health, and this

health has consequences for all economic and social levels of human society. NPP is limited by sunlight and nutrient availability. These constraining environmental conditions have well-defined seasonal patterns that describe ~60% of the ocean's stock variability [10] – we note here that our analysis suggests a much higher influence (~90%). At inter-annual and multi-annual time scales, NPP is impacted by changes in climate and atmosphere-ocean dynamics [7]. The main inter-annual climatic driver of global NPP is El Niño – Southern Oscillation (ENSO), as its global annual changes develop closely with ENSO variability [11], and during an ENSO phase transition event can induce anomaly of 1-2 Pg.C sequestered by phytoplankton [11,12]. A very recent review shows that on decadal time scales, the most important global NPP changes appear to be driven by ENSO and/or the Pacific Decadal Oscillation [7]. However, past decade NPP global trends [13,14] have a similar pattern to the one induced by ocean warming [11]. Ocean warming, on the other hand, can be a clear indicator of anthropogenic induced climate change in last 18 years [15].

Unfortunately, NPP global record time series are comparatively short to the multi-decadal time series needed (~40 years) to be able to distinguish a global warming trend from natural variability [14]. Observational studies on global trends in NPP are scarce in the literature due to the relatively poor coverage in space and/or short record in time. A few *in situ* time series, that are freely available, cover about 20 years in record length, e.g., the Hawaii Ocean Time-series [16] and the Bermuda Atlantic Time-series [17]. However, even these relatively continuous records are only a couple of decades in length, while describing NPP variability at single sites in a vast global ocean.

An important advance has been that some satellite remote sensing missions have been able to provide near-global coverage of ocean colour (estimates of surface

chlorophyll) in the last few decades. Simultaneous regional-scale coverage was achieved with the advent of ocean colour remote sensing Coastal-Zone-Color-Scanner (CZCS), which provided 8 years of measurements (October 1978 to June 1986). The more sophisticated Sea-viewing Wide Field-of-view Sensor (SeaWiFS) had a lunar-viewing calibration, more measurements on the visible band of the electromagnetic spectrum and also a permanent recording [18]. SeaWiFS provided near continuous global observations commencing in September 1997, following an 11-year gap after the close of CZCS, until December 2010. Satellite estimates of chlorophyll-*a* (Chl), however, are restricted to the surface [19]. Chl is a pigment that exists in all phytoplankton organisms. It provides a technique for ocean colour remote observing sensors to calculate the oceanic NPP distribution with a more complete spatial coverage, relatively high spatial resolution and higher frequency sampling than *in situ* measurements, which typically require costly field cruises [20].

Algorithms that estimate NPP through satellite derived Chl concentrations are fairly common in the literature. Here, we use the Vertically Generalized Production Model (VGPM) [21] as it is simple to implement and its results have proven to be, at least, as good as any other model available [38]. This model takes into account several environmental characteristics, including the daily photoperiod, sea surface daily photosynthetically active radiation, and, the euphotic depth, as well as the remote estimates of Chl concentrations. Satellite driven NPP values, however, might be underrated by biomass indicators such as surface Chl measurements, as total global phytoplankton biomass is consumed every 2-6 days [21]. Further, NPP estimates calculated by the VGPM are still far to represent its true variability, specifically in the ENSO set of the Tropical Pacific ($r = 0.57$) [22]. Nevertheless, this model is still one the best available models to work with, amongst the available ones.

Using empirical orthogonal function (EOF) analysis on non-seasonal NPP monthly anomalies (NPPA) over 10 years (Oct 1997 - Dec 2007), the first two modes correspond to (i) ENSO (EOF1), and (ii) pattern and timing consistency with a decadal trend in NPP [14] and/or the ocean warming induced NPP [11] (EOF2), which includes a NPP a high amplitude change at the western and north Tropical Pacific. On closer analysis of the monthly mode time series (Fig 1), we find that EOF2 is strongly and significantly correlated at zero lag ($r = 0.86$, $p = 0.02$) with the improved El Niño – Modoki index (IEMI) [23]. For the corresponding 10-month running average series, the correlations and confidence is even higher ($p < 0.01$, $r = 0.94$) (Fig. 1a). The projected global SST anomalies (SSTA) spatial pattern of the non-seasonal NPPA EOF2 (Fig. 1c) characterizes the El Niño – Modoki mode [24,25].

The El Niño – Modoki, also referred as Date Line El Niño [26] or Central Pacific warming [25], is a relatively recent (~6 years) identified phenomenon [26]. Its relationship with the canonical ENSO is unknown [27]. Unlike the 'classical' cold-tongue El Niño, the El Niño – "Modoki" (from the Japanese word for "similar but different", hereafter abbreviated EM) mode is characterized by a lens of maximum warming in the central-western equatorial Pacific, flanked to the west and east by cool SSTA. While the EOF2 pattern is not isolated to the central equatorial Pacific (Fig. 1c), the NPPA time series projected onto global SSTA provides a compelling pattern correspondence that couples the NPPA ~ -1 g C m^{-2} d^{-1} in the equatorial central-western Pacific (in the NINO4 region) with SSTA ~ +5 ºC in the same region (Fig. 1c) [24]. While the EOF2 time series correlates with the NINO4 index at the 90% confidence level ($r = 0.62$, $p = 0.10$). However, when reconstructing EOF2 time series back in time by projecting the EOF2 correspondent SSTA spatial pattern, onto SSTA global observations from 1870 [28]. The century-scale backward-reconstructed EOF2 time series shows no significant

difference from the IEMI since 1870 (Fig 2) ($r = 0.83$, $p << 0.01$). Nevertheless, This method assumes that the 1997 to 2007 observed relationship between NPPA and SSTA persist since 1870, which is arguably acceptable. We contend, therefore, that EOF2 identifies the EM influence on global NPP, since it is completely consistent with our current understanding of the climate system dynamics underpinning EM [23,24,29,30]. We note once again, however, that the spatial pattern of EOF2 synoptically resembles a decadal trend (1997-2007) in NPPA/Chl [7,14], and the pattern induced during an ocean warming period [11].

It is important to note two points here. First, the observed global-scale multi-decadal ocean warming trend detected in recent decades is attributed to anthropogenic climate change [29]. Second, a very recent study argues that anthropogenic climate change may actually induce an increase in EM intensity [27].

To corroborate this point, the EM connected NPPA mode (EOF2) is affected by the decadal NPPA trend, by increasing its amplitude and advancing the NPPA response by almost a season. Removing the long-term linear trend from the data, before performing the EOF analysis, does not change EOF1 significantly (not shown), but makes an important difference to EOF2 (Fig. 3). The NPPA EOF2 spatial patterns, i.e., original (Fig 1) and linearly detrended (Fig 3), correlate significantly ($r = 0.69$, $p << 0.01$), indicating that the decadal trend pattern in NPPA is similar to the EM pattern for this decade. The EOF2 time series from analysis of the linearly detrended NPPA follows the IEMI (Fig. 3a) with the same statistical significance ($r = 0.71$, $p = 0.02$) as the original signal, and maximum lagged significance was found when the IEMI leads EOF2 by four months ($r = 0.73$, $p = 0.01$). This suggests that the NPPA including the trend responds to EM four months earlier than without the current decadal trend. This is corroborated by the projected SSTA EOF2 from

analysis of the linearly detrended NPPA (Fig. 3d), which is resembles the spatial pattern of an EM event ~4 months later, i.e., during summer [24]. The influence of the decadal trend on EM, as seen in EOF2, adds 0.15 Pg C yr^{-1} of NPP to the negative anomaly of 0.52 Pg C yr^{-1} during the Oct 1997 – Dec 2007 period.

As discussed throughout the literature, ENSO is the dominant inter-annual mode of global climate variability. Here, the first non-seasonal EOF (10% of the global non-seasonal variance) from analysis of the NPPA (Fig. 4), identifies the classical 'cold tongue' ENSO mode [7]. This is clearly evident from the highly significant correlations between the NPPA EOF1 time series and the Multivariate ENSO index (MEI; $r = 0.93$, $p << 0.01$) during the past decade (Fig. 4a). The relationship between the global-SSTA ENSO index (GEI) [31] and the back-reconstructed EOF1 time series to 1870 is even stronger ($r = 0.77$, $p << 0.01$; Fig. 5). The relationship is most apparent in the EOF and SSTA projected patterns, which show a large amplitude warmth anomaly across the tropical Pacific, as the opposed phase of the characteristic "cold tongue" ENSO (Fig. 4c,d).

The classical ENSO characteristics are evident. The characteristics for a 'composite'-style El Niño (La Niña) are an anomalous decrease (increase) in the strength of the trade winds, suppressed (intensified) upwelling in the eastern tropical Pacific, anomalously high (low) eastern equatorial Pacific SST, and an anomalous increase (decrease) in sea level pressure (SLP) over the Western Pacific Warm Pool (WPWP) region. These characteristics are clearly evident when projecting the NPPA EOF1 time series onto the SSTA and SLPA (Fig. 4d). During El Niño, the Indo-Pacific Ocean region NPPA is significantly affected, with substantial declines ~ 1 g C m^{-2} d^{-1} in the equatorial central-eastern Pacific, and increases of ~ 1 g C m^{-2} d^{-1} in the WPWP. Increases (decreases) in NPP are also evident in the oligotrophic waters of

the interior Pacific subtropical gyres during El Niño (La Niña) – consistent with commensurate changes in nutrient supply to the euphotic depth, and in strong agreement with previously reported influences of ENSO dynamics on NPP [32].

EOF1 is also characteristic of the Indian Ocean Dipole (IOD) pattern in the Indian Ocean region [33]. This apparent 'co-dependence' is, however, not really surprising given that numerous studies have endeavoured to separate the IOD from ENSO, and debates continue as to whether the IOD is an entity in its own right [34,35]. The IOD and ENSO are often found in phase [36], which was the case for the strongest IOD/ENSO event couplet that occurred during the decade of interest here, i.e., the +IOD/El Niño of 1997/98. Further, the IOD Mode index (IODMI) is also significantly correlated with the NPPA EOF1 time series ($r = 0.49$, $p = 0.02$; Fig. 4a), suggesting that NPP is coupled across the Indo-Pacific modes.

EOF1 accounts for inter-annual variations of ±0.75 Pg C yr^{-1} about the estimated mean (47.8 Pg C yr^{-1}), corresponding to the same amount in the equatorial Pacific during the 1997/98 ENSO phase transition [12]. We estimate that the very strong 1997/98 El Niño/+IOD event induced a near-global maximum anomaly of -2.5 Pg C in December 1997, which contributed to a cumulative maximum anomaly over 7 months of -16.7 Pg C, when the 1997/98 El Niño finally switched to its La Niña phase (Fig. 4b). In total, EOF1 explains a rate of 90 Pg C of NPP during the whole period associated with ENSO/IOD climate variability.

A statistically identical EOF1 and EOF2 patterns of variability are obtained when using remote sensed Chl concentrations, which is SST independent unlike the used NPP estimates [21]. The leading mode correlates significantly with the MEI ($r = 0.90$, $p << 0.01$), and from a total of 2.82×10^3 g m^{-3} of Chl observed in the ocean during this period, where most is due to seasonal variability (89%), EOF1 mode

explains slightly less than VGPM estimates of NPP inter-annual variability (7.12%). Further, the spatial and temporal patterns of both, Chl and NPP, leading modes from separate EOF analyses, were highly significantly correlated with each other (r = 0.97 for spatial correlation, r = 0.99 for temporal correlation, and, both relations show $p << 0.01$).

Satellite derived surface Chl can be used to estimate NPP rates using the Eppley model, $PP_{Eppley}(x,y,z) = \sqrt{Chl(x,y,z)} \times 1000$, where x,y, z correspond to longitude, latitude and time - here we multiply by 1000 to calibrate these units with the VGPM [37], thus offering an excellent baseline for global comparison. Since the Eppley model calculates NPP as a direct function of Chl only, it assumes that NPP is solely dependent on biomass, ignoring environmental conditions. Despite its relative simplicity, the Eppley algorithm is quite successful in capturing the overall ocean NPP [38]. Furthermore, in the Tropical Pacific it provides good correlation (r = 0.53) with a very low degree of bias (+0.04 g C m^{-2} d^{-1}) when compared to *in situ* values [22]. However, the Eppley model appears to underestimate NPP (by about 28%) compared with the VGPM estimates. Despite this, the EOF1 and EOF2 patterns and time series arising from analyses of NPP estimates using either algorithm, give highly significant correlations with each other ($p << 0.01$).

Global ocean primary productivity has been examined here in relation to established inter-annual climate variability modes. While it is clear that natural climate variability affects NPP distributions globally, the oceanic characterisation of anthropogenic climate change, observed as a global warming trend [39], is projected in the EOF analysis of NPP variability. Despite the oceanic impacts of anthropogenic climate change disrupting NPP natural variability, such as ocean temperature

increases or acidification [40], we have shown here that for the satellite ocean colour observing decade, the inter-annual variability of NPP is largely described by the canonical ENSO and El Niño – Modoki 'modes'. While both of these sources of inter-annual variability are arguably first-order components of our natural coupled ocean-atmosphere system, the El Nino – Modoki 'mode' apparently intensifies significantly its influence on NPP natural variability under the increasing ocean warming trend.

Methods

Chl and VGPM estimates of NPP datasets were obtained from the Oregon State University Ocean Productivity (http://www.science.oregonstate.edu/ocean.productivity/). Both datasets are comprised of global monthly means, from October 1997 to December 2007 (n=123), with Chl in $mg.m^{-3}$ and VGPM in $mg.C.m^{-2}.d^{-1}$. Each data matrix is composed of 1080 x 2160 pixels, and each pixel corresponds to 18km x 18km at the equator decreasing polewards.

Inter-annual values were calculated by $NPP_{(x,y,t)} = PP_{(x,y,t)} - 10^{a}$, where x is longitude and y latitude and t a specific month, a is the log-distributed average of the PP for the specific location and month of the year (tm), i.e., $a = \overline{\log_{10}\left(PP_{(x,y)}\right)_{(tm)}}$.

The EOF analysis comprises the calculus of the main eigenvalues and eigenvectors from the covariance matrix of the monthly anomalies of the datasets to isolate the main patterns of variability [41]. Additionally, to evaluate the underlying physical drivers of each independent mode, the eigenvectors of the biological variables were projected onto the monthly anomalies of SLP and SST covering the same time period. SLP data was obtained from the NOAA Earth System Research Laboratory (http://www.ncdc.noaa.gov/oa/climate/research/slp/). It consists of monthly means at 2.5º zonal and meridional global grid in hectopascals (hPa). The

SST global maps were obtained from the Met Office Hadley Centre (http://www.metoffice.gov.uk/hadobs/hadisst/) and consist of 1º x 1º grid global monthly SST maps (in degrees - ºC) since 1871 [28]. This dataset is a product of the combined analysis of *in situ* and remote sensing SST observations, with additional data quality improvement techniques applied. Such techniques include bias adjustment, reconstruction of *in situ* data fields, reduced space optimal interpolation and bias-adjusted AVHRR SSTs. Additionally we took into account the serial correlation in each of our time series by reducing the effective number of degrees of freedom [42].

To reconstruct EOF time series, we calculated the EOF from Chl data instead of the NPP, so this mode is independence from SST observations. Further, EOF2 from VGPM and Chl show no significant differences between them, either in the temporal coefficients or the correspondent spatial patterns (i.e., $p << 0.01$ for both). The reconstructed EOF time series were calculated by extracting the projected SSTA EOF spatial pattern from a SSTA dataset from 1871 [28].

Climate indices were obtained from the NOAA Earth System Research Laboratory (MEI, http://www.esrl.noaa.gov/psd/enso/mei/), Japan Agency for Marine-Earth Science and Technology (respectively IODMI and EMI, http://www.jamstec.go.jp/frsgc/research/d1/iod/). The SLP dataset is a product of the NCEP/NCAR Reanalysis 1 project (http://www.esrl.noaa.gov/psd/data/gridded/data.ncep.reanalysis.derived.surface.html) [43].

Acknowledgements

This work was supported by MQRES, PGRF and MI form Macquarie University, Sydney, Australia, and part of it done when visiting the School of Geography, University of Tasmania, Hobart, Australia.

References

[1] Mackas, D. L., *Nature* **472** (7342), E4-E5 (2011).

[2] Rykaczewski, R. R. and J. P. Dunne, *Nature* **472** (7342), E5-E6 (2011).

[3] McQuatters-Gollop, A. *et al.*, *Nature* **472** (7342), E6-E7 (2011).

[4] Nealson, K. H. and P. G. Conrad, *Philosophical Transactions of the Royal Society B: Biological Sciences* **354** (1392), 1923-1939 (1999).

[5] Field, C. B., M. J. Behrenfeld, J. T. Randerson, and P. Falkowski, *Science* **281** (5374), 237-240 (1998).

[6] Behrenfeld, M. J. *et al.*, *Science* **291** (5513), 2594-2597 (2001).

[7] Chavez, F. P., M. Messié, and J. T. Pennington, *Annual Review of Marine Science* **3** (1), 227-260 (2011).

[8] Murtugudde, R., J. Beauchamp, C. R. McClain, M. Lewis, and A. J. Busalacchi, *Journal of Climate* **15** (5), 470-486 (2002).

[9] Sabine, C. L. *et al.*, *Science* **305** (5682), 367-371 (2004).

[10] Yoder, J. A. and M. A. Kennelly, *Global Biogeochemical Cycles* **17** (4), 23-1 (2003).

[11] Behrenfeld, M. J. *et al.*, *Nature* **444** (7120), 752-755 (2006).

[12] Chavez, F. P. *et al.*, *Science* **286** (5447), 2126-2131 (1999).

[13] Demarcq, H., *Progress in Oceanography* **83** (1-4), 376-385 (2009).

[14] Henson, S. A. *et al.*, *Biogeosciences* **7** (2), 621-640 (2010).

[15] Trenberth, K. E., *Nature* **465** (7296), 304-304 (2010).

[16] Chiswell, S. M. and R. Lukas, *EOS, Transactions of the American Geophysical Union* **71** (1990).

[17]Michaels, A. F., in *Ecological Time Series*, edited by Powell, T. M. and J. H. Steele (Chapman & Hall Publishing, New York, 1995), pp. 181-208.

[18]McClain, C. *et al.*, *An overview of the SeaWiFS project and strategies for producing a climate research quality global ocean bio-optical time series*. (Elsevier, Kidlington, ROYAUME-UNI, 2004).

[19]O'Reilly, J. E. *et al.*, in *SeaWiFS Postlaunch Calibration and Validation Analyses, Part 3*, edited by Hooker, S. B. and E. R. Firestone (NASA, Goddard Space Flight Center, Greenbelt Maryland., 2000), Vol. 11, pp. 9-23.

[20]Antoine, D., J. M. Andre, and A. Morel, *Global Biogeochemical Cycles* **10** (1), 57-69 (1996).

[21]Behrenfeld, M. J. and P. G. Falkowski, *Limnology and Oceanography* **42** (1), 1-20 (1997).

[22]Friedrichs, M. A. M. *et al.*, *J. Mar. Syst.* **78** (1), 113-133 (2008).

[23]Li, G., B. Ren, C. Yang, and J. Zheng, *Advances in Atmospheric Sciences* **27** (5), 1210-1220 (2010).

[24]Ashok, K., S. K. Behera, S. A. Rao, H. Weng, and T. Yamagata, *Journal of Geophysical Research C: Oceans* **112** (11) (2007).

[25]Di Lorenzo, E. *et al.*, *Nature Geosci* **3** (11), 762-765 (2010).

[26]Larkin, N. K. and D. E. Harrison, *Geophys. Res. Lett.* **32** (13), L13705 (2005).

[27]Yeh, S.-W. *et al.*, *Nature* **462** (7273), 674-674 (2009).

[28]Rayner, N. A. *et al.*, *J. Geophys. Res.* **108** (2003).

[29]Barnett, T. P. *et al.*, *Science* **309** (5732), 284-287 (2005).

[30]Willis, J. K., D. P. Chambers, and R. S. Nerem, *J. Geophys. Res.* **113** (C6), C06015 (2008).

[31]Smith, T. M., R. W. Reynolds, R. E. Livezey, and D. C. Stokes, *Journal of Climate* **9** (6), 1403-1420 (1996).

[32]Murtugudde, R. G. *et al.*, *Journal of Geophysical Research C: Oceans* **104** (C8), 18351-18366 (1999).

[33]Saji, N. H., B. N. Goswami, P. N. Vinayachandran, and T. Yamagata, *Nature* **401** (6751), 360-363 (1999).

[34]Dommenget, D. and M. Jansen, *Journal of Climate* **22** (18), 4930-4938 (2009).

[35]Cai, W., A. Sullivan, and T. Cowan, *Journal of Climate* **24** (6), 1688-1704 (2011).

[36]Meyers, G., P. McIntosh, L. Pigot, and M. Pook, *Journal of Climate* **20** (13), 2872-2880 (2007).

[37]Eppley, R. W., E. Stewart, M. R. Abbott, and H. U., *Journal of Plankton Research* **7** (1), 14 (1985).

[38]Carr, M. E. *et al.*, *Deep-Sea Research Part II: Topical Studies in Oceanography* **53** (5-7), 741-770 (2006).

[39]Lyman, J. M. *et al.*, *Nature* **465** (7296), 334-337 (2010).

[40]Kim, J.-M. *et al.*, *Geophys. Res. Lett.* **38** (8), L08612 (2011).

[41]Bjornsson, H. and S. A. Venegas, *A manual for EOF and SVD analyses of climate data*, 52 p. (1997).

[42]Davis, R. E., *Journal of Physical Oceanography* **6** (3), 249-266 (1976).

[43]Kalnay, E. *et al.*, *Bulletin of the American Meteorological Society* **77** (3), 437-471 (1996).

Figures

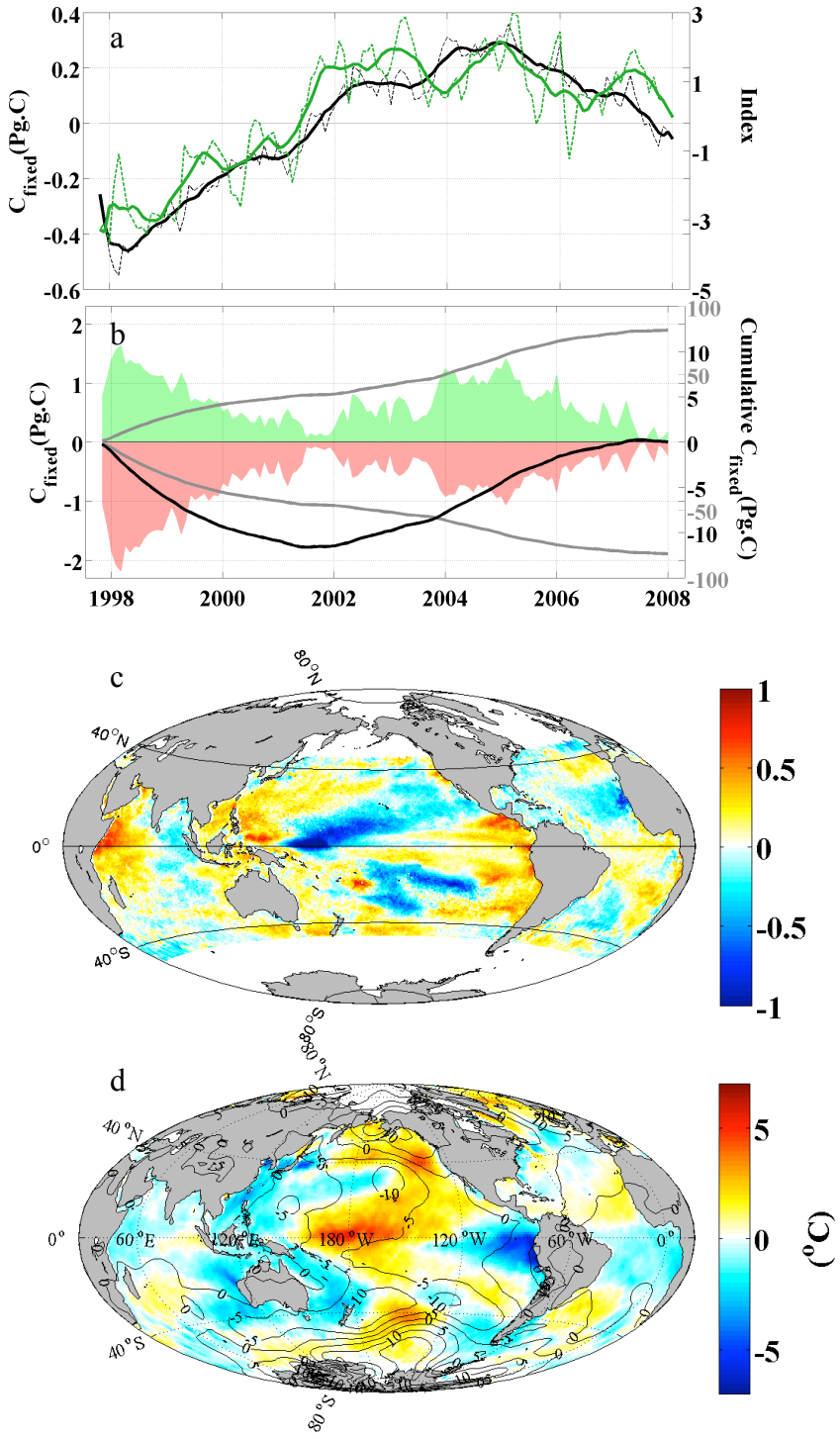

Figure 1 | a, Relationship between the NPPA EOF2 time series (black dashed line) and IEMI (green dashed line) – the solid lines show the corresponding 10-month running average series. Note: the decadal trend is included in the analysis. **b,** EOF2 positive NPPA (green shading) and negative NPPA (red shading; left y-axis), respective cumulative curves (grey lines, right y-axis), and the cumulative net of EOF2 NPPA (black line, right y-axis). **c**, NPPA spatial pattern amplitudes (dimensionless). **d,** Global distribution SSTA (ºC) and SLPA (hPa, contoured) spatial patterns under EOF2 time series projected.

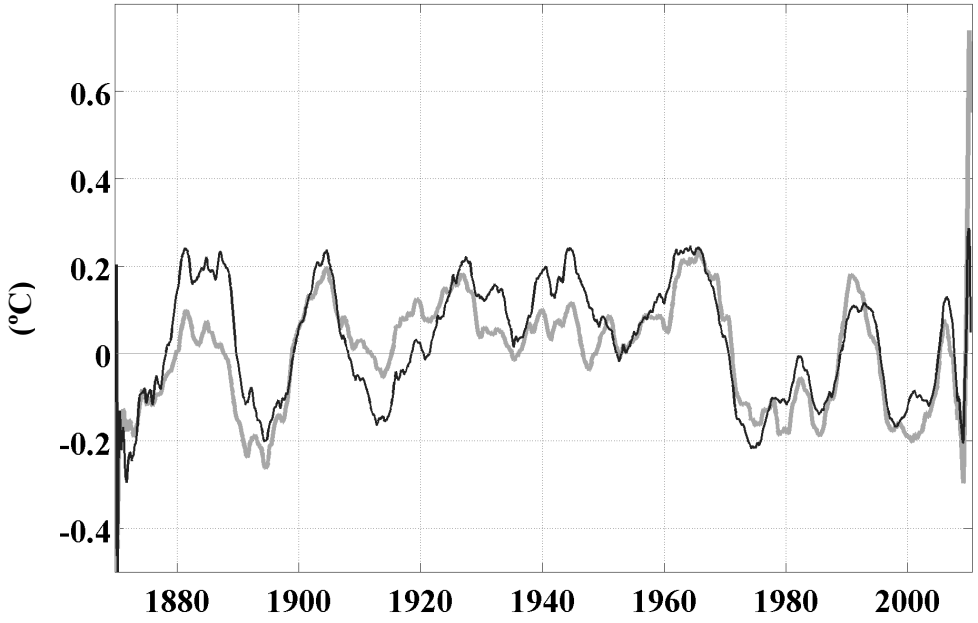

Figure 2 | Comparison between the back-reconstructed EOF2 time series (black line) and the IEMI (grey line) since 1870. The reconstruction was achieved by extracting the projected EOF2 SSTA pattern onto global SSTA observations [28] since 1870.

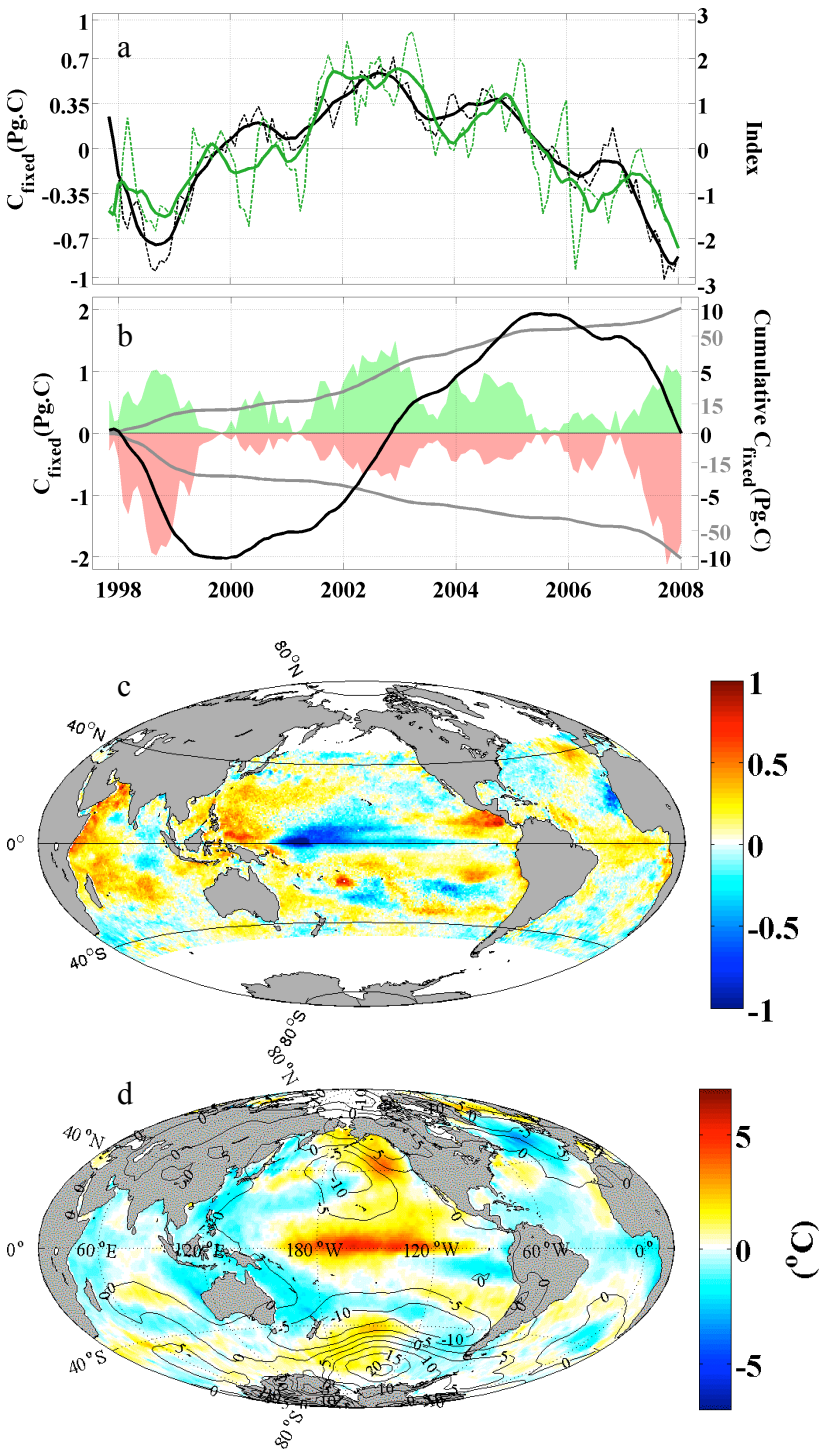

Figure 3 | a, Relationship between the detrended NPPA EOF2 time series (black dashed line) and detrended IEMI (green dashed line) –the solid lines show the 10-month running average series. **b,** detrended EOF2 positive NPPA (green shading) and negative NPPA (red shading; left y-axis), respective cumulative curves (grey lines, right y-axis), and the cumulative net of EOF2 NPPA (black line, right y-axis). **c**, NPPA spatial pattern amplitudes (dimensionless). **d,** Global distribution SSTA (ºC) and SLPA (hPa, contoured) spatial patterns under EOF2 time series projected.

.

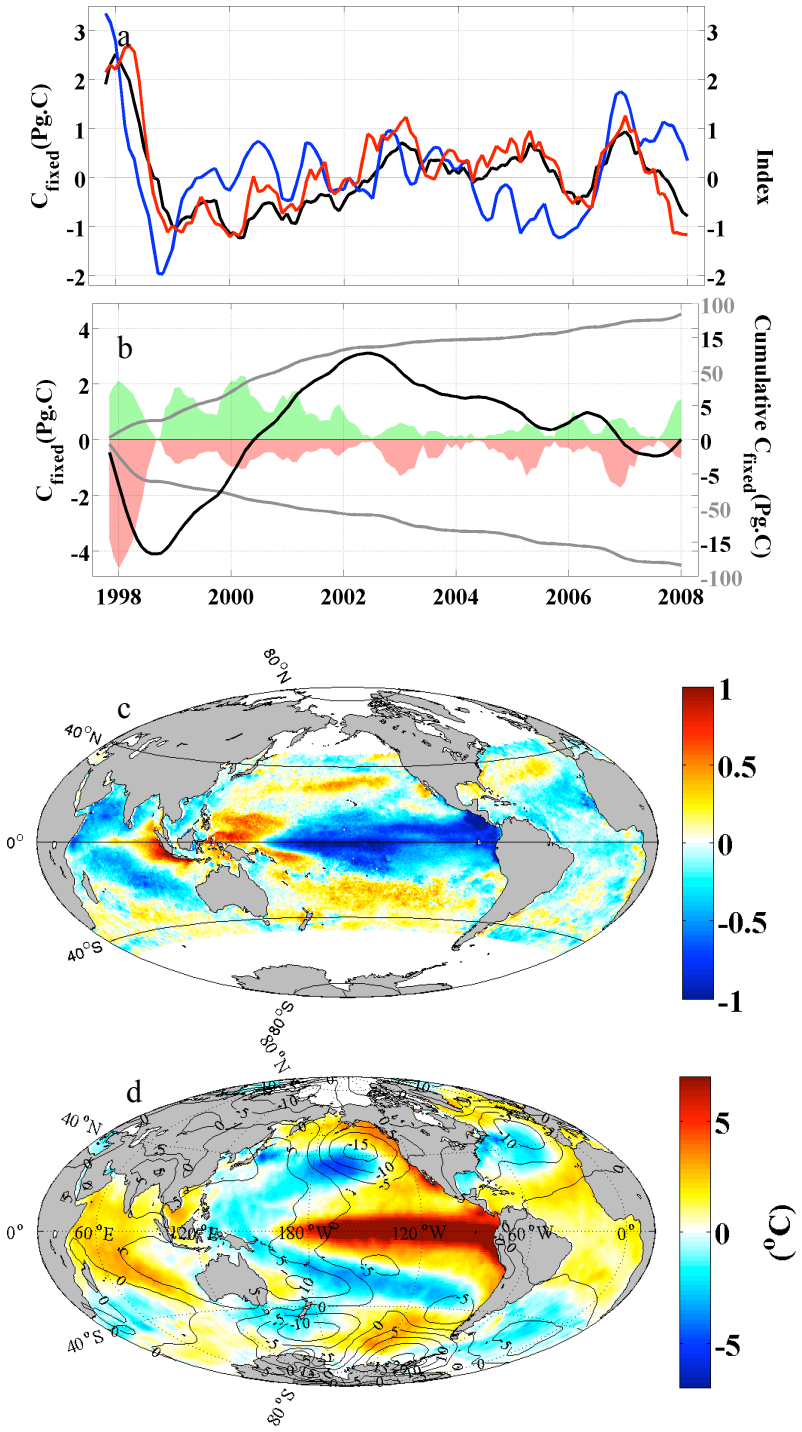

Figure 4 | a, Relationship between the NPPA EOF1 time series (black line), MEI (red line) and IODMI (blue line). **b,** EOF1 positive NPPA (green shading) and negative NPPA (red shading; left y-axis), respective cumulative curves (grey lines, right y-axis), and the cumulative net of EOF1 NPPA (black line, right y-axis). **c**, NPPA spatial pattern amplitudes (dimensionless). **d,** Global distribution SSTA (ºC) and SLPA (hPa, contoured) spatial patterns under EOF1 time series projected.

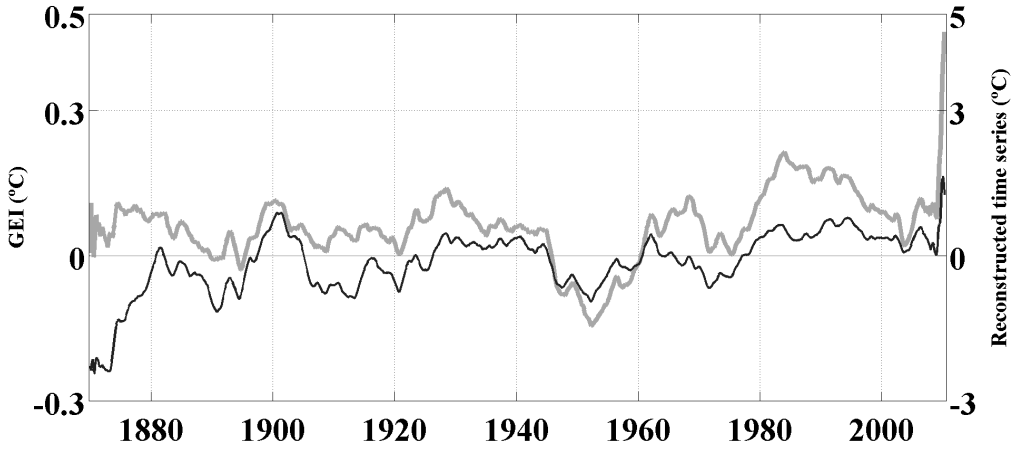

Figure 5 | Comparison between the back-reconstructed EOF1 time series (black line) and the IEMI (grey line) since 1870. The reconstruction was achieved by extracting the projected EOF1 SSTA pattern onto global SSTA observations [28] since 1870.

3.3 CHAPTER SUMMARY

The results of this chapter show that in the past decade global inter-annual NPP variability was primarily related to two different modes of variability. The leading mode was found to be related to ENSO, which explained 90 Pg.C fixed in the ocean (10% of NPP inter-annual variability), and the second mode related to EM, which explains 64 Pg.C (6%). Further, the last decadal trend was observed to significantly enhance EM NPP mode, by +18 Pg.C, suggesting that this mode is connected to anthropogenic climate change. In fact, the justification of EM as a distinct phenomenon has been highly argued in contemporary literature, and possible links with ENSO have been argued, such as that EM is possibly the modified state of ENSO by anthropogenic induced climate change (Yeh *et al.*, 2009), or, that EM is nonetheless non-linear ENSO variability (Takahashi *et al.*, 2011).

CHAPTER 4

Inter-annual propagating features on global chlorophyll-*a* concentrations

4.1 CHAPTER OVERVIEW

In the previous section, we identified the main mode of NPP inter-annual variability to be connected to ENSO dynamics using the EOF tool. However, EOF is limited to analysing standing oscillation features. Further, it is known that ENSO propagation plays a significant role in climate dynamics via atmosphere and ocean circulation, thus affecting phytoplankton distribution. In this chapter, we investigate global Chl inter-annual variability related to ENSO. Also, we assess the connection of inter-annual Chl variability using EEOF, which isolates propagating features, and evaluate its connection with ENSO dynamics. As with the previous chapter, this chapter also addresses the first objective of the thesis.

The main text of this section is a paper, entitled 'Global phytoplankton standing and propagating ENSO variability signals from satellite derived chlorophyll-*a*', which was accepted as a peer-reviewed proceedings paper to be presented at the Global Conference on global Warming 2011 (GCGW-11), held in Lisbon, Portugal, between 11 and 14 July 2011. It is a paper co-authored by A. B. Couto and A. M. Maharaj.

Candidate's contribution to this paper

For this paper, I obtained the dataset, wrote the scripts and performed all data analysis. I also produced the figures and drafted the manuscript, which was posterior evaluated by Dr. Maharaj.

Global phytoplankton standing and propagating ENSO variability signals from satellite derived chlorophyll-*a*

André B. Couto[1] and Angela M. Maharaj[2]

Abstract —Understanding how propagating signals influence phytoplankton distribution at the euphotic layer is a subject of enormous scientific interest. The proposed mechanisms range from meridional advection, uplift/downlift of the community, and upwelling/downwelling of nutrients. These will increase phytoplankton in a specific area by either gathering them or allowing better conditions for reproduction (i.e., increased access to light or nutrients). It is known that ENSO and its associated propagation play a significant role on ocean circulation and climate variability. In the present study we provide empirical evidence of an immediate and lagged influence of ENSO on SeaWiFS and MODIS Aqua derived global Chlorophyll *a* concentrations (Chl). We demonstrate that the influence of ENSO on phytoplankton dynamics occurs in well defined oceanic regions, which are neither restricted to the Tropical Pacific nor to a specific timeframe. Chl distributions suggest that zonal phytoplankton communities react in different phases to the shoaling/deepening of the thermocline. An analysis of propagating signals suggests that ENSO driven propagation explains a substantial amount of interannual phytoplankton variability throughout the Tropical Pacific. Thus, to better understand the importance of ENSO on phytoplankton distribution, further work has to be done on ENSO driven propagation and its associated dynamics.

Keywords — ENSO, Propagation, Satellite derived chlorophyll-*a*

1 Introduction

El Niño - Southern Oscillation (ENSO) is a Tropical Pacific phenomenon with worldwide climatic teleconnections. Despite the unknown relationship between ENSO and global warming, several studies have also linked an increase in the amplitude of ENSO [1], as well an increase in the predominance and intensity of the El Niño phase of ENSO to global warming [2]. ENSO is a coupled atmosphere-ocean system that occurs in the Tropical Pacific. Its oscillation, driven by the Walker circulation [3], determines the state of ocean physical characteristics, such as the mixed layer depth. The mixed layer depth is crucial for phytoplankton, since it determines the abundance of nutrients in the euphotic depth, where these photoautotroph organisms are limited to live. In this study we aim to investigate how global phytoplankton patterns are distributed, in space and time, due to ENSO dynamics. Remote sensing tools have proven to overcome the greatest limitations that classical observational methods suffer by providing global coverage and a continuing sampling rate. Sensors such as the recently terminated SeaWiFS project and the on-going MODIS *Aqua*, are passive ocean colour instruments that measure water leaving radiance which can be converted into Chlorophyll-*a* (Chl) concentrations. Due to the presence of this molecule in all phytoplankton organisms, Chl is commonly used as a phytoplankton biomass indicator throughout the water column.

2 Data and Methods

The Multivariate ENSO Index (MEI) represents ENSO atmosphere-ocean interactions by taking into account six observed variables over the Tropical Pacific. These are: sea level pressure, both components of surface wind, sea surface temperature, surface air temperature, and total cloudiness fraction of the sky [4]. The MEI is the time series of the leading mode yielded when performing an empirical orthogonal function (EOF) analysis of all six fields together. A negative/positive index period is related to a La-Niña/El-Niño event, i.e., a cold/warm ENSO phase respectively.

Remote sensing has proven to be an ideal observational tool, since it provides a continuous sampling of the global ocean. In this study we use SeaWiFS, from October 1997 to December 2007, and MODIS Aqua, from January 2008 to October 2010, monthly averaged global ocean maps of Chl observations. These maps represent, in their original grid form, 18 km^2 per pixel at the equator, reducing zonally towards the poles, then were interpolated to a four times larger grid, i.e., to a 72 km^2 at a latitude of 0º. Chl maps were converted

1. *A. B. Couto is with the Department of Environtment and Geography, Macquarie University, Sydney, 2109 NSW, Australia. E-mail: Belo.Couto@gmail.com*
2. *A. M. Maharaj is with the Department of Environtment and Geography, Macquarie University, Sydney, 2109 NSW, Australia. E-mail: angela.maharaj@mq.edu.au*

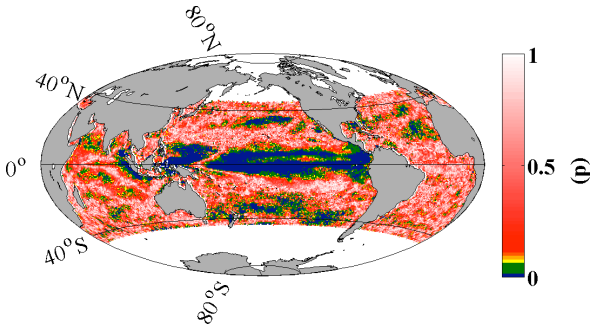

Fig. 1. Significance (p-value) of the probability that MEI has the same distribution as Chl time series for each grid point (p), green are values between 0.01 and 0.1. Calculated with reduced number of intervals [5].

to log-distribution and monthly averages were then subtracted from the time series, which was then divided by its standard deviation to normalise the intra-annual cycles of the Chl values. The data was smoothed over each three months prior to being detrended. Posterior analysis was only performed on grid points which had full time coverage, i.e., n=157. Additionally, all correlations between MEI and each grid point time series were estimated using a reduced number of degrees of freedom [5]. Cross-correlation were carried out to determine the time lag of the best fit between MEI and each Chl grid point time series.

The classical Empirical Orthogonal Function (EOF) is a common mathematical tool used in atmospheric sciences to identify the patterns that explain most of the variability within a set of observations [6]. While the technique yields a standing wave-like pattern, propagating signals are often isolated into different modes with a similar temporal series. Furthermore, if the data is truncated into a series of predefined lag times prior to performing the EOF, the result isolates modes that explain all the variance within a propagation mode that best fits the predefined lag. This method is called an extended EOF (EEOF) and is commonly used to study propagating features in atmospheric sciences [7]. Here, we use it to isolate oceanic Chl propagation that occurs with the same cycle as the MEI maximum spectrum (L = 28 months).

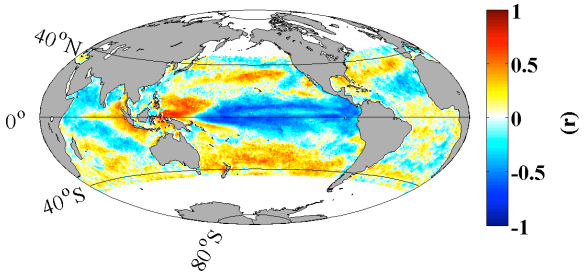

Fig. 2. Coefficient relation (r) when testing the relationship between MEI and Chl time series for each grid point.

3 Results

Fig. 1 shows the spatial distribution of statistical significance between the MEI and Chl time series. ENSO has a more significant influence on Chl concentrations over the Pacific then in other ocean basins. Nevertheless, significant relationships are also found in the Indian Ocean (mainly off the Java and Sumatra west coasts) and within the centre of the North Atlantic gyre (Fig. 1). Furthermore, significant relationships are found to exist not only in the Tropical region of the Pacific but also further poleward to 35° in both hemispheres. These extra-tropical regions also display high correlation coefficients, albeit with an inverse relationship to that observed throughout the Tropical Pacific, with the exception of the west side of the basin where a positive correlation coefficient is observed (Fig. 2). Direct and highly significant relationships are also found in the subtropical regions.

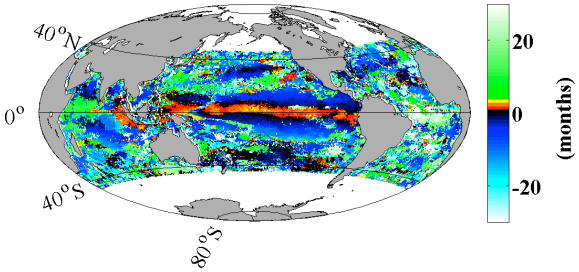

Fig. 3. Time lag (months) of best coefficient correlation (r) between MEI and Chl time series for each grid point. Positive values mean that Chl is leading.

Interestingly, while all these Chl regions track well with the MEI, they display different timing with respect to a best fit with the ENSO signal. As we can see in Fig. 3, the Chl temporal series over the Equatorial Pacific and also at the west coast of Java and Sumatra in the Indian basin (with either a direct or inverse relation to the MEI) has a positive (leading) best fit to the MEI, and in some regions at three or more months earlier. This best fit is delayed towards the poles. However, in the mid latitude Pacific where a significant relationship with the MEI is observed, the best correlation fit occurs simultaneously with the MEI. The same best fit of near zero lag occurs between the MEI and Chl patterns in the North Atlantic gyre.

The EOF analysis yielded two independent modes of variability [8] with time coefficients that are significantly related to the MEI: EOF mode 2 at $r = 0.83$ ($p << 0.01$), and the third EOF mode with a MEI lead lag of 8 months for the best fit ($r = -0.76$, $p << 0.01$) (Fig. 4). These two modes together explain 14% of the Chl inter-annual variability, mostly in the Tropical Pacific region and off the west coasts of Java and Sumatra. However, the

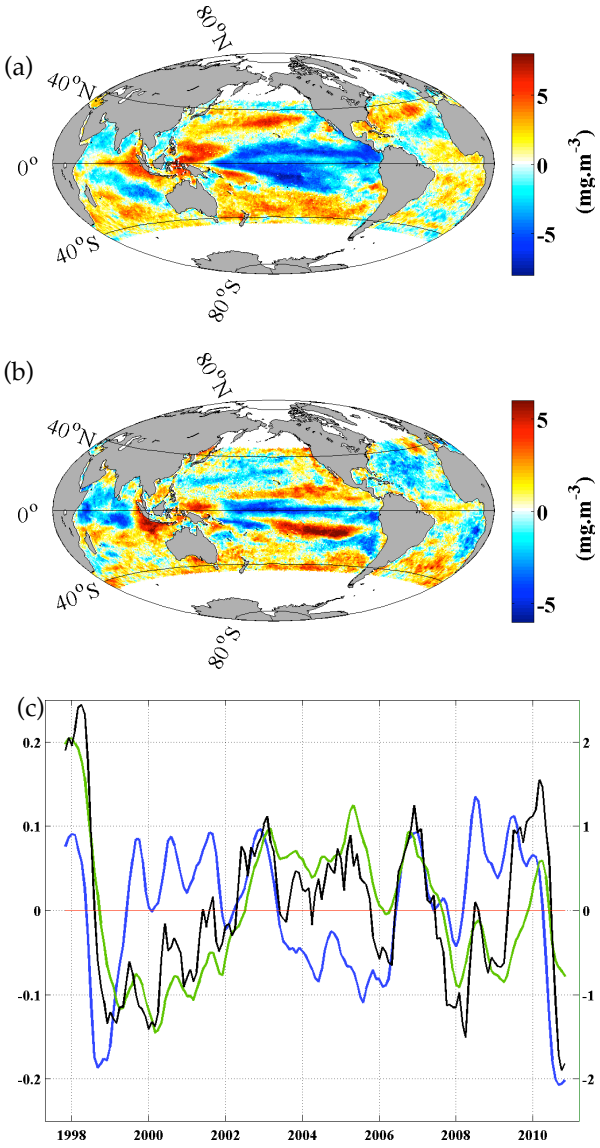

Fig. 4. EOF modes that significantly related to MEI. (a) EOF mode 2 spatial pattern explaining 9% of Chl interannual variability between October 1997 and October 2010; (b) EOF mode 3 spatial pattern explaining 5% of same as the previous; (c) EOF modes 2 (blue) and 3 (green), and MEI (black) time series.

EOF mode 3 spatial pattern is quite different from the pattern in mode 2. Whereas in mode 2 the spatial pattern resembles Fig. 2, reminiscent of the same regions where Chl distribution is strongly influenced by ENSO, the mode 3 pattern shows a strong signal along the equatorial line, and an equally strong amplitude of the opposite signal northward and southward off the equator. This suggests that ENSO dynamics drive a Chl interannual variability signal at the Tropical Pacific, the spatial pattern of which is best represented by the EOF mode 3 in Fig. 4, and occurring 8 months after changes in the regional climate mode.

The EEOF analyses yielded only one mode that significantly tracked MEI, mode 2 ($r = 0.79$, $p = 0.001$), as seen in Fig. 5a. This mode explains 6% of the Chl interannual variability pattern propagating mainly along the Tropical Pacific (Fig. 5b), although, variability patterns are observed at higher latitudes of the Pacific, as well as in the North Atlantic and Indian Ocean in the same regions where a significant relationship was previously found. This propagating EEOF mode 2 has a good correlation with the spatial patterns of both EOF modes discussed before that showed a highly significant relationship with ENSO. The EOF mode 2 spatial pattern shows the best significant relationship with EEOF mode 2 at the first time step ($r = 0.96$, $p << 0.001$) of the series, whilst EOF mode 3 is better represented by EEOF mode 2 step 11 ($r = 0.63$, $p <<0.001$; Fig. 6). This not only strongly indicates that EEOF mode 2 is due to ENSO dynamics, but also confirms that EOF mode 3 is an ENSO propagation signal.

4 Discussion

The near equatorial trough between the subtropical high-pressure systems located in both hemispheres at the eastern Pacific and western Atlantic accelerate air masses towards the equator, which with coriolis deflection makes the easterly trade winds. The associated wind stress will drag the warm ocean surface layer westward uncovering a deeper lower layer of nutrient rich cooler waters on the eastern side of the Equatorial

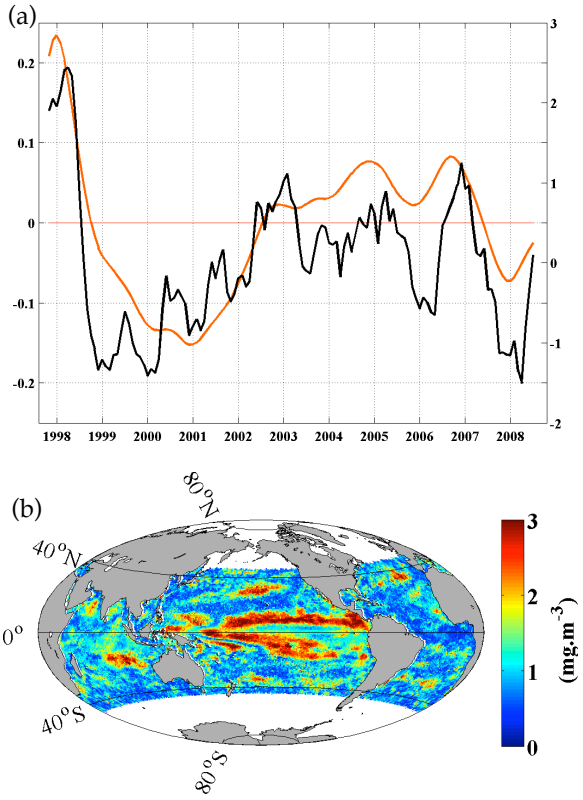

Fig. 5. EEOF mode 2 of interannual Chl: (a) EEOF time series (orange) and MEI; (b) EEOF standard deviation of mode 2.

Pacific basin, which is also dragged westward by the same force. The impact of the thermocline shoaling due to the trade wind forcing in the Eastern Tropical Pacific on phytoplankton communities [9], and also the impact of ENSO dynamics on global ocean phytoplankton distribution [10] have been previously reported. However, the influence of ENSO in phytoplankton distribution in subtropical latitudes, in either Pacific basins, or in the North Atlantic, as reported here (Fig. 1), is not clear in the current literature. Further to this, the various timing of best fits with MEI suggest that depending on the zonal location along the Tropical Pacific, phytoplankton communities have a different phase of reaction to ENSO fluctuations (Fig. 3). It is worth noting that the MEI is an index representing the entire Tropical Pacific domain [4], and not specifically reflecting propagating atmospheric or oceanic waves that occur, e.g., when ENSO is shifting phase. Nevertheless, taking the MEI as an average of propagating modes occurring throughout the Tropical Pacific, our results indicate that this index is significantly coupled and synchronous with Chl patterns that occur off the equatorial belt, and lagged with the patterns at the equator. Indeed, the EOF analysis suggests that the Chl pattern has a highly significant correlation to the MEI at an 8 month lag in addition to the dominant and synchronous pattern driven by ENSO. The ENSO related out of phase Chl variability EOF mode 3 (Fig. 4), is actually quite similar to a result reported by Behrenfeld et al., [11], as the difference between two consecutive La Niña events of similar intensity. This suggests that mode 3 might represent the signal of a persistent ENSO phase. Nevertheless, the EEOF propagation analysis includes such a pattern in its ENSO related propagation mode, in addition to the synchronously related EOF mode 2.

5 Conclusions

In summary, we demonstrate that the influence of ENSO on phytoplankton dynamics occurs in well defined oceanic regions, which are neither restricted to the Tropical Pacific nor to a specific frequency. Chl distributions suggest that zonal phytoplankton communities react in different phases to the shoaling/deepening of the thermocline. An analysis of propagating signals suggests that ENSO driven propagation explains a substantial amount of interannual phytoplankton variability throughout the Tropical Pacific. We speculate that the observed delayed reaction to ENSO variability might be due to several mechanisms, including the persistence of an ENSO phase. Thus, to better understand the importance of ENSO on phytoplankton distribution, further work has to be done on ENSO driven propagation and its associated dynamics.

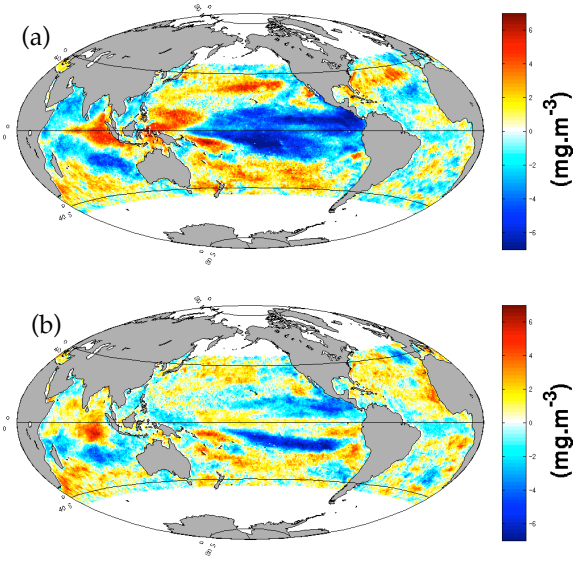

Fig. 6. Chl interanual EEOF mode 2 spatial patterns of step 1 (top) and 11 (bottom).

References

[1] Zhang Q, Guan Y, Yang H. ENSO amplitude change in observation and coupled models. Advances in Atmospheric Sciences 2008;25(3):361-6.

[2] Fedorov AV, Philander SG. Is El Niño Changing? Science 2000 June 16, 2000;288(5473):1997-2002.

[3] Wang C, Enfield DB. A Further Study of the Tropical Western Hemisphere Warm Pool. Journal of Climate 2003;16(10):1476-93.

[4] Wolter K, Timlin MS. Monitoring ENSO in COADS with a seasonally adjusted principal component index. Proc of the 17th Climate Diagnostics Workshop; 1993; Norman, OK, NOAA/NMC/CAC, NSSL, Oklahoma Clim. Survey, CIMMS and the School of Meteor., Univ. of Oklahoma; 1993. p. 52-7.

[5] Davis RE. Predictability of Sea Surface Temperature and Sea Level Pressure Anomalies over the North Pacific Ocean. Journal of Physical Oceanography 1976;6(3):249-66.

[6] Bjornsson H, Venegas SA. A manual for EOF and SVD analyses of climate data. Montréal, Québec: McGill University; 1997.

[7] Holbrook NJ, S-L CP, Venegas SA. Oscillatory and propagating modes of temperature variability at the 3–3.5- and 4–4.5-yr time scales in the upper southwest Pacific Ocean. Journal of climate 2005;18:719-36.

[8] North GR, Bell TL, Cahalan RF, Moeng FJ. Sampling Errors in the Estimation of Empirical

Orthogonal Functions. Monthly Weather Review 1982 July 01, 1982;110(7):699-706.
[9] Pennington JT, Mahoney KL, Kuwahara VS, Kolber DD, Calienes R, Chavez FP. Primary production in the eastern tropical Pacific: A review. Progress in Oceanography 2006;69(2-4):285-317.
[10] Behrenfeld MJ, O/'Malley RT, Siegel DA, McClain CR, Sarmiento JL, Feldman GC, et al. Climate-driven trends in contemporary ocean productivity. Nature 2006;444(7120):752-5.
[11] Behrenfeld MJ, Randerson JT, McClain CR, Feldman GC, Los SO, Tucker CJ, et al. Biospheric primary production during an ENSO transition. Science 2001;291(5513):2594-7.

4.3 CHAPTER SUMMARY

In this chapter we assessed Chl interannual variability related to ENSO dynamics. We observed that ENSO related Chl dynamics occurs mostly in the Tropical Indo-Pacific, but reacts at different phases (-3 to 3month lags) to the Multivariate ENSO index (MEI). Further, two of the first three leading EOF modes of Chl inter-annual variability were highly related to the MEI, mode 2 and 3. Whilst mode 2 had a 0 lag maximum correlation, $r = 0.83$ ($p << 0.01$) mode 3 correlated higher a lag of 8 months ($r = 0.76$), and related with EEOF propagating mode month 11 hence ($r = 0.67$, $p << 0.01$), suggesting that ENSO has a significant propagating influence on global Chl variability.

CHAPTER 5

South Hemisphere chlorophyll-*a* patterns of variability

5.1 CHAPTER OVERVIEW

In this chapter we limit our study area to the South Hemisphere, and apply the EOF technique to analyse Chl intra- and inter-annual patterns variability. To this end, the EOF tool was used on unfiltered and deseasonalised satellite derived global Chl. Further, we assess if the inclusion/exclusion of the Tropical Pacific, the region where ENSO occurs, influences the Chl inter-annual variability leading mode. This chapter addresses objective 2 of the thesis.

The main text of this section is a paper entitled 'Climatic Influences on Southern Hemisphere Oceanic Primary Production Derived from Satellite Remote sensing observations', presented at the International Conference on South Hemisphere Meteorology and Oceanography 2009 (ICSHMO-09), hold in Melbourne, Australia, between 9 and 13 February 2009. It is a paper co-authored by A. B. Couto, A. M. Maharaj and N. J. Holbrook.

Candidate's contribution to this paper

In this paper I obtained the dataset, script and performed all data analysis, produced the figures and drafted the paper, which was evaluated by both co-authors. Additionally, input from both co-authors was attained regularly during this process.

CLIMATIC INFLUENCES ON SOUTHERN HEMISPHERE OCEANIC PRIMARY PRODUCTION DERIVED FROM SATELLITE REMOTE SENSING OBSERVATIONS

Andre B. Couto[1]*, Angela M. Maharaj[1], Neil J. Holbrook[2]
[1]Macquarie University, Sydney, Australia, [2]University of Tasmania, Hobart, Australia

1. INTRODUCTION

Oceanic phytoplankton growth is essential to the sustainability of ocean biota (Field et al. 1998). Ocean's primary productivity varies in response to environmental conditions, such as grazing, sunlight and nutrient availability. These factors restrain the reproduction and growth of drifting algae. In the southern hemisphere several climate signals exist which may modulate ocean primary productivity such as the El Niño Southern Oscillation (ENSO), the Indian Ocean Dipole (IOD) in the tropical Indo-Pacific region (Saji et al. 1999; Wolter; Timlin 1998); and the Southern Annular Mode (SAM) in the polar and sub-polar regions (Mo 2000a). Ocean primary productivity is thought to respond indirectly to these climate modes of variability, by the circulation changes that these induce (Behrenfeld et al. 2006). Changing circulation patterns may induce an anomalous upwelling (or downwelling), leaving anomalous nutrient signatures in the euphotic layer, where primary productivity will anomaly correspond (Lovenduski; Gruber 2005). Additionally, the southern hemisphere also includes the unique region of the Southern Ocean, which is a critical component of the global circulation and the biogeochemical cycles of nutrients and carbon (Arrigo et al. 2008). Phytoplankton growth patterns adapt to different regions depending on the intrinsic conditions of each region.

As vast and rapidly changing as the ocean is, satellite imagery provides an ideal tool to observe and illustrate, at a high sampling rate, several oceanic characteristics, including its colour (McClain et al. 2004). Using the appropriate algorithm, one is able to retrieve not only chlorophyll concentrations, and from these also phytoplankton estimates (Morel; Berthon 1989).

In this study we use Empirical Orthogonal Functions (EOF) to evaluate satellite derived chlorophyll concentrations. The use of EOF is an ideal tool to observe cyclical patterns within continuous observations (Bjornsson; Venegas 1997).

This paper explores the relationship between large-scale climate modes of variability (ENSO, IOD and SAM) and phytoplankton distribution patterns, using chlorophyll estimates as an indicator, across the southern hemisphere oceans.

* *Corresponding author address*: Andre B. Couto, Faculty of Science, Department of Environment & Geography, Macquarie university, NSW, 2109 Australia; e-mail: abelodoc@mq.edu.au.

2. DATA AND ANALYSIS

Remote sensing derived ocean chlorophyll *a* concentrations were used in this study. The OC4-v4 chlorophyll algorithm product from SeaWiFS reprocessed version 5.1 oceanic global maps were obtained from NASA's Ocean Color website (http://oceancolor.gsfc.nasa.gov). These maps were retrieved at a 2,160 x 4,320 pixel resolution originally (*i.e.* one pixel at the equator represents 9 km of the planet's surface) then interpolated to a 4x larger scale (540 x 1080 pixel, *i.e.* 36 km/pixel at the equator). More than ten years of satellite imagery was used (from September 1997 to December 2007) with a time resolution of one month. The time resolution was chosen to maximize sampling. Due to the presence of clouds, higher time resolution maps often show a succeeding degradation with increase of the sample coverage, making time averaged joined maps an improved research dataset. The region of interest, the southern hemisphere, was selected from data imagery, and posterior analyses were carried. Although to evaluate southern hemisphere ocean's primary production patterns with and without ENSO signal, other areas were selected from the original data, as from 20ºN to south pole, as well as from 20ºS to 80ºS. this first area is expected to show a better relationship with ENSO and IOD signals than the original region of interest. The second area, without tropical region, was done to focus more on the subpolar and polar climate events, such as SAM. When data is deseasonalised, the EOF analyses illustrate chlorophyll patterns, which are related to interannual influences, allowing one to focus on climate events that might influence the primary productivity signal. To remove the season signal from the data and calculate monthly anomalies, monthly averages were calculated and subtracted from data. In order to evaluate primary production distribution patterns in the ocean, we use an empirical orthogonal function (EOF) analyses. EOF is a mathematical tool that decomposes the data into cyclical patterns, both spatial and temporal, ordered by the explained variance within the data (Bjornsson; Venegas 1997).

Climate signal indicators used were include: the Multivariate ENSO Index (MEI), Southern Oscillation Index (SOI) which is calculated from Darwin (Australia) and Tahiti (French Polynesia) measurements, for the tropical region and the Southern Annular Mode (SAM) for the polar and sub-polar regions. MEI data was acquired from http://cdc.noaa.gov/people/Klaus.wolter/MEI, SOI data from http://www.eldersweather.com.au/ and SAM data from http://www.cpc.noaa.gov/products/precip/CWlink/.

MEI is based on six different atmosphere-ocean interaction characteristics. These variables are: sea-level pressure, zonal and meridional components of the surface wind, sea surface temperature, surface air temperature and total cloudiness fraction of the sky (Wolter; Timlin 1998). SAM is defined by the dominant pattern of non-seasonal tropospheric circulation variations southward of 20ºS. SAM is characterized by pressure anomalies in the centre of the Antarctic, and opposed to anomalies in the 40ºS to 50ºS (Mo 2000b).

Time resolution used was the same as the chlorophyll imagery. In order to evaluate the relationship between chlorophyll concentrations and climate variability, the temporal variability of various regional climate indicators were statistically compared against the calculated EOF time series.

3. RESULTS

3.1 EOFs Of Chlorophyll Maps

The first six modes of the EOF analysis of chlorophyll maps show a strong seasonal component, the first mode being more dominant (87.74%), however altogether explain about 91.5% of chlorophyll variability in the data. The temporal and spatial patterns of the mode 1 (Figure 1) showed that, essentially, primary productivity in the southern hemisphere ocean is mostly synchronized with a seasonal cycle, and a similar pattern with the mean chlorophyll distributions for southern hemisphere ocean. Mode 1 spatial pattern suggests lowest variability regions are those of oligotrophic waters in the centre of the oceanic gyres, either South Pacific, South Atlantic, and Indian oceans. In opposition, highest values of variability were observed in the coastal areas such as the Angola, Namibia and South Africa, in the south Atlantic eastern boundary, and River Plate (estuary between Uruguay and Argentina) the western south Atlantic boundary. In the Pacific Ocean the Ecuadorian, Peruvian and some regions in the Chilean coast, showed high variability values, as well as some localities in the coastal Indonesian waters. In the subpolar and polar regions it is observed a poleward decrease to explain chlorophyll variability by this mode show. It is known that in ocean gyre centre regions of the Indian, South Pacific and South Atlantic, phytoplankton is limited on iron availability (Field, 1998), which explains the observed low chlorophyll *a* concentrations. Further phytoplankton growth is also limited due to the lack of sunlight availability, which is possibly the cause of the observed low chlorophyll *a* concentrations towards the polar region. Nevertheless, higher concentrations observed in coastal areas, probably due to the well mixed and nutrient rich waters, particularly in estuaries.

Though, the amplitude of this mode does not vary much (±0.04), suggesting that 87.74% of primary productivity variability is a very relaxing seasonal cycle, in the southern hemisphere oceanic tropical region.

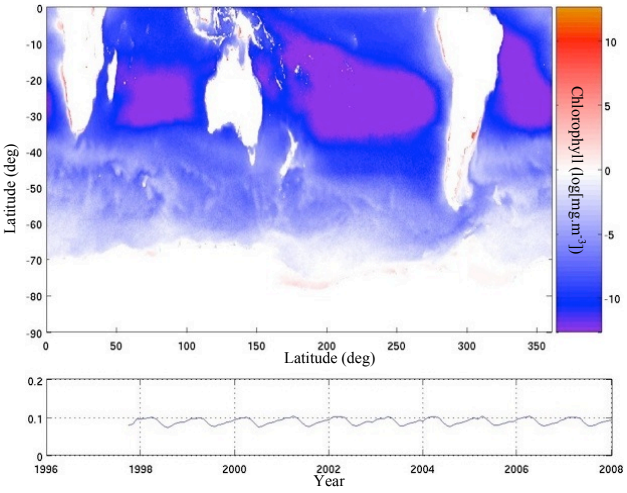

Figure 1. Mode 1 of EOF analysis from chlorophyll *a* southern hemisphere maps (87.74% of the variance).

Mode 2 suggests great dynamics of chlorophyll *a* at high latitudes of the southern hemisphere ocean (Figure 2). With almost 2% of variability, this mode showed a high dynamical seasonal pattern (amplitude range ~0.3), suggesting optimum growth conditions alternate with bad growth conditions seasonally. The spatial pattern shows roughly 4-stripped regions alternated with positive and negative values of variability. With positive, 48ºS downwards until Antarctic coast and, with less intensity, between ~30ºS to 45ºS. This illustration shows a similar pattern with the climate pattern of variation defined by SAM (Thompson; Solomon 2002). These differences may be explained by the different sun and nutrient availability that each ocean is characteristic with (Southern Ocean rich in nutrients and poor in sun availability, and vice-versa for tropical regions). Therefore, in regions where these two have the opportunity to blend synchronized with the seasons, an extreme seasonal variability of primary production occurs.

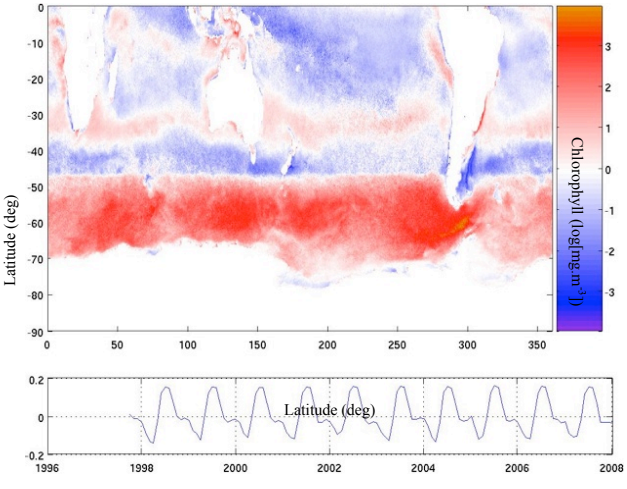

Figure 2. Mode 2 of EOF analysis from chlorophyll *a* southern hemisphere maps (1.94% of the variance).

3.2 EOFs Of Deseasonalised Chlorophyll Maps

The first mode of the EOF analysis made from the chlorophyll anomalies explained 4.42% of the total relative variance (Figure 3). Comparing to Figure 1, this leading mode of deseasonalised chlorophyll illustrates a more complex, less dynamical, however, more intensive pattern of chlorophyll anomalies. This mode shows bigger patches of positive loads, and stronger variability in the tropical Indo-Pacific Ocean region. The correspondent time series (Figure 3) indicates a transitional stage to positive amplitudes for the positive patches, in the first two years, with rather slow changes in the signal during the rest of the period. Nevertheless, the high range of amplitudes (~0.5), suggests an intensive chlorophyll concentration patterns. In common, both leading modes, one from original data and the other from deseasonalised data, decrease load polewards.

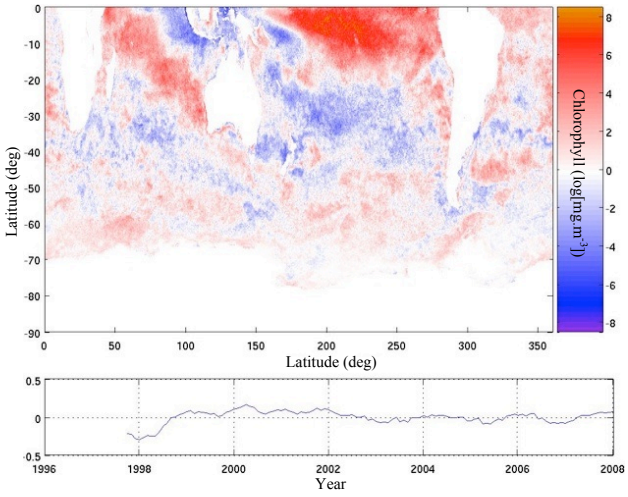

Figure 3. Mode 1 of EOF analysis from deseasonalised chlorophyll *a* southern hemisphere maps (4.42% of the variance).

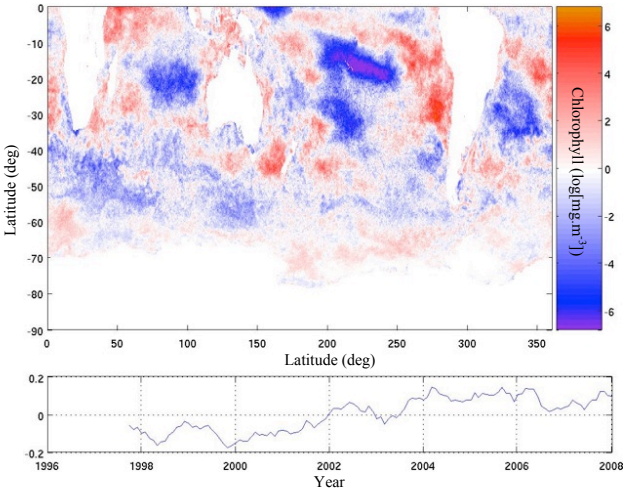

Figure 4. Mode 2 of EOF analysis from deseasonalised chlorophyll *a* southern hemisphere maps (3.80% of the variance).

With 3.8% of variance, mode 2 of deseasonalised data, in Figure 4, shows a very complex spatial and temporal pattern.

3.3 Comparing chlorophyll and climate signals

The comparisons made between the two leading modes of different regions of chlorophyll anomalies and climate modes of variability indices (MEI, SOI and SAM) is summarised in Table 1. Although the amplified study region showed an increase of variance explained (5.34%), an improve relationship was not observed when its time series was correlated with MEI. This was expected since the amplified region area is highly influenced by ENSO (as observed in the southern hemisphere ENSO region) (Field, 1998). Yet, the original study area mode 1 time series showed a better relationship (R^2=0.63), than the amplified region analysis (R^2=0.58) (Figure 5 and 6).

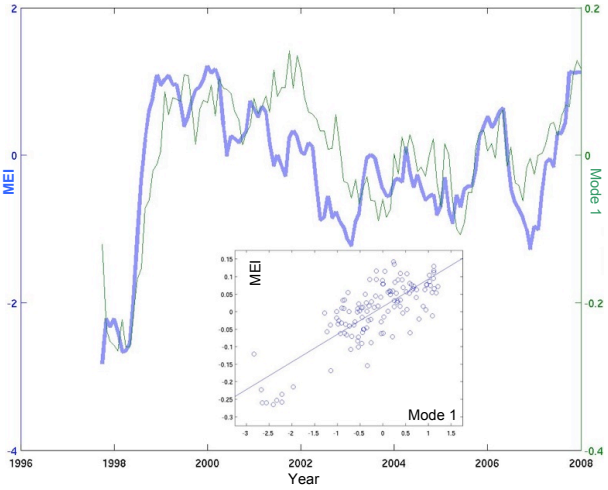

Figure 5. Comparison between Mode 1 of EOF analysis from un-seasonalised chlorophyll *a* southern hemisphere maps time series with MEI (R^2=0.63).

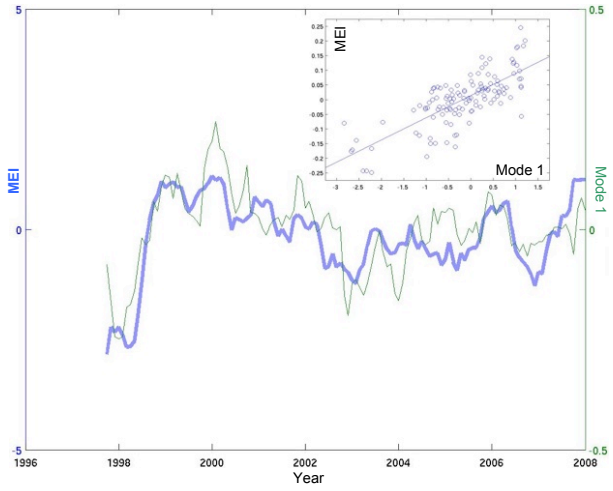

Figure 6. Comparison between Mode 1 of EOF analysis from extended un-seasonalised chlorophyll *a* region time series with MEI (R^2=0.58).

For the Indo- Western Pacific region, it is known that the climate mode of variability known as IOD, act upon this area. Spatially some resemblance can be seen by synoptic view of the leading mode for the original and extended regions of study.

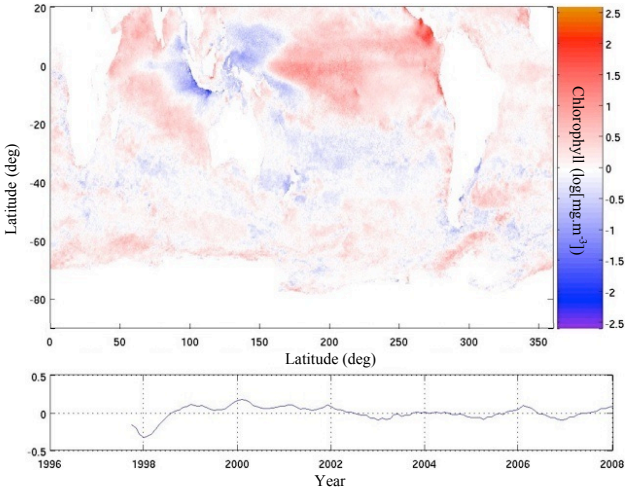

Figure 7. Mode 1 of EOF analysis from un-seasonalised chlorophyll *a* amplified area (5.34% of the variance).

When comparing these two regions both leading modes with the other indices taken into account (SOI and SAM), these showed a very weak or non-existent correlation. SAM also showed no visible correlation with the southern hemisphere ocean chlorophyll patterns (Table 1). Not even in the selected region to try to enhance this connection (20ºS to 80ºS). Nonetheless, both the leading modes of this last region analysis showed longitudinal patches along polar region in both modes, and the sub polar region in the second mode (Figures 8 and 9).

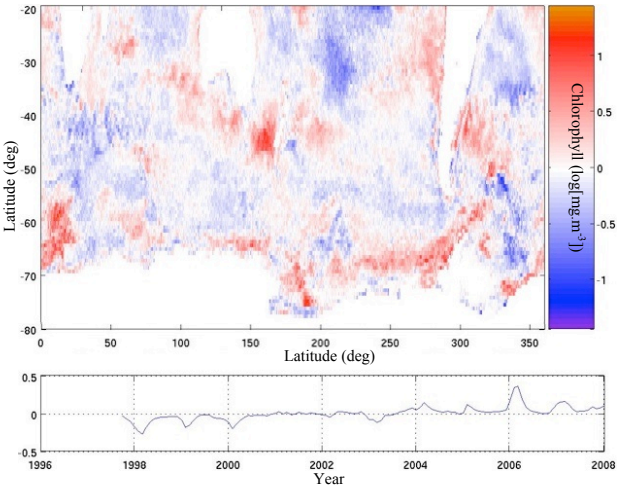

Figure 8. Mode 1 of EOF analysis from un-seasonalised chlorophyll *a* reduced area (4.03% of the variance).

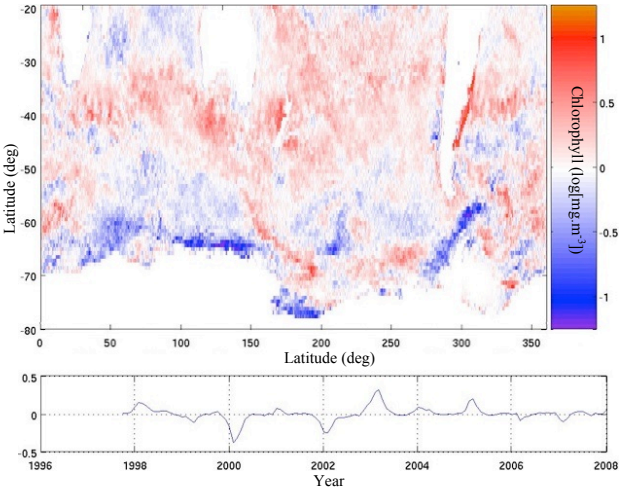

Figure 9. Mode 2 of EOF analysis from un-seasonalised chlorophyll *a* reduced area (3.68% of the variance).

Both these modes yield from the EOF analysis of the reduced area, show a pattern that suggests some association between the primary productivity and SAM (Lovenduski; Gruber 2005).

All statistic tests here discussed showed result of p<0.01.

Table 1. Coefficient of determination (R^2) of the linear regression relationship between the leading modes (1 & 2) of chlorophyll anomalies and three climate modes of variability indices for different regions observed (p<0.01, for all tests).

Region	Mode of time series	MEI	SOI	SAM
0º to 90ºS	1	0.63	0.25	0.00
	2	0.03	0.01	0.01
20ºN to	1	0.58	0.33	0.05
90ºS	2	0.13	0.05	0.02
20ºS to	1	N/A	N/A	0.05
80ºS	2	N/A	N/A	0.01

4. CONCLUSIONS & FUTURE WORK

Southern hemisphere primary productivity variability distribution was observed to be essentially seasonal, with a spatial pattern similar to the one showed by averaged chlorophyll concentrations. Meaning that high variability is enhanced by optimised conditions of growth, and vice-versa.

Most of the southern hemisphere chlorophyll variability is located in the Atlantic, Indian and Pacific Oceans, since the leading modes always focused on these regions. However, the temporal distribution showed to be quite smooth, in contrast with the sub polar and polar regions. Here, the seasonal cycle corresponds to very dynamic alternation from highly productive to non-productive regions.

Despite of phytoplankton being regulated in a seasonal basis, this study showed that most interannual variability is located in the Tropical Indo-Pacific Ocean. By synoptic view this region was easily related with ENSO and IOD. Furthermore, ENSO index (MEI), showed to have a good correlation with southern hemisphere's chlorophyll concentration interannual variability (R^2=0.63).

Sub polar and polar oceanic regions showed no relationship in statistical tests used, however, by synoptic view this climate mode may be easily related.

Future work may include the analysis of other ocean and atmospheric teleconnection signals through the examination of indices such as the Tropical Atlantic SST Index (TASI), the Dipole Mode Index (DMI) and the South Western Indian Ocean (SWIO) SST index. On the other hand, specific physical variables such as sea surface temperature, wind stress or the heat flux, could potentially be used to assess oceanic chlorophyll distribution.

5. REFERENCES

Arrigo, K. R., G. L. van Dijken, and S. Bushinsky, 2008: Primary production in the Southern Ocean, 1997-2006. *Journal of Geophysical Research C: Oceans*, **113**.

Behrenfeld, M. J., and Coauthors, 2006: Climate-driven trends in contemporary ocean productivity. *Nature*, **444,** 752-755.

Bjornsson, H., and S. A. Venegas, 1997: A manual for EOF and SVD analyses of climate data, 52 pp.

Field, C. B., M. J. Behrenfeld, J. T. Randerson, and P. Falkowski, 1998: Primary production of the biosphere: Integrating terrestrial and oceanic components. *Science*, **281,** 237-240.

Lovenduski, N. S., and N. Gruber, 2005: Impact of the Southern Annular Mode on Southern Ocean circulation and biology. *Geophysical Research Letters*, **32**.

McClain, C. R., G. C. Feldman, and S. B. Hooker, 2004: An overview of the SeaWiFS project and strategies for producing a climate research quality global ocean bio-optical time series. *Deep-Sea Research Part II: Topical Studies in Oceanography*, **51,** 5-42.

Mo, K. C., 2000a: Relationships between Low-Frequency Variability in the Southern Hemisphere and Sea Surface Temperature Anomalies. *Journal of Climate*, **13,** 1.

——, 2000b: Intraseasonal modulation of summer precipitation over North America. *Monthly Weather Review*, **128,** 1490-1505.

Morel, A., and J. F. Berthon, 1989: Surface pigments, algal biomass profiles, and potential production of the euphotic layer: relationships reinvestigated in view of remote-sensing applications. *Limnology & Oceanography*, **34,** 1545-1562.

Saji, N. H., B. N. Goswaml, P. N. Vinayachandran, and T. Yamagata, 1999: A dipole mode in the tropical Indian ocean. *Nature*, **401,** 360-363.

Thompson, D. W. J., and S. Solomon, 2002: Interpretation of recent Southern Hemisphere climate change. *Science*, **296,** 895-899.

Wolter, K., and M. S. Timlin, 1998: Measuring the strength of ENSO events - how does 1997/98 rank? *Weather*, **53,** 9.

5.3 CHAPTER SUMMARY

When applying the EOF technique on unfiltered Chl, we observed that the seasonal cycle explained 88% of the October 1997 to December 2007 Southern Hemisphere Chl monthly variability, whilst the interannual variability was firstly connected to ENSO dynamics, corroborating the global observations of chapter 3. Further, by excluding the Tropical region of the initial study area from the analysis, i.e. cropping from 20ºS to 90ºS, we observe that the leading mode is unrelated to ENSO. However, if the Northern Tropical region is included in the analysis, i.e. the study area augmented from 20ºN to 90ºS, the amount of Chl variability related with ENSO dynamics increases significantly. As suggested in the results from chapter 4, this indicates that ENSO mostly influences phytoplankton interannual variability within tropical latitudes.

CHAPTER 6

Seasonal patterns of chlorophyll-*a* in the Tropical and South Pacific

6.1 CHAPTER OVERVIEW

This chapter addresses the Chl seasonal variability characterization throughout the Tropical and South Pacific. As indicated by previous sections of this thesis, ENSO was the main driver of phytoplankton inter-annual variability in the past decade. In addition, ENSO influence is mostly localized to the Tropical Pacific.

Here, we evaluate the major unfiltered seasonal cycle of Chl, and relate it to atmosphere and ocean physical and chemical characteristics in the ENSO region. This chapter provides an insight to the major mechanisms and forcing variables related to the phytoplankton seasonal cycle, which explain most of its variability, within the ENSO region. This paper covers the third objective of the thesis.

The main text of this section is a fully drafted paper entitled 'The seasonal harmony between the atmosphere-ocean dynamics and satellite derived chlorophyll–*a* in the Tropical and South Pacific', intended for submission to the Journal *Geophysical Research Letters*, co-authored by A. B. Couto, A. M. Maharaj and N. J. Holbrook.

Candidate's contribution to this paper

In this paper, I obtained the datasets, scripts, performed all the data analysis, produced the figures and wrote the paper draft, which was evaluated by both co-authors. However, the precursor idea for the analysis rose during a group discussion by myself, Dr. McCreary, Dr. Sutton and Dr. Holbrook. The idea was pursued and

developed by myself, and input from Dr. Holbrook was attained regularly during this process.

The seasonal relationship between the atmosphere-ocean dynamics and satellite derived chlorophyll-*a* in the Tropical and South Pacific

André B. Couto

Department of Environment and Geography, Macquarie University, Sydney, New South Wales, Australia

Angela M. Maharaj

Department of Environment and Geography, Macquarie University, Sydney, New South Wales, Australia

Neil J. Holbrook

School of Geography, University of Tasmania, Hobart, Tasmania, Australia

For submission to *Geophysical Research Letters*

Abstract

Chlorophyll–*a* (Chl) is a photo-pigment present in all phytoplankton , which can be large-scale and therefore best observed with satellite instruments. Phytoplankton is directly dependent on nutrients and sunlight availability and thus can be inferred from Chl variability. The Tropical and South Pacific is divided into several bio-geographical regions where the availability of these restrictors/limiters changes with seasonal atmospheric and ocean forcing. This study assesses Chl seasonal pattern across the Tropical and South Pacific with atmospheric and oceanic regional characteristics. Our findings indicate that 40% of the studied area has a simultaneous

variation between Chl and sea surface temperature (SST). In the Tropical Pacific regional atmosphere-ocean mechanisms may act to condition phytoplankton growth, thus influencing surface Chl. Atmospheric convergence zones, specifically the ITCZ and SPCZ, are regions where seasonal dynamics have a profound impact on Chl. Using a linear regression model, Chl can be significantly ($p<0.01$) predicted for ~60% of the study area using SST, photosynthetically active radiation and sea surface height.

This study highlights the intra-annual development of surface chlorophyll-*a* abundance related to atmospheric-ocean dynamic system, and provides insights on oceanic chlorophyll forecast.

1. Introduction

Phytoplankton plays a key role in biological, biogeochemical and climate processes and therefore it is important to comprehend its interannual variability Phytoplankton provides nutrition for the upper trophic levels in the marine ecosystem, varying mostly in a inter-annual cycle [*Yoder and Kennelly*, 2003]. Additionally, through the process of photosynthesis, these microorganisms are an important component of the cycle of several chemical elements such as the oxygen and carbon.

Ocean color platforms enabled a comfortable near-global scale monitoring of phytoplankton. Since the launch of the Coastal Zone Color Scanner Experiment (CZCS) in the 1970s, near global-scale observations of chlorophyll-*a* (Chl) have been a reality. Despite being a relatively short and disrupted program (91 months), this first global ocean color observer hailed the beginning of a new era in understanding ocean biology. Followed by other remote sensors, such as the Sea-viewing Wide Field-of-view Sensor (SeaWiFS), and the European Medium Resolution Imaging Spectrometer

(MERIS), these sensors were designed to measure ocean color, i.e., measurement of the radiation of visible spectra from the seas, which enables the quantification of surface chlorophyll-*a* concentrations that are linked directly to phytoplankton abundance [*Carr et al.*, 2006; *O'Reilly et al.*, 2000].

As phytoplankton growth is limited by nutrient (N, P, Si, Fe) concentration and sunlight intensity, environmental oceanic and atmospheric processes have a crucial role on regulating phytoplankton delimiters, and its productivity. Across the Tropical and South Pacific Ocean, the regional physical and chemical characteristics divide the open ocean into several bio-geographic regions [*Longhurst et al.*, 1995]. Here, different atmospheric and/or oceanic patterns conduct the seasonal changes in the physical and chemical cycles, which are determinant for the regional phytoplankton cycle. Whilst the Tropical region has a complex wind driven current structure due to the Coriolis effect on different hemispheres of the planet, pushing and mixing nutrient-rich waters in the euphotic layer, thus, inducing complex phytoplankton seasonality patterns [*Dandonneau et al.*, 2004]. The more extensive South Pacific region has a large-scale counter-clockwise surface circulation, which accumulates poor nutrient waters onto the subtropical gyre, making this region oligotrophic, and thus, a biological ocean desert [*Dandonneau et al.*, 2004].

The importance of accurate diagnosis of phytoplankton over the seasonal cycle, is an essential step to providing better evaluation and potential forecasts and target a healthier and sustainable system at the intra- and inter-annual time-scales. The contribution of these microorganisms to the planetary system, e.g., on a biogeochemical cycle and climate dynamics level; or energy production [*Anemaet et al.*, 2010], and food supply level, has advanced considerably in the last two decades. Prediction methodologies are the ultimate tool towards the full comprehension of the

role of phytoplankton on the planetary system. However, the system's great complexity turn these ideal tools into scenarios with high levels of uncertainty [*deYoung et al.*, 2004].

In this paper, we connect regional atmosphere and ocean monthly climatologies of photosynthetically active radiation (PAR), sea level pressure (SLP), wind speed (WS), sea surface height (SSH), sea surface temperature (SST), nitrate concentration and outgoing long-wave radiation (OLR), to satellite-derived estimates of monthly-averaged Chl concentrations, in order to understand the seasonal coupling between atmosphere-ocean drivers, feedbacks and ocean productivity. We provide a conceptual framework for understanding the atmosphere and ocean dynamics that underpins the seasonal Chl concentrations across most of the Tropical and South Pacific. We demonstrate that the seasonality of the Inter-tropical Convergence Zone (ITCZ) and South Pacific Convergence Zone (SPCZ) are important for changes in Chl. Finally, using a linear regression model, we demonstrate that up to ~60% of the seasonal Chl concentration anomalies across the study domain can be estimated with high significance ($p < 0.01$), using SST, PAR and SSH information.

2. Data and Methods

The Chl data used in this study were derived from Sea-viewing Wide Field-of-view Sensor (SeaWiFS) and Moderate-resolution Imaging Spectroradiometer (MODIS)-Aqua remotely sensed observations of ocean color reprocessing R2009.1. Chl concentrations ($mg.m^{-3}$) are in the format of matrices spatially representing the global surface. The global time series maps have spatial dimensions of 1080 × 2160 pixels, corresponding to a surface resolution of 18.5 km^2 at the equator reducing in

area poleward. Each matrix corresponds to a monthly-averaged composite of daily Chl observations from October 1997 to December 2007 for the SeaWiFS data product, and from January 2008 to December 2009 for the MODIS-Aqua (n=147) data. From near-global data, the Pacific region of 20ºN - 60ºS, 140ºE - 70ºW was selected, comprising of the South Pacific and tropical Pacific extending to 20^{o}N. In order to speed up the numerical calculations while still retaining the important information relevant to large-scale ocean dynamics (but smoothing across eddy-scales), the data were investigated as averages on a ~1º latitude and longitude grid. A pixel mean was calculated for each calendar month for the 12 years, producing monthly-averaged regional climatology maps across the region.

The oceanic characteristics taken into account are remotely sensed sea surface temperature (SST) and height (SSH), and the *in situ* observed nitrate concentration at 10 m. SST data were sourced from the Advanced Very High-Resolution Radiometer (AVHRR) product provided by the NOAA Satellite and Information Service, but obtained from the same site as Chl data (see Acknowledgements section for details). Monthly-averaged SST (ºC) values are spatially resolved at 1024 × 2048 pixels across the global surface, i.e., 19.5 km^2 resolution at the equator. SSH data are from the Archiving, Validation and Interpretation of Satellite Oceanographic (AVISO) web service (http://www.aviso.oceanobs.com/). These data represent the global sea surface height (SSH) in reference to the ellipsoid at 1/3º × 1/3º resolution. SSH (cm) values result from the merging of Jason-1 and -2, and TOPEX/Poseidon altimeter observations [*Le Traon et al.*, 2003]. Nitrate concentrations (µmol.l^{-1}) were retrieved from the World Ocean Atlas 2009 [*Garcia et al.*, 2010]. Nitrate concentration data consist of interpolated mean values for each calendar month in each 1º longitude-latitude cell at standard depths calculated from *in situ* ship-based observations.

Atmospheric variables examined are wind speed (WS, $m.s^{-1}$), outgoing long-wave radiation (OLR, $W.m^{-2}$), sea level pressure (SLP, hPa) and photosynthetically active radiation (PAR). The WS data represent a cross-calibrated multi-platform product retrieved from the physical oceanography distributed active archive center (PODAAC) of the Jet Propulsion Laboratory, at the California Institute of Technology from NASA [*Atlas et al.*, 1996]. WS are composed of global monthly means on a 1/4º × 1/4º grid. The OLR and SLP data products are NOAA Earth System Research Laboratory monthly composites provided on a 2.5º × 2.5º grid derived from NOAA remote sensing instruments. PAR was obtained from the same website where Chl dataset was retrieved, and is time-space resolution and coverage are identical to the Chl data characteristics.

All fields were interpolated onto the same Chl data spatial grid (1º cells), and monthly climatology maps were calculated. Correlation coefficients and p-value statistics (using the t-statistic method, calculated with n-2 degrees of freedom) maps were calculated at each spatial grid point between Chl and each physical variable. Chl was also regressed onto the physical fields. Analyses were only performed where pixels with valid Chl data is available (Note that Chl data does not cover the entire region, as data is inexistent for regions with long periods of natural light absence, i.e., during the winter at high latitudes). Hence regions above ~45ºS may not present values in figures. However, the region bellow 45ºS is shown in maps as all physical variables have full coverage. Maps of these results are plotted on a Lambert projection.

3. Results

3.1. Correlation analysis

The Pacific Chl seasonal pattern varies harmonically with atmosphere and ocean fields across certain regions. Specifically, SST, WS and OLR were significantly correlated with each other (at ≥ 95% confidence level) over extensive regions of the study domain (Fig 1). Perhaps surprisingly, nitrate concentrations, an indicator of nutrient availability, are not correlated as strongly with Chl across the domain as the other variables, although we expect this to be at least partly due to the sparse coverage of *in situ* nitrate observations that have been provided on a regular grid.

Forty percent of the study area has a seasonal SST pattern that highly significantly (at the 99% level) co-varies with Chl (Figure 1a and 1b). In these regions, the correlation coefficients are either highly positive ($r > 0.9$) or highly negative ($r < -0.9$), with the majority of the region explained by the very strong and highly significant negative relationship between Chl and SST. In the higher latitudes of the region (>40ºS), in particular the southwest Pacific basin, a highly significant positive ($r > 0.8$) relationship between Chl and SST is observed. Conversely, highly significant correlations <-0.8 (at zero lag) between Chl and SST are observed across the zonal band from the mid-latitudes through the subtropics (40-45ºS to ~20ºS). Furthermore, stronger negative correlations ($r < -0.9$) are also observed from about 10º-15ºS and from 180º-140ºW. Across the central-eastern equatorial Pacific cold tongue (and upwelling zone), Chl is positively correlated with SST through the seasonal cycle. North of the equator, through the tropics, a significant negative correlation pattern is again observed through the seasonal cycle, as per much of the South Pacific. This extends from Mexico in the east to the eastern edge of the Western Pacific Warm Pool (WPWP) in the NW Pacific, where the correlation changes sign.

WS, on the other hand, is typically positively correlated with Chl over the seasonal cycle across much of the Pacific domain of interest (Figure 1c and d), i.e., stronger seasonal winds occur with a corresponding seasonal Chl maximum. Interestingly, the spatial pattern of the seasonal correlations between Chl and WS (Fig 1c) match well the pattern between Chl and SST (Fig 1a), albeit of opposite sign. Overall, there is strong coherence between the relationships of both WS and SST with Chl that is summarized by the significant negative relationship between WS and SST over much of the study area (Figure 1e).

Chl co-varies significantly ($p < 0.01$) with WS over 30% of the study area. We know that strong winds occur in regions of high horizontal SLP gradients. Correspondingly, Chl and SLP co-vary significantly across 22% of the study area. The north-south shift from positive to negative correlation essentially corresponds to the subtropical ridge of high atmospheric pressure around 30ºS. Chl and SLP co-vary harmonically throughout the subtropics and tropics, but are anti-correlated in the ITCZ from 0º-10ºN (Figure 2a) – we identify the ITCZ as being the region of lowest OLR (<240 Wm^{-2}) north of the equator. In the SPCZ region – which extends east-southeast from the WPWP in the tropical southwest Pacific - Chl is positively and highly significantly correlated ($p<0.01$) with SLP through the seasonal cycle (Figure 2b). In each case, we use OLR as the indicator of the position of the ITCZ and SPCZ, which also correlates reasonably well with SLP (see contours overlaying each figure). Seasonal variations in OLR and Chl are positively correlated in the ITCZ region ($p<0.01$), while the WPWP region is characterized by correlations of opposite sign (Figure 2c). In total, 29% of the area-wide Chl seasonal cycle varies highly significantly with the OLR (i.e., $p < 0.01$) (Figure 2d).

In an extension of our analysis , we find that a fascinating relationship exists

between Chl and SSH within the regions of these atmospheric convergence zones (Figure 3). In contrast to the broader Pacific study domain where Chl is significantly and negatively correlated with SSH through the seasonal cycle, Chl and SSH are positively correlated within the WPWP, ITCZ and SPCZ regions (Figure 3a). Specifically, in the regions of the North Equatorial Current (Figure 3c, adapted from Tomczak and Godfrey [2003]), WPWP, SPCZ, central Tropical and South Pacific (7ºS - 15ºS, 140ºW - 120ºW) all show significant positive relationships between Chl and SSH. In contrast, regions defined by ocean dynamic features including the East Australian Current, Peru Current, South Equatorial Current, and the North Equatorial Countercurrent, showed a significant negative seasonal correlations between SSH and Chl.

Other than phytoplankton abundance being indirectly influenced by atmosphere-ocean physical characteristics, nutrients and PAR, as a measure of sunlight availability, directly enable phytoplankton growth [*Behrenfeld and Falkowski*, 1997]. Despite this, we found that the seasonal variability of nitrate concentration only showed a highly significant relationship across 6% of the study area (at $p < 0.01$) where the correlation spatial pattern is very irregular at the surface and at 10 m depth (Figure 4a). This small area of significant relationship with Chl is possibly due to the poor spatial and temporal coverage of the nutrients observations. However, PAR, has a seasonal cycle that pairs positively and significantly with Chl at high latitudes, i.e., ~45ºS polewards, and negatively in the Coral Sea and subtropical gyre centre (Figure 4b). Overall, PAR showed highly significant seasonal variability to Chl over 27% of the study area.

3.2 Regression analysis

We now consider Chl as the predictand in a simple linear regression analysis, in an attempt to better understand the relationship between seasonal variations in atmosphere/ocean drivers and phytoplankton concentrations. We start by using a two-predictor model as follows:

$$\text{Chl}\,(x,y) = a\,(x,y) \times \textit{variable 1}\,(x,y) + b\,(x,y) \times \textit{variable 2}\,(x,y) + c\,(x,y) \qquad (1)$$

where x and y are east and north coordinates, a and b are the regression coefficients, and *variable 1* and *variable 2* are any two of the selected predictors (SST, SSH, WS, SLP, OLR, PAR, nitrate) and c is the offset. Each Chl value is analyzed on the same space-time (monthly-averaged) grid as the predictand, Chl. This relatively simple linear regression approach proves to be very successful in highlighting important relationships across specific regions.

In short, the best and most robust model estimates of Chl concentrations are found using any two-predictor model combinations of SST, PAR and/or SSH, but not nitrate concentration. Using nitrate in combination with any other variable to predict Chl gives the lowest correlations. In contrast, using SST in combination with either PAR or SSH gives the largest correlations. When examining residuals between the observed Chl and the model-regressed Chl, using SST and PAR in the two-predictor model, 55% of the study area had highly significant correlations between the model-estimated Chl seasonality and the observations ($p < 0.01$) shown as the region in blue in Figure 5a. This area comprises most of the South Pacific and to the north of the equator with a mean coefficient determination (r^2) of 0.83 (Figure 5b), demonstrating the very strong relationship that exists between the regression model fit and the observed Chl on seasonal time scales.

Regressing Chl onto two-predictor combinations of either SST and SSH or PAR

and SSH (figures not shown) explain 48% and 46% ($p<0.01$), respectively, of the seasonal Chl variance across the study area compared with observed Chl. Additionally, for both experiments, the area where $p<0.01$ is observed has a mean r^2 of 0.80. Using a two-predictor model of SST and WS to estimate Chl resulted in over 46% of the study area variance explained with a mean r^2 of 0.83.

For the two-atmosphere predictor regression models used to estimate Chl, and based on combinations of OLR, WS and/or SLP, yielded less significant results. However, these atmosphere variable combinations were again best served when combined with SST.

Finally, using a three-predictor regression model formulation, generated by simply adding the extra term, $c\,(x,y) \times variable\ 3\,(x,y,t)$ to Equation (1), we found that the best and most robust model estimates of Chl are provided using a combination of SST, PAR and SSH. For this three-predictor model, highly significant correlations are found between observed seasonal variations in Chl concentrations and model estimates ($p<0.01$) over 58% of the study area, with a mean $r^2 = 0.87$ over these significant regions.

4. Discussion

Phytoplankton seasonal concentration is balanced by productivity (conditioned by nutrient and sunlight supply) and loss processes (such as grazing and advection). Environmental regional mechanisms can regulate phytoplankton distribution by controlling the availability of nutrient and sunlight conditions, towards a favourable productivity rate.

Our findings argue that, for most of the South Pacific, phytoplankton and the environment co-evolve seasonally together at a high level of significance (Table 1).

However, the area within the domain where a significant parallel between the biological and environmental seasonal cycles is found, is reduced to 40% at the most (when comparing with SST) if stronger confidence is required (99%). This indicates that, even though phytoplankton is susceptible to seasonal environmental dynamics, direct indicators are restricted to specific regions. Further, such indicators can give us an insight to a mechanism that regulates local phytoplankton seasonal distribution.

We find that the best environmental variables that link to Chl seasonality are SST, r = 62.4%, and WS, r = 55.2%, (values at 90% confidence, Table 1). SST and WS are generally indicators of two seasonal mechanisms linked with surfacing nutrient rich waters, SST with upwelling and WS with vertical mixing. Additionally, the patterns of these two environmental indicators are naturally found to be inversely related (Figure 1e). Yet, we find that the southern region of the Coral Sea and the area east of this is an exception, as this region has an inverse wind seasonal cycle [*Holbrook and Bindoff*, 1999]. Thus, Chl seasonal cycle has a low significance of similarity with the WS cycle, but keeps following the SST cycle significantly in this specific region.

Furthermore, we found that patterns of high correlation between Chl seasonality and environmental variables occured to a greater extent at subtropical latitudes. However, at tropical latitudes patterns of good correlation are observed to be more complex. We know that the tropical Pacific is generally a nutrient depleted region with infusive local upwelling systems, such as the eastern tropical pacific upwelling system [*Pennington et al.*, 2006], and the equatorial upwelling [*Le Bouteiller et al.*, 2003]. Generally, regions of low nutrients peak in phytoplankton concentrations when winds are strong, and SST is cool. However, these infusive persistent upwelling systems have a dissimilar seasonal cycle [*Pennington et al.*, 2006] hence, inducing a

complex pattern of seasonal productivity in the region. This is manifested in the results as small areas where the seasonal cycles of Chl and environmental variables follow each other with great significance, but with a less significant relationship if considering the tropical Pacific region as a whole.

However, in the western side of the tropical Pacific, in the Western Pacific Warm Pool (WPWP), we find that Chl seasonal variability corresponds significantly with both, SST and WS seasonality patterns . This suggests that, even though these WPWP waters are of an oligotrophic nature and thus, the Chl seasonal cycle is of quite low amplitude (Figure 6), here the Chl seasonal pattern is likely to be driven by environmental large-scale dynamics, rather than nonlinear local mechanisms.

Nevertheless, in this same region, patterns of relationship between Chl seasonality and other environmental variables such as SLP or OLR show a completely different structure. In fact, the patterns yielded suggest a significant positive coupling with the seasonal migration of the ITCZ (on the northern and eastern flanks) throughout the tropical Pacific. This suggests that the high rain intensity and low solar intensity in the ITCZ is connected to the low concentrations of Chl. A connection between the ITCZ seasonal migration and Chl was previous reported in the Atlantic [*Grodsky et al.*, 2008].

In the southern region of the WPWP (Figure 2c, the blue region north of Papua New Guinea), we find a negative OLR-Chl and SLP-Chl seasonal relationship. This suggests that high deep convection and consequent heavy rain in the region are coupled with increases of Chl concentration, which might be due to the presence of the north and south equatorial currents. These equatorial currents are composed by mesotrophic high nutrient, low chlorophyll waters, which together with vertical

mixing from their meanders, induce Chl increase in the region [*Messié and Radenac*, 2006].

The cumulous cloud band in the SPCZ, extending from the WPWP south-eastward towards French Polynesia [*Vincent et al.*, 2009], has a similar seasonal relationship with Chl as the ITCZ across the Pacific. This suggests that large atmospheric convergence zones may play an important role on Chl patterns, despite of the zonal or meridional range.we know that these convergence zones are linked to heavy precipitation [*Kiladis et al.*, 1989], thus increasing SSH where these occur. We find that exactly in these regions, Chl and SSH seasonality match positively with a very high degree of confidence (Figure 3b). This indicates, unintuitively, that in CZ regions Chl increases with SSH , even north of Papua New Guinea where the OLR and SLP relationship with Chl is disrupted, thus reinforcing the idea that this disruption might be due to the uplifting of the nutricline by the intrusion of equatorial currents meanders, as suggested by Missié and Radenac [2006].

Additionally, we find that Chl-SSH seasonal patterns also match highly significantly but negatively, just to the east of where these CZ positive patterns are found (Figure 3). This means that Chl and SSH seasonality are inversely related, suggesting that SSH is inversed and that possibly there is westwardmovement of waterswhich could be enhanced by high evaporation rates near the CZ. Further, we know that during the austral winter, when primary productivity generally increases in the oligotrophic regions, the North and South Equatorial Currents flow more strongly towards the WPWP, hence increasing the WPWP SSH at this time [*Qu et al.*, 2008].

Our results and these previously discussed findings are pertinent a better understanding of how phytoplankton relates to its environment, and possibly to

empirically map biogeographic boundaries of the ocean. In addition to this, it can be used to develop the seasonal predictability in specific regions, using environmental descriptors, as generally environmental variables are easier to observe and record than biological variables which are mostly achieved at poor spatial and temporal resolution via costly sea cruises.

Our findings show that seasonal Chl can be better estimated when using SST. Additionally, using a simple linear regression model where different fields can be combined to make Chl predictions, the area of significant predictability (with 99% confidence interval) in the Tropical and South Pacific can be increased from 40% (using only SST) to 56% (by combining SST and PAR observations), and at most 58% (by adding SSH to the latter) with the used variables. This means that, using only three parameters, seasonal Chl distribution can be predicted in most of the domain with a very high degree of confidence.

Of course a greater challenge would be to predict primary productivity, as many authors have unsuccessfully tried [*Carr et al.*, 2006]. Since productivity is the rate of photosynthetic activity it is also an indicator of available organic energy for upper trophic levels throughout the ocean, and, of carbon and oxygen cycling. However, productivity can only be measured *in situ* at this technological stage. And, as the usage in this study of the nutrient variables has indicated, this data lacks in spatial and temporal resolution. As such, satellite Chl measusrements are indispensable, since it is the only oceanic biological variable currently measured in large scale with regular time resolution allowing us to have an insight of oceanic production at a large scale.

5. Acknowledgements

Chl, SST and PAR data were obtained from the Ocean Productivity website at the Oregon State University (http://www.science.oregonstate.edu/ocean.productivity /). We would like to thank to Mauro Vargas, Peter Strutton and Jay McCreary for helpful discussions and suggestions at various stages of this work.

6. References

Anemaet, I. G., M. Bekker, and K. J. Hellingwerf (2010), Algal Photosynthesis as the Primary Driver for a Sustainable Development in Energy, Feed, and Food Production, *Marine Biotechnology*, *12*(6), 619-629.

Atlas, R., R. N. Hoffman, S. C. Bloom, J. C. Jusem, and J. Ardizzone (1996), A multiyear global surface wind velocity data set using SSM/I wind observations, *Bull. Amer. Meteor. Soc.*, *77*, 869–882.

Behrenfeld, M. J., and P. G. Falkowski (1997), A consumer's guide to phytoplankton primary productivity models, *Limnology and Oceanography*, *42*(7), 1479-1491.

Carr, M. E., et al. (2006), A comparison of global estimates of marine primary production from ocean color, *Deep-Sea Research Part II: Topical Studies in Oceanography*, *53*(5-7), 741-770.

Dandonneau, Y., P.-Y. Deschamps, J.-M. Nicolas, H. Loisel, J. Blanchot, Y. Montel, F. Thieuleux, and G. BÈcu (2004), Seasonal and interannual variability of ocean color and composition of phytoplankton communities in the North Atlantic, equatorial Pacific and South Pacific, *Deep Sea Research Part II: Topical Studies in Oceanography*, *51*(1-3), 303-318.

deYoung, B., M. Heath, F. Werner, F. Chai, B. Megrey, and P. Monfray (2004), Challenges of Modeling Ocean Basin Ecosystems, *Science*, *304*(5676), 1463-1466.

Garcia, H. E., R. A. Locarnini, T. P. Boyer, J. I. Antonov, M. M. Zweng, O. K. Baranova, and D. R. Johnson (2010), World Ocean Atlas 2009. Vol. 4, Nutrients (phosphate, nitrate, silicate)*Rep.*, 398 pp, National Oceanic and Atmospheric Administration, Washington, D.C.

Grodsky, S. A., J. A. Carton, and C. R. McClain (2008), Variability of upwelling and chlorophyll in the equatorial Atlantic, *Geophysical Research Letters*, *35*(3).

Holbrook, N. J., and N. L. Bindoff (1999), Seasonal temperature variability in the upper southwest Pacific Ocean, *Journal of Physical Oceanography*, *29*(3), 366-381.

Kiladis, G. N., H. von Storch, and H. Loon (1989), Origin of the South Pacific Convergence Zone, *Journal of Climate*, *2*(10), 1185-1195.

Le Bouteiller, A., A. Leynaert, M. R. Landry, R. Le Borgne, J. Neveux, M. Rodier, J. Blanchot, and S. L. Brown (2003), Primary production, new production, and growth rate in the equatorial Pacific: Changes from mesotrophic to oligotrophic regime, *Journal of Geophysical Research C: Oceans*, *108*(12), EBE 6-1 - EBE 6-16.

Le Traon, P. Y., Y. Faugère, F. Hernandez, J. Dorandeu, F. Mertz, and M. Ablain (2003), Can we merge GEOSAT follow-on with TOPEX/Poseidon and ERS-2 for an improved description of the ocean circulation?, *Journal of Atmospheric and Oceanic Technology*, *20*(6), 889-895.

Longhurst, A., S. Sathyendranath, T. Platt, and C. Caverhill (1995), An estimate of global primary production in the ocean from satellite radiometer data, *Journal of Plankton Research*, *17*(6), 1245-1271.

Messié, M., and M.-H. Radenac (2006), Seasonal variability of the surface chlorophyll in the western tropical Pacific from SeaWiFS data, *Deep Sea Research Part I: Oceanographic Research Papers*, *53*(10), 1581-1600.

O'Reilly, J. E., et al. (2000), Ocean color chlorophyll a algorithms for SeaWiFS, OC2, and OC4: Version 4. In: SeaWiFS Postlaunch Technical Report Series, in *SeaWiFS Postlaunch Calibration and Validation Analyses, Part 3*, edited by S. B. Hooker and E. R. Firestone, pp. 9-23, NASA, Goddard Space Flight Center, Greenbelt Maryland.

Pennington, J. T., K. L. Mahoney, V. S. Kuwahara, D. D. Kolber, R. Calienes, and F. P. Chavez (2006), Primary production in the eastern tropical Pacific: A review, *Progress in Oceanography*, *69*(2-4), 285-317.

Qu, T., J. Gan, A. Ishida, Y. Kashino, and T. Tozuka (2008), Semiannual variation in the western tropical Pacific Ocean, *Geophys. Res. Lett.*, *35*(16), L16602.

Tomczak, M., and J. S. Godfrey (2003), *Regional oceanography: an introduction*, 2nd ed., xi+390p pp.

Vincent, E., M. Lengaigne, C. Menkes, N. Jourdain, P. Marchesiello, and G. Madec (2009), Interannual variability of the South Pacific Convergence Zone and implications for tropical cyclone genesis, *Climate Dynamics*, *36*(9), 1881-1896.

Yoder, J. A., and M. A. Kennelly (2003), Seasonal and ENSO variability in global ocean phytoplankton chlorophyll derived from 4 years of SeaWiFS measurements, *Global Biogeochemical Cycles*, *17*(4), 23-21.

7. Figures

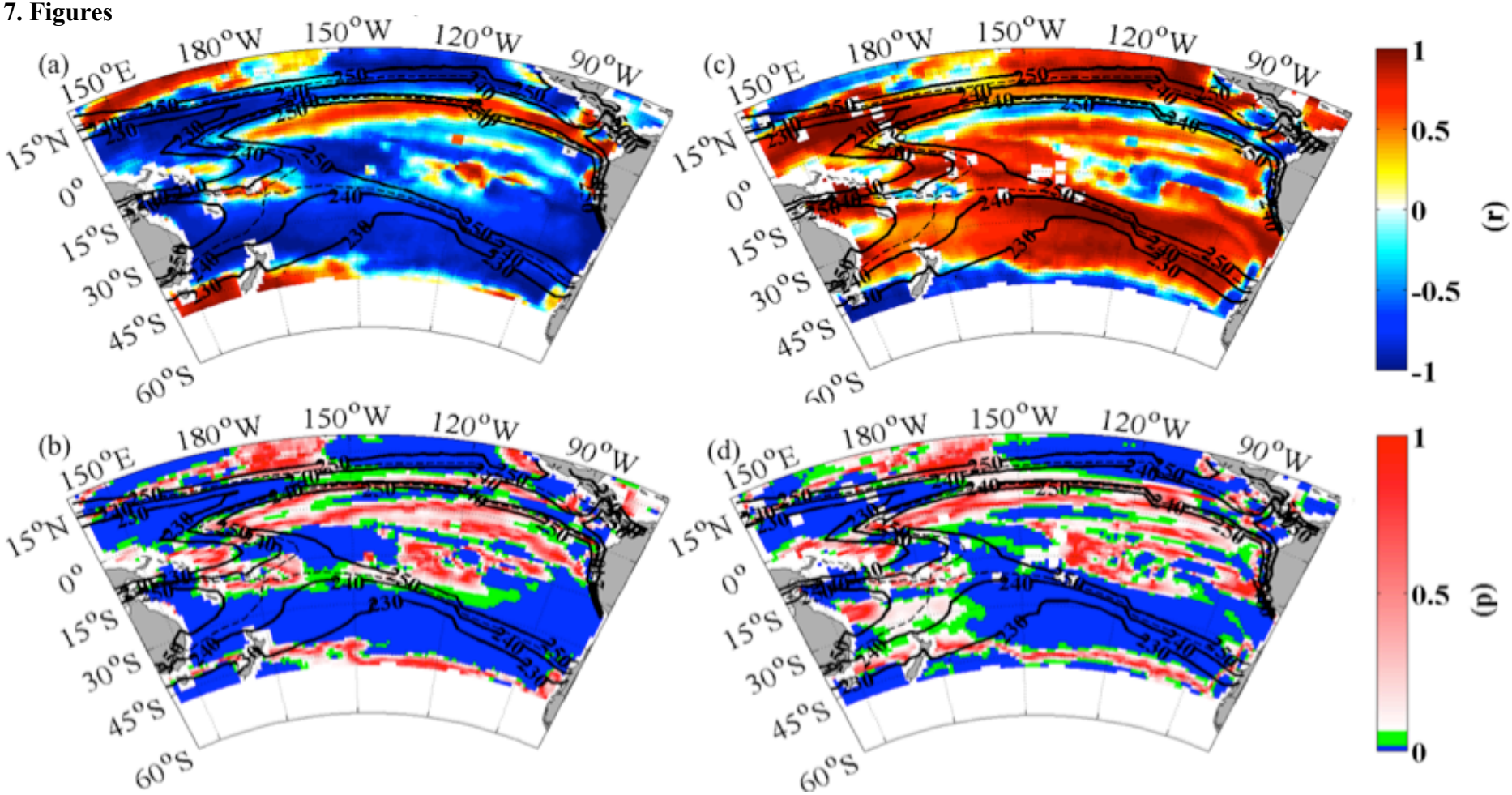

Figure 1. Spatial pattern of the correlation coefficient, r (a), and the significance value, p (b) between Chl and SST seasonal cycles. And, the spatial pattern of r (c) and p (d) from Chl and WS, and, SST and WS (e). The blue color in the color scale of p corresponds to 99% confidence, and green to 95%. Solid contours are OLR annual average, expressed in $W.m^{-2}$, and dashed contours the 245 $W.m^{-2}$.

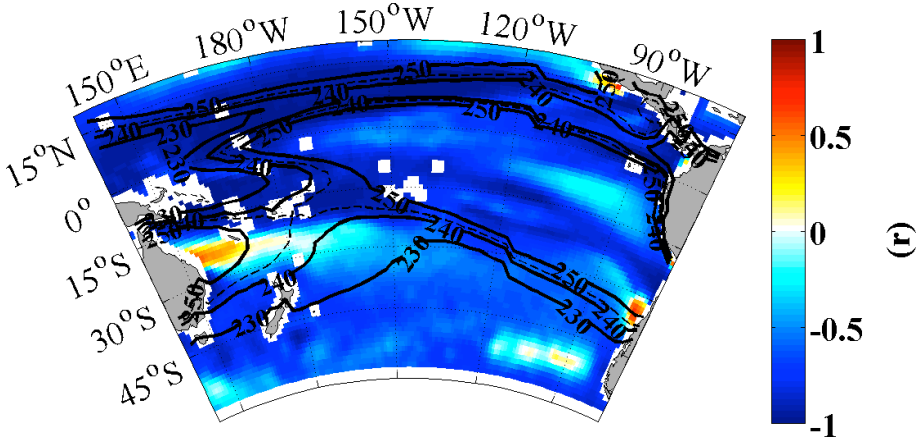

Figure 1. Continuation.

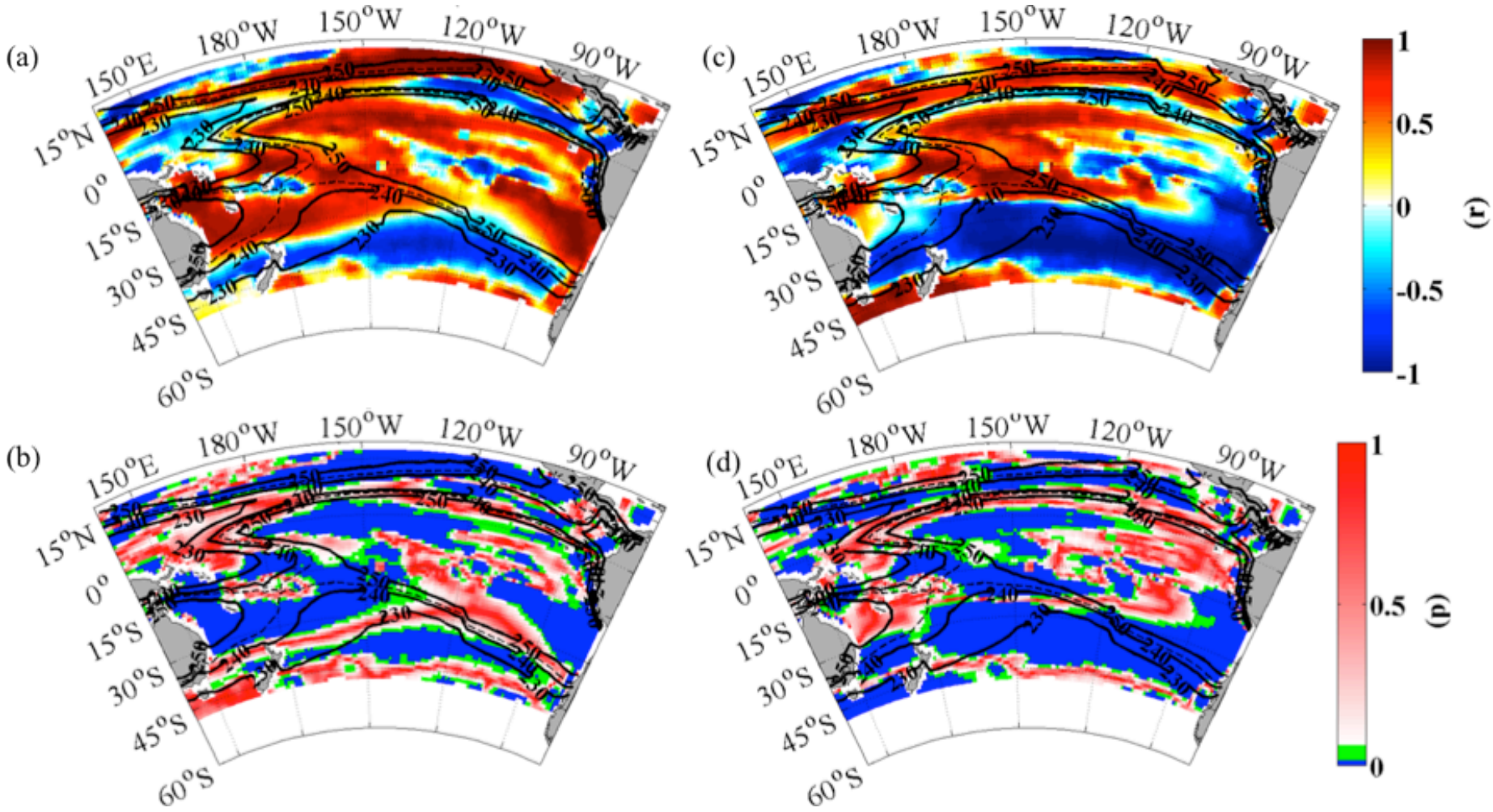

Figure 2. Spatial pattern of the correlation coefficient, r (a), and the significance value, p (b) between Chl and SLP seasonal cycles. And, the spatial pattern of r (c) and p (d) from Chl and OLR (c). The blue color in the p-value color scale corresponds to 99% confidence, and green to 95%. Solid contours are OLR annual average, expressed in $W.m^{-2}$, and dashed contours the 245 $W.m^{-2}$.

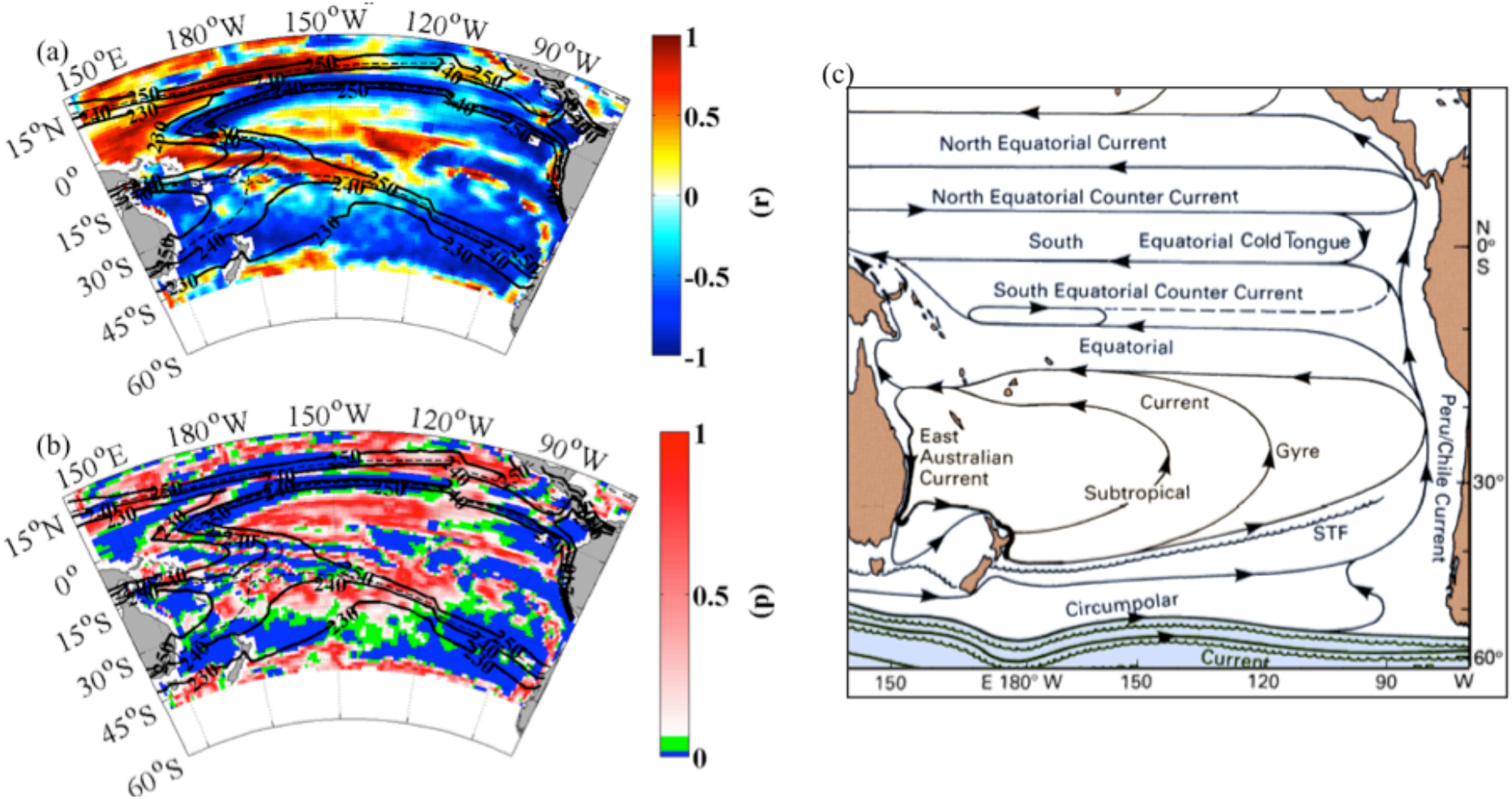

Figure 3. Spatial pattern of the correlation coefficient, r (a), and the significance value, p (b) between Chl and SSH seasonal cycles. The blue color in the p-value color scale corresponds to 99% confidence, and green to 95%. Solid contours are OLR annual average, expressed in $W.m^{-2}$, and dashed contours the 245 $W.m^{-2}$. (c) Surface currents of the South Pacific (adapted from Tomczak and Godfrey [2003]).

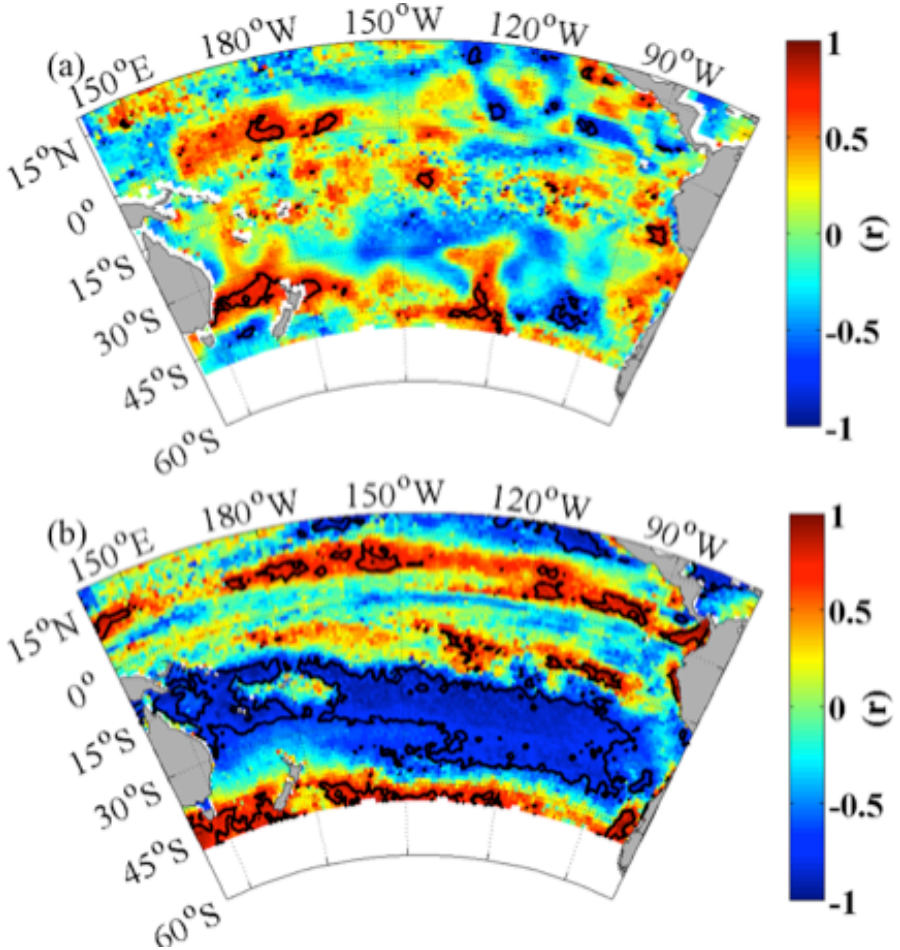

Figure 4. Spatial pattern of the correlation coefficient, r between Chl and nitrate at 10 m depth (a), and, between Chl and PAR (b) seasonal cycles (Contour lines show where p = 0.01).

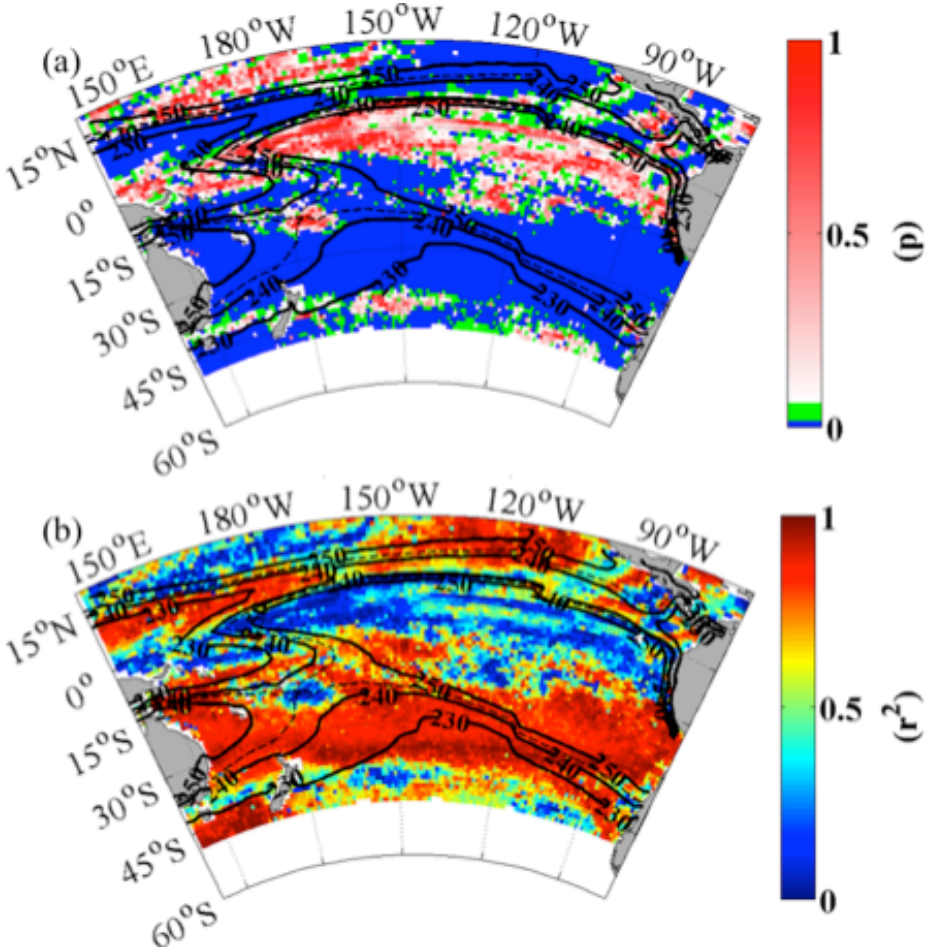

Figure 5. Spatial pattern of the significance value, p (a), and coefficient of determination, r^2 (b), when comparing the observed Chl seasonal distribution with the Chl seasonality calculated using SST and PAR seasonal

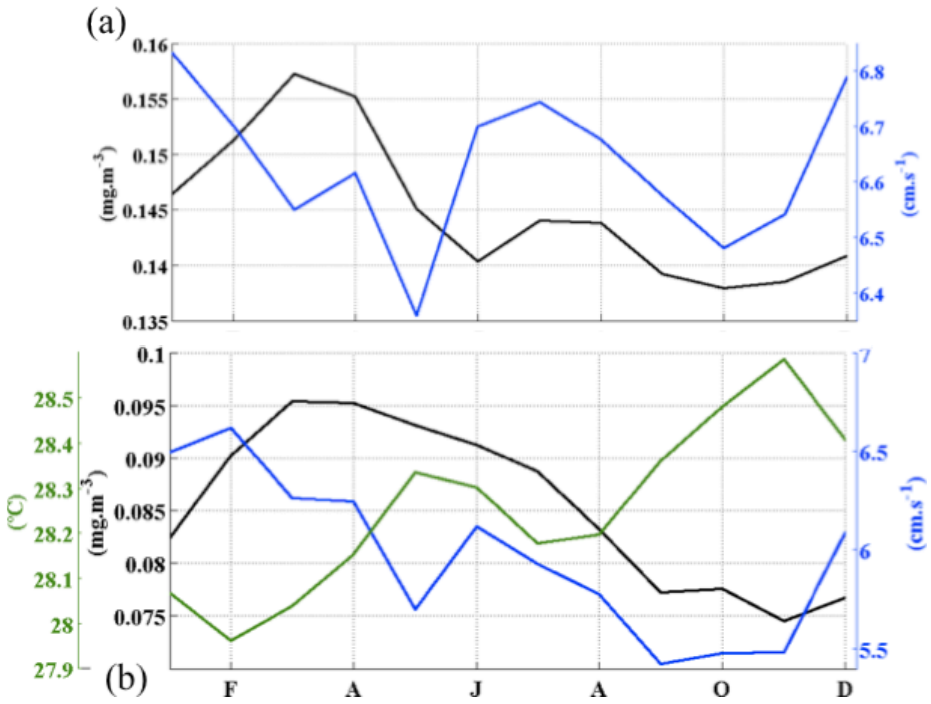

Figure 6. Seasonal time series profile of Chl and WS at the Tropical Pacific (a), from 20ºN to 23.5ºS. And time series of Chl, WS and SST at the WPWP (b), 15ºN to 15ºS and 150º to !80º Longitude.

Table 1. Are of the domain where Chl and environmental field seasonal cycles match at different levels of confidence.

Significance level (p)	SST	WS	OLR	PAR	SLP	SSH	nitrates (10 m)
99%	40.4%	30.2%	29.2%	27.6%	21.7%	20.6%	6.4%
95%	54.6%	45.9%	43.9%	45.3%	37.4%	35.9%	16.2%
90%	62.4%	55.2%	51.8%	53.3%	45.8%	45.3%	24.7%

6.3 CHAPTER SUMMARY

In this chapter, we demonstrate that atmospheric and ocean seasonal characteristics across the Tropical Pacific develop differently from those observed in the South Pacific. In the Tropical Pacific, the small variations of Chl during the intra-annual cycle are easily enhanced or reduced by atmosphere and/or ocean forcing mechanisms, such as the presence of an atmospheric convergence zone, the wind driven up/downwelling in the eastern Equatorial region, or the equatorial counter currents seasonal intensity. Throughout the South Pacific, the Chl seasonal cycle develops in synchrony with SST and WS. Nevertheless, SST is a good proxy for surface Chl seasonal cycle for only 40% of the Tropical and South Pacific surface area. However, by combining PAR, SSH and SST, almost 60% of this region can be significantly predicted.

CHAPTER 7

Inter-annual patterns of chlorophyll-*a* in the Tropical and South Pacific

7.1 CHAPTER OVERVIEW

In the previous chapters, the main climatic drivers for inter-annual phytoplankton global variability were identified. These are, firstly, the 'classic' ENSO mode, followed by the EM mode (regardless of its connection to ENSO). Here, we address the fourth objective of this thesis. We utilise the EEOF tool to evaluate Chl propagation variability across the Tropical and South Pacific specific to these two mechanisms main cycle.

The main text of this section is a fully drafted paper entitled 'Can we detect ENSO influences on South Pacific chlorophyll-*a*', intended for submission to the *Journal of Geophysical Research*, co-authored by A. B. Couto, A. M. Maharaj and N. J. Holbrook.

Candidate's contribution to this paper

In this paper I obtained the datasets, script and performed all data analysis, produced the figures and wrote the manuscript, which was evaluated by both co-authors. Input from Dr. Holbrook was attained regularly during this process.

Can we detect ENSO influences on South Pacific chlorophyll-*a*?

André B. Couto

Department of Environment and Geography, Macquarie University, Sydney, New South Wales, Australia

Angela M. Maharaj

Department of Environment and Geography, Macquarie University, Sydney, New South Wales, Australia

Neil J. Holbrook

School of Geography, University of Tasmania, Hobart, Tasmania, Australia

For submission to *Journal of Geophysical Research – Oceans*

Abstract

El Niño – Southern Oscillation (ENSO) is regarded as the main driver of phytoplankton inter-annual variability. Since the advent of remote sensing acquisition of surface chlorophyll-*a* (Chl), a molecule present in all phytoplankton organisms, it has been possible to observe and examine phytoplankton variability at a resolution and scale which allows for the investigation of the impact of climate signals such as ENSO. We use more than 13 years of Chl remote sensing observations across the Tropical and South Pacific to isolate and research the spatial development of Chl during ENSO: its canonical variability mode, and, arguably, its non-linear evolution El Niño – Modoki (EM) mode using the extended empirical orthogonal function

technique. Here we describe how an canonical ENSO phase transition affects Chl, and identify the Chl inter-annual El Niño – Modoki (EM) mode of variability induced spatial pattern. Further, we argue that EM is more influential on Chl inter-annual variability than the canonical ENSO during the period considered, and finally, that EM mode might be the mechanism responsible for the reported decadal Chl spatial trend, connecting it to the non-natural anthropogenic forced climate change.

1. Introduction

Canonical El Niño – Southern Oscillation (ENSO) and El-Niño Modoki (EM) climate modes of variability share the same spatial region, but are considered to have a distinct physical evolution and proprieties [*Li et al.*, 2010]. Independency of EM from ENSO phenomenon has been commonly accepted in literature in the last few years [*Ashok et al.*, 2007], more recently EM was described to be the non-linear evolution of ENSO [*Takahashi et al.*, 2011], thus, that both leading modes of global climate variability represent the same climatic mechanism. Nevertheless, each mode represents a unique relationship of interaction dynamics between the atmosphere and the ocean, albeit, with similar but subtly different environmental characteristics.

The classical (cold-tongue) ENSO has been considered and recognized very broadly as a large-scale phenomenon for just over 40 years now, since the seminal work by Bjerknes [1969]. The classical ENSO mode is commonly described in terms of a basin-wide coupling of the ocean and atmosphere across the tropical Pacific that manifests itself as a quasi-periodic variability of the climate system on a time scale of 2-7 years. In the neutral 'phase' of ENSO (i.e., neither El Nino nor La Nina conditions), the climatic conditions are characterized by high sea level pressure (SLP) over the central-eastern subtropical Pacific, with strong trade winds pushing the

surface waters westward into the Western Pacific Warm Pool (WPWP). This statistically averaged state of the tropical Pacific climate provides deeper cooler waters to upwell along the eastern and equatorial boundaries creating a cold tongue that extends from the East to Central Tropical Pacific. The effect of this cold tongue is to enrich the phytoplankton response around the equator, since the upwelling brings nutrient rich waters into the euphotic zone where it is needed by these organisms. The For the composite El Niño phase of ENSO, SLP in the central-eastern subtropical Pacific tends to be reduced, the trade winds are weaker, and the central-eastern equatorial Pacific is anomalously warm and nutrient-depleted due to the reduction in upwelling. El Niño events tend to concomitantly show an anomalous decrease of phytoplankton in the Tropical Pacific [*Behrenfeld et al.*, 2001], except in the WPWP region, where the deep nutrient rich waters have a greater chance to surface with the help of local mechanisms such as the island mass effect [*Messié and Radenac*, 2006]. Conversely the La Niña phase of ENSO, which is associated with an enhancement of the trade wind flow beyond the neutral phase, leads to an anomalous increase of phytoplankton in the central-eastern equatorial Pacific.

As suggested by its name, El Nino 'Modoki' (modoki being the Japanese word for 'similar') has some obvious similarities with classical ENSO, in particular regarding the zone of sea surface temperature anomaly (SSTA) variability across the Tropical Pacific [*Ashok et al.*, 2007]. However, it has been noted that EM displays also a strong decadal periodicity [*Ashok et al.*, 2007; *Di Lorenzo et al.*, 2010]. Like classical ENSO, the El Niño phase of EM is also characterized by an anomalous warming of SSTs in the central equatorial Pacific. However, notably unlike its 'brother', the El Nino phase of EM is flanked by anomalously cool SST along the equator to the west and east. It is thought that EM El-Niño events are excited by

anomalous westerly winds in the western Pacific, which push the surface warm water layer from the off-equatorial western Pacific towards the equator, driving downwelling equatorial Kelvin waves, which induces a deepening of the thermocline from the central to the eastern Pacific [*Ashok et al.*, 2007]. This is followed by easterly anomalies in the eastern Pacific creating water convergence into the central Pacific, further deepening the Central Pacific thermocline. Thus the SST warming in the Central Pacific is further strengthened by downwelling equatorial Kelvin waves from the west, and Rossby waves from the east [*Ashok et al.*, 2007]. The influence of EM on phytoplankton distribution and variability is, to our knowledge, absent from the current literature.

Traditional *in situ* measurements of phytoplankton in the remote ocean are too sparse in space and time to effectively investigate the influence of large-scale climatic phenomena. In contrast, satellite derived observations, which have large-scale coverage in space and repeat information in time, have proven to be very useful for the assessment of the role of large-scale atmosphere-ocean interactions on phytoplankton distribution. By comparison, these measurements provide an excellent frequency-sampling rate (~ 1 day) and near-global coverage to enable such research. Ocean Color remote sensors, such as the Coastal Zone Color Scanner (CZCS), Sea-viewing Wide Field-of-view Sensor (SeaWiFS) and Moderate Resolution Imaging Spectroradiometer (MODIS), have been used to record water leaving-radiance at specific wave-lengths in the visible domain of the spectrum, that enable reliable estimates of surface chlorophyll-*a* (Chl) concentrations [*O'Reilly et al.*, 2000]. The Chl molecule is a photosynthetic pigment present in all phytoplankton, and is often used to indicate phytoplankton abundance [*Carr et al.*, 2006]. Phytoplankton abundance is mostly explained by the seasonal cycle, where the availability of

nutrients and solar radiation play essential roles. Inter-annual atmosphere-ocean dynamics instead induce conditions that vary the seasonal phytoplankton variability patterns significantly [*Chavez et al.*, 2011].

In this paper, we aim to describe and interpret the Tropical and South Pacific Chl patterns in the context of the dominant inter-annual mode(s) of Pacific (and global) climate variability – classical ENSO and, debatably, El Nino Modoki (EM). Based on our results, we demonstrate that Chl signal is more connected with the EM structure than with the classical ENSO mode. Further, we describe how an ENSO transition affects Chl; and, identify how EM has an effect on decadal Chl concentrations.

2. Data

The primary data investigated in this study are satellite derived Chl observations. These data were retrieved from the Oregon State University Ocean Productivity website, and is combination of r2009.1 SeaWiFS and MODIS-Aqua satellites Chl products. The dataset comprises of monthly-averaged matrices of 1080 by 2160 pixels, representing the equatorial transect by 1/6º of a degree per pixel, reducing polewards. The Chl observations were derived from SeaWiFS in the period October 1997 - December 2007 and MODIS-Aqua from January 2008 - October 2010.

The phases of ENSO are characterized by several time series (or indices). For the present study, we selected the multivariate ENSO index (MEI) since it is the most comprehensive index for basin-scale climate investigations, taking into account six observed atmosphere and ocean physical variables across the tropical Pacific. These are: sea level pressure, zonal and meridional surface wind components, sea surface

temperature, surface air temperature and total cloudiness fraction of the sky [*Wolter and Timlin*, 1993]. The MEI was obtained from the U.S. National Oceanic and Atmospheric Administration.

EM has only been described as a distinct climatic phenomenon relatively recently [*Ashok et al.*, 2007]. Consequently, there have been fewer simple metrics developed to this point to diagnose and/or monitor EM changes. Here we have used the improved EM index (IEMI), developed by Li et al. [2010] which we calculated using remotely-sensed sea surface temperature (SST) measurements. SST measurements are derived from two different sensors covering different times ranges. For the period covered by SeaWiFS measurements of Chl (October 1997 to December 2007), SST was measured by the Advanced Very High-Resolution Radiometer (AVHRR). For the period covered by MODIS derived observations (January 2008 to October 2010), both Chl and SST were measured simultaneously from the same satellite platform. AVHRR SST data comprise of monthly-averaged 1024 x 2048 pixel global ocean maps interpolated to the same scales as the Chl and MODIS SST.

3. Methods

For the purposes of this study, we selected a tropical and South Pacific basin-wide area that extends meridionally from 20ºN-60ºS and zonally from 140ºE-70ºW. To simplify the analysis, we coarsened the Chl data to the 1º grid-scale. Chl anomalies (ChlA) were calculated by removing the log-normal monthly average of the log-normal distribution of each pixel. All data were linearly de-trended in time. The power spectra for both climate indices (IEMI and MEI) were calculated for the same period as the Chl dataset using Fourier techniques [*Frigo and Johnson*, 1998]. This yielded peaks with maximum power, above the mean red noise spectrum and

95% confidence levels [*Torrence and Compo*, 1998], that correspond to 28- and 128-month periodicities, for the MEI and IEMI respectively (Figure 1). These two power spectra maxima were thus taken as the lag (L) periods for the extended empirical orthogonal function (EEOF) analysis.

The empirical orthogonal function (EOF) is a commonly used technique in geophysical research since it can often summarise large datasets in space and time into only a few distinct modes that may be linked to important mechanisms [*Bjornsson and Venegas*, 1997]. However, one of the limitations of EOF analysis is that it is unable to account for leads and lags in the propagating patterns, which might in some cases be identified as two (or more) modes in quadrature when in fact they are simply part of a single dynamically propagating process. By virtue of its name the extended EOF (EEOF) provides an extension to the regular EOF by taking account of lag sequences in the time series, and hence propagation within individual modes. This is enabled through the pre-cropping the data into several subsets of predefined time lengths, lags (L; also known as 'lag-sequence lengths'), and concatenating these before performing the EOF analysis. For a comprehensive explanation of the EEOF technique, the reader is referred to *Venegas* [2001]. Example applications of the technique are provided by *White and Peterson* [1996] and *Holbrook et al*. [2005a; 2005b]. In practice the technique is often applied using predefined time increments that are longer than the actual data intervals, since the analysis can be otherwise very computationally expensive. Here, however, we use the monthly grid-scale directly from the data as our time increment for the analysis. We applied the EEOF analysis for two predefined lag-sequence lengths. These are L=28 months, based directly on the maximum analysed power in the Multivariate ENSO index (MEI) that we assume to characterise the more classical ENSO, and L=128 months corresponding to the

maximum power in the El Nino Modoki index (IEMI). The EEOF time series and the climate indices were then tested for any statistical relationships. Significance of the correlations take account of the effective number of degrees of freedom according to [*Davis*, 1976] accounting for autocorrelation in the time series.

Additionally, the EEOF time series were projected onto the SST, thus identifying SST patterns that may relate directly with the ChlA EEOFs. This allowed us to obtain the SST patterns that relate to Chl propagating patterns.

4. Results

4.1. EEOF L = 28

When using L = 28 months in the EEOF analysis, the first 10 modes explain about 30% of the total ChlA variance, with both leading modes (mode 1= 7% and mode 2= 5%) being independent of each other according to the North et al. [1982] test (Figure 2). The EEOF1 time series is highly significantly correlated (at the 98% confidence level) with the El Nino Modoki index (IEMI), and remains insignificantly correlated with our more classical ENSO index (the MEI) at even the 80% confidence level. In contrast, EEOF2 is highly significantly correlated (at the 99.5% level) with the MEI over the first 130 months, and significantly correlated with the MEI at the 80% (84%) confidence level over the entire time record. Nevertheless these two curves seem to be slightly out of phase (Figure 3).

The L28 EEOF2 ChlA spatial pattern sequence is shown in Fig. 4. ChlA is strongly negative (< -0.2 $mg.m^{-3}$) in the central and eastern Tropical Pacific in the first month of the cycle and positive (~0.1 $mg.m^{-3}$) in the western Pacific warm pool (WPWP) region and across the South Pacific. From month 1 to 10, a positive anomaly develops along the equator, whilst the negative anomalies (< -0.1 $mg.m^{-3}$) persist

away from the equator. From months 10 to 16, a strong negative ChlA (< 0.15 mgm^{-3}) develops in the western-central equatorial Pacific (~170ºE), whilst the negative ChlA along the southern tropical region still persists until the last month. From months 16 to 28, the positive ChlA pattern in the western-central Equatorial Pacific strengthens further (> 0.2 $mg.m^{-3}$) and slowly propagates westward in the last six months of the lag sequence.

Projecting EEOF2 onto SSTA yields a similar spatial pattern to the ChlA, albeit that the sign is negative (Figure 5). The sequence commences with a negative SSTA < -7ºC in the central-eastern Equatorial Pacific (from ~15ºN to ~15ºS), while positive SSTAs exist in the subtropical gyre centre, WPWP and Tasman Sea regions. At the equator, the cooler waters warm from the west, until reaching the eastern Tropical Pacific. Then, a positive anomaly pattern starts to develop in the central equatorial Pacific from month 8 until the end of the 28-month sequence, with maximum SSTAs found in the 22 - 25month period. In the eastern Tropical Pacific, negative SSTAs are observed at the end of the 28-month sequence, while in the southwest corner of the South Pacific, anomalous positive SSTAs are seen to propagate eastward.

4.2. EEOF L = 128

The 10 leading L = 128-month EEOFs yielded twice the explained inter-annual ChlA variance (~60%) compared with the leading 10 L= 28-month EEOFs (~30% variance) (Figure 6). EEOF1 explains 13% of the total inter-annual ChlA variance at L = 128 months, and is highly significantly correlated with the El Nino Modoki index (IEMI, $r = 0.84$, $p << 0.01$). We note, however, that the leading modes are degenerate according to the North et al. test [*North et al.*, 1982]. Further, the EEOF1 time series is very smooth compared with the IEMI (Figure 7). This is due to the fact that the

EEOF time series represents the 128-month cycle evolution in the few monthly steps (30) that comprise this period within the Chl dataset (n = 157).

The L128 EEOF1 ChlA spatial pattern sequence (Figure 8) is characterized by high variability within the Tropical Pacific region, and is strongest in the western and southern parts. In month 1, the eastern Tropical Pacific displays a negative ChlA (< -1.5 $mg.m^{-3}$). In the western region, at the same latitude, the ChlA is positive (~+1.5 $mg.m^{-3}$) whereas across most of the South Pacific, ChlA alternates from positive to negative - however, the anomalies are not as large as in the Tropics. Following month 1, the eastern Tropical Pacific negative anomaly disappears in the first couple of months, and the western Tropical Pacific positive ChlA extends eastward. At the same time that the eastward positive ChlA reaches the eastern side of the basin (by month 6), a positive ChlA also develops along east Tropical Pacific. From month 12 onwards, positive ChlAs (~+0.07 $mg.m^{-3}$) develop off the equator, i.e., in one northern and one southern branch, joined near the equator in the western Pacific. This branched pattern remains for 10 months, until the eastern Tropical Pacific positive ChlA reaches maximum amplitude, with ChlA concentrations > 1.5 $mg.m^{-3}$. From month 22 onwards, the western Tropical Pacific positive ChlA at 170ºE disappears, giving rise to a negative ChlA pattern that intensifies until month 44, and a second negative ChlA core that develops to the east of the 180º meridian in the following months. At this point in the sequence, the eastern Tropical Pacific displays a low amplitude positive ChlA pattern. From month 54 to 64, two negative ChlA patterns are observed – one in the western equatorial Pacific between 160º-170ºE, extending northeastwards, and another in the Central Pacific extending southeastwards from just south of the equator. These anomaly patterns change sign at month 120. Interestingly,

the southern ChlA pattern is clearly seen to propagate west-northwestward over the period of about 40 months, from around month 60 to month 100.

The L128 EEOF1 projected SSTA pattern shows large variability within the central Tropical Pacific (Figure 9). The SSTA sequence commences with a cool anomaly in the central equatorial region, flanked by warmer SSTAs to the east in the eastern Tropics and to the west, in the Coral Sea as well as north of the equator. By month 6 of the 128-month sequence, a warm pattern in the Tropical Pacific has developed similar to the projected L28 EEOF2 SSTA pattern for month 1 described earlier. This SSTA pattern remains until month 23, and is coupled with the formation of two ChlA branches that extend off the equator, and described in the previous paragraph. In the following 20 months, a SSTA pattern with a sign reversal to the one observed in the first month develops, with warm SSTAs in the central equatorial Pacific flanked by cool SSTA waters to the east in the eastern Tropical Pacific, and to the west just north of the equator and in the Coral Sea. This is concurrent with the western equatorial Pacific negative ChlA pattern. The occurrence of a similar pattern but with opposite sign (in month 40) as the one in the commencing month of the L28 EEOF1 sequence suggests that both are the extremes of the cyclic pattern period. However, we note the development from here onwards is quite different from the one observed at the commencement of the sequence. Instead of the now positive SSTA in the equatorial Pacific developing to occupy the eastern side of the basin, it instead remains flanked on the eastern side by a cool SSTA pattern until the month 66. After month 66, the warm equatorial SSTA pattern starts to cool and from month 93 through to month 111, the region is totally replaced by negative SSTAs which move westward to the WPWP region towards the end of the sequence. Simultaneously, warm SSTAs develop in the eastern Tropical Pacific.

4.3. Results summary

We have shown that for the L = 28-month EEOF analysis, EEOF2 is highly significantly correlated with the basin-wide ENSO time series metric, the Multivariate ENSO index (MEI). In contrast, for the L = 128-month EEOF analysis, EEOF1 is highly significantly correlated with the improved El-Nino Modoki index (IEMI). However, we note similarities across the analyses. In the L = 28-month EEOF analysis, the leading mode (i.e., EEOF1) was better related to the IEMI than it was to classical ENSO – which might be considered a little surprising given that for analyses of longer record SSTA fields, classical ENSO is typically always the leading EOF found in inter-annual climate variability studies. We further note that the second maximum power peak from a spectral analysis of the IEMI is at the 32-month periodicity. We found that while the second mode correlates significantly with the MEI in the L = 28 EEOF analysis, it remains coupled with the leading mode.

Further, EEOFM2, seems to illustrate the evolution of a phase transition of ENSO event, where central and east equatorial Pacific high amplitudes of Chl and SST change signal. In EEOFM1, a persistent structure of Chl high amplitude anomalies in the west central equatorial Pacific connect through propagating features with northern off Equatorial Pacific region, coupled with central Equatorial Pacific SST high amplitude pattern.

5. Discussion

5.1. Similarities/differences between L28 EEOF1 and EEOF2

The dominant spectral peaks identified in an analysis of the classical ENSO metric (MEI) and the El Nino Modoki index (IEMI) are respectively 28 and 128 months, for

the period 1997 to 2010. While published literature typically shows that ENSO has a quasi-periodicity of between 2 and 8 years, e.g., *Trenberth* [1994], *Torrence* [1998], although for long time series, it is not uncommon for spectral peaks to be in the range of around 3.5-4.5 yr. For the shorter record here (1997-2010), the dominant 2.3-yr period in the MEI demonstrates the relatively high frequency that characterises ENSO in recent years. Importantly here, ENSO quasi-biennial cycles are often treated as noise [*Huang and Morimoto*, 2008]. Noise in the ENSO signal refers to high-frequency forcing and smaller time scale processes, such as Kelvin wave propagation, which can determine, for example, the initialisation or termination of an ENSO event [*Huang and Morimoto*, 2008], having enormous implications for phytoplankton populations [*Masotti et al.*, 2011]. We caveat here that our study period commences with the very large 1997/98 El Nino event, and its phase transition, which contributes to the shorter 28-month (2.3-yr) period. A second spectral peak was also found in the MEI at the 85-month periodicity (7.1 years) - however, this peak was not significant against the background red noise threshold.

Similarities between the L = 28-month EEOF2 ChlA pattern propagation and its projected SSTA field indicate that the spatial patterns are consistent with published studies of the evolution of classical cold-tongue ENSO [*Chavez et al.*, 2011]. Examples that confirm this are: the strong values of ChlA from the Costa-Rica Dome in the eastern equatorial Pacific during classical ENSO events [*Pennington et al.*, 2006], the opposite signed ChlA in the West Pacific Warm Pool (WPWP); and the substantial projected warm SSTA pattern that corresponds to the cold tongue region in the first month of the sequence.

It is important to note that while the L28 EEOF2 timing is characteristic of classical ENSO, the pattern sequence also includes El Nino Modoki characteristics.

As seen in month 28 of the projected SSTA sequence, a central equatorial Pacific SSTA pattern is flanked - in the east, south and northwest regions - by patterns of opposite sign characteristic of an El Nino Modoki event [*Ashok et al.*, 2007]. Keeping in mind that since the time series of this mode is highly correlated ($r = 0.75$, $p = 0.01$) with MEI (i.e., ENSO), and not IEMI (which related to another mode from the same analysis), this mode is definitely an ENSO related mode. Here, we argue that the EEOF analysis might have wrongly picked up only part of the spatial propagating pattern, or that these two different signals share similar mechanisms and have similarities on induced spatial patterns, which can be originated by the common climate phenomenon, ENSO, as suggested by Takahashi [2011].

Importantly, while our analysis has identified a quasi-decadal time scale characteristic of El Nino Modoki in this record, it has been previously characterised also at the 4-year (48-month) inter-annual time scale [*Ashok et al.*, 2007]. We find that the second spectral maximum of the IEMI time series was 28 months, with >95% confidence above red noise, which is also characteristic of the MEI time series, albeit that it does not dominate in the IEMI spectra. This result suggests some connection between both modes of variability. Further, the fact that EEOF when performed with a $L = 28$ yields a leading mode that related better with EM mode, suggests that the EM lower frequency signal was stronger than canonical ENSO oscillations during the period considered. However, since these two leading modes failed a modal dependency screening which also suggests a link between them and therefore maybe the relatively small scale and higher frequency process, between both modes of variability are similar. In fact, the EEOF ($L = 28$) ChlA spatial patterns of mode 1 in month 1 seem to be the inverse pattern of the mode 2 month 24 (Figure). Also, SSTA projected patterns of mode 1 month 1, which agree with a La Niña EM event SSTA

patterns [*Ashok et al.*, 2007], are quite similar to the inverse pattern of mode 2 month 28 (Figure 4 and 5). Yet, both ChlA and projected SSTA spatial patterns mode 2 month 1 are quite distinct from any other 28-month cycle of mode 1, related to EM (not shown).

5.2. ENSO propagation

The influence on ChlA of a transition from an El Niño to a La Niña event was first reported in the literature following the very strong El Nino event transition that occurred in 1997/98, and was only really made possible with the advent of un-precedented satellite global Chl observations during that time (e.g., [*Behrenfeld et al.*, 2001]). EEOF2 yielded a spatial pattern sequence that not only highlights a classical 'composite'-like ENSO in Chl in the leading month, but by month 8 the evolving spatial pattern is quite similar to reports in the literature describing the difference between the La Niña to El Niño observations [*Behrenfeld et al.*, 2001]. This further corroborates that the L28 EEOF2 sequence is characteristic of the propagating pattern of transition between ENSO phases which we observe as: a reduction in the ChlA from the Costa Rica dome through to just north and south of the equator; the development of a central-eastern Tropical Pacific positive ChlA; and development of an equatorial egative ChlA pattern. The corresponding SSTA consists of a westward anomalous warming of the equatorial cold tongue and the development of cool anomalies in the central equatorial Pacific.

5.3. EM propagation

The way El Nino Modoki develops across the Pacific Ocean is described in detail by Ashok et al. [2007]. The L128 EEOF1 projected SSTA propagating pattern

shown in the present study (Fig. 9) is consistent with Ashok et al.'s (2007) description of an El Nino Modoki event. EM at the end of 1997 was in a La Niña phase, i.e., an anomalously cool Central Pacific flanked with warming to the east, south and northwest. By month 54, the spatial pattern has reversed sign, when the IEMI is also strongly positive (the Modoki El Niño phase). The El Nino Modoki returns to the La Niña phase by month 108 (Figure 9). The SSTA pattern evolution between these phases, however, is not the same. Rather, when El Nino Modoki is weak, other mechanisms, such as the evolution of classical cold tongue ENSO, may also significantly influence SSTA, and consequently ChlA. In fact, in the development of the ChlA and SSTA pattern, in the intervening period between the two phases of Modoki (i.e., between months 1 and ~58), a signature pattern that resembles a cold tongue ENSO event [*Chavez et al.*, 2011] is observed at around month 20 (Figure 8 and 9).

As discussed in Section 1, studies relating El Nino Modoki with ChlA are, to our knowledge, absent from the literature. Here, the patterns found to correspond to an EM event are described mainly by a strong ChlA in the western-central equatorial Pacific, connected with north and south off-equatorial ChlA patterns of the same sign (Figure 8). We note, however, that this ChlA EM pattern is very similar to: the last decade trend pattern [*Demarcq*, 2009; *Henson et al.*, 2010], the pattern occurring during a period of ocean warmth [*Behrenfeld et al.*, 2006], or, the inter-decadal variability pattern [*Martinez et al.*, 2009] in phytoplankton distribution, i.e., a high amplitude negative anomaly in the western-central Pacific connected with two branches in either subtropical regions of the Pacific. Since here we empirically connect a similar pattern to EM, which is essentially a decadal climate mechanism, we suggest that all these published patterns might be due to EM variability. Further, it

was suggested that EM is nonetheless than a nonlinear evolution of ENSO [*Takahashi et al.*, 2011], which could be induced by a flattening of the thermocline in the Equatorial Pacific, as in response to a warming ocean induced by anthropogenic climate change have been put forward [*Yeh et al.*, 2009]. Which, suggests a linkage between anthropogenic induced climate change and the decadal propagating mode of ChlA here observed.

6. Conclusions

In this study, we identified the power spectra maximum periodicity in the Multivariate ENSO index (MEI) and El Nino Modoki index (IEMI) from Oct 1997 - Oct 2010 as being 28 months and 128 months, respectively. We found that the MEI power spectral maximum of 28 months relates to ENSO high frequency processes which might represent a transition between phases, which is observed in the isolated EEOFM2 Chl pattern. This transition occurs with the decrease in intensity of the ChlA in the off-equatorial region, and the SSTA in the cold tongue, followed by the development of an positive ChlA pattern in the western-central equatorial region.

In the present study, using an EEOF analysis approach applied to the most recent 12-yr satellite record of Chl-a coincident with SST, we have shown that classical ENSO explained less ChlA variability than the El Nino Modoki mode. While we have demonstrated that El Nino Modoki has a quasi-decadal climate signature,, it nevertheless also responds at higher frequencies. The isolated pattern in the main El Nino Modoki lag-sequence of 128 months shows the occurrence of a large amplitude ChlA pattern in the western-central equatorial Pacific, which then develops just north of the equator. Hence, our results strongly suggest that the previously reported trends in phytoplankton over the last decade, inter-decadal differences and ocean warming

period, are due to the recent increases in El Nino Modoki, which might represent the non-linear ENSO evolution [*Takahashi et al.*, 2011] forced by anthropogenic induced climate change [*Yeh et al.*, 2009].

Acknowledgements

Chl and SST data were obtained from the Ocean Productivity website at the Oregon State University (http://www.science.oregonstate.edu/ocean.productivity/). We would like to thank Mauro Vargas for his insights in our discussions of this work.

References

Ashok, K., et al. (2007), El Niño Modoki and its possible teleconnection, *Journal of Geophysical Research C: Oceans*, *112*(11).

Behrenfeld, M. J., et al. (2001), Biospheric primary production during an ENSO transition, *Science*, *291*(5513), 2594-2597.

Behrenfeld, M. J., et al. (2006), Climate-driven trends in contemporary ocean productivity, *Nature*, *444*(7120), 752-755.

Bjerknes, J. (1969), Atmospheric teleconnections from the Equatorial Pacific, *Monthly Weather Review*, *97*(3), 163-172.

Bjornsson, H., and S. A. Venegas (1997), A manual for EOF and SVD analyses of climate data, 52 pp, McGill University, Montréal, Québec.

Carr, M. E., et al. (2006), A comparison of global estimates of marine primary production from ocean color, *Deep-Sea Research Part II: Topical Studies in Oceanography*, *53*(5-7), 741-770.

Chavez, F. P., et al. (2011), Marine Primary Production in Relation to Climate Variability and Change, *Annual Review of Marine Science*, *3*(1), 227-260.

Davis, R. E. (1976), Predictability of Sea Surface Temperature and Sea Level Pressure Anomalies over the North Pacific Ocean, *Journal of Physical Oceanography*, *6*(3), 249-266.

Demarcq, H. (2009), Trends in primary production, sea surface temperature and wind in upwelling systems (1998-2007), *Progress in Oceanography*, *83*(1-4), 376-385.

Di Lorenzo, E., et al. (2010), Central Pacific El Nino and decadal climate change in the North Pacific Ocean, *Nature Geosci*, *3*(11), 762-765.

Frigo, M., and S. G. Johnson (1998), FFTW: An Adaptive Software Architecture for the FFT, *Proceedings of the International Conference on Acoustics, Speech, and Signal Processing*, *3*, 1381-1384.

Henson, S. A., et al. (2010), Detection of anthropogenic climate change in satellite records of ocean chlorophyll and productivity, *Biogeosciences*, *7*(2), 621-640.

Holbrook, N. J., et al. (2005a), Corrigendum, *Journal of Climate*, *18*(1637-1639).

Holbrook, N. J., et al. (2005b), Oscillatory and propagating modes of temperature variability at the 3–3.5- and 4–4.5-yr time scales in the upper southwest Pacific Ocean, *Journal of climate*, *18*, 719-736.

Huang, Z., and H. Morimoto (2008), Wavelet based fractal analysis of El Niño/La Niña episodes, *Hydrological Research Letters*, *2*, 70-74.

Li, G., et al. (2010), Indices of El Niño and El Niño Modoki: An improved El Niño Modoki index, *Advances in Atmospheric Sciences*, *27*(5), 1210-1220.

Martinez, E., et al. (2009), Climate-Driven Basin-Scale Decadal Oscillations of Oceanic Phytoplankton, *Science*, *326*(5957), 1253-1256.

Masotti, I., et al. (2011), Large-scale shifts in phytoplankton groups in the Equatorial Pacific during ENSO cycles, *Biogeosciences*, *8*(3), 539-550.

Messié, M., and M.-H. Radenac (2006), Seasonal variability of the surface chlorophyll in the western tropical Pacific from SeaWiFS data, *Deep Sea Research Part I: Oceanographic Research Papers*, *53*(10), 1581-1600.

North, G. R., et al. (1982), Sampling Errors in the Estimation of Empirical Orthogonal Functions, *Monthly Weather Review*, *110*(7), 699-706.

O'Reilly, J. E., et al. (2000), Ocean color chlorophyll a algorithms for SeaWiFS, OC2, and OC4: Version 4. In: SeaWiFS Postlaunch Technical Report Series, in *SeaWiFS Postlaunch Calibration and Validation Analyses, Part 3*, edited by S. B. Hooker and E. R. Firestone, pp. 9-23, NASA, Goddard Space Flight Center, Greenbelt Maryland.

Pennington, J. T., et al. (2006), Primary production in the eastern tropical Pacific: A review, *Progress in Oceanography*, *69*(2-4), 285-317.

Takahashi, K., et al. (2011), ENSO regimes: Reinterpreting the canonical and Modoki El Niño, *Geophys. Res. Lett.*, *38*(10), L10704.

Torrence, C., and G. P. Compo (1998), A Practical Guide to Wavelet Analysis, *Bulletin of the American Meteorological Society*, *79*(1), 61-78.

Trenberth, K. E., and J. W. Hurrell (1994), Decadal atmosphere-ocean variations in the Pacific, *Climate Dynamics*, *9*(6), 303-319.

Venegas, S. A. (2001), Statistical methods for signal detection in climate, Danish Centre for Earth System Science, Niels Bohr Institute for Astronomy, Physics and Geophysics, University of Copenhagen, Denmark.

White, W. B., and R. G. Peterson (1996), An Antarctic circumpolar wave in surface pressure, wind, temperature and sea-ice extent, *Nature*, *380*(6576), 699-702.

Wolter, K., and M. S. Timlin (1993), Monitoring ENSO in COADS with a seasonally adjusted principal component index., paper presented at Proc. of the 17th Climate

Diagnostics Workshop, Norman, OK, NOAA/NMC/CAC, NSSL, Oklahoma Clim. Survey, CIMMS and the School of Meteor., Univ. of Oklahoma.

Yeh, S.-W., et al. (2009), El Niño in a changing climate, *Nature*, *462*(7273), 674-674.

Figures

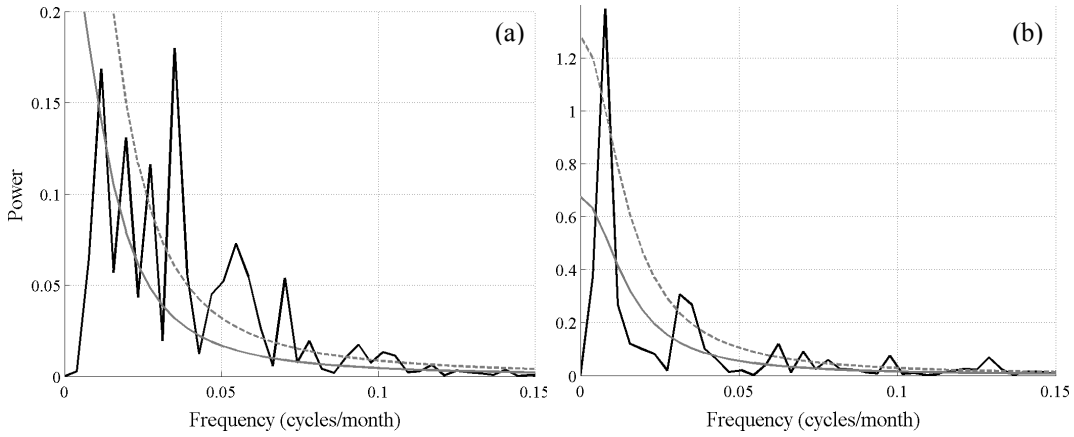

Figure 1. MEI (a) and IEMI (b) power spectra (black line), red noise spectra (solid grey line), and 95% confidence line (dashed grey line). The peak maximum power for the MEI is 28 months, and for the IEMI is 128 months. These maxima are significant against the background red noise and at the 95% confidence level.

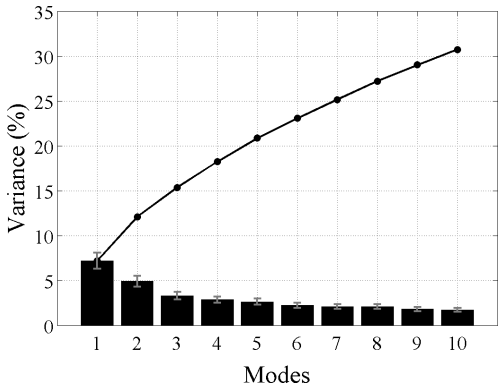

Figure 2. Variance and cumulative variance explained by the first 10 EEOFs (L = 28). EEOF1, which is highly significantly correlated with the IEMI, explains 7% of the inter-annual ChlA variance. EEOF2, identified as the classical ENSO mode, explains 5% of the inter-annual ChlA variance. The error bars were calculated according to the North et al. (1982) test for mode independence.

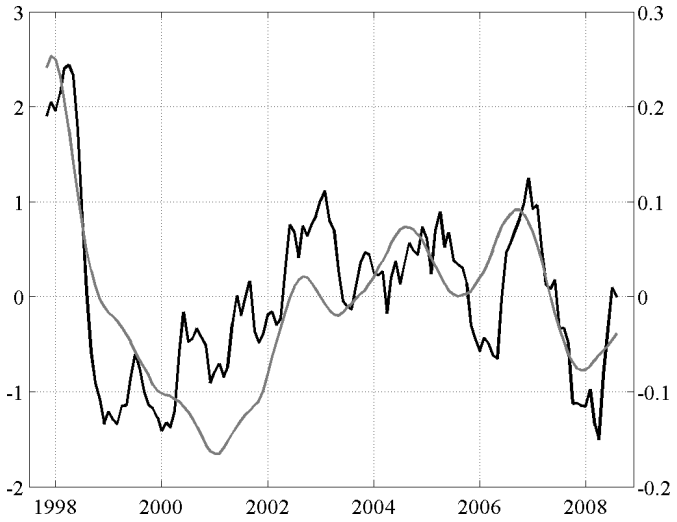

Figure 3. The MEI time series (black) for 130 months starting in October 1997 until August 2008. The EEOF2 (L = 28-month) time series from the analysis of ChlA (grey) is also shown (note that the exact timing is not provided in the EEOF analysis). The series compare with $r = 0.75$ and $p < 0.01$, taking account of serial correlations according to Davis (1976).

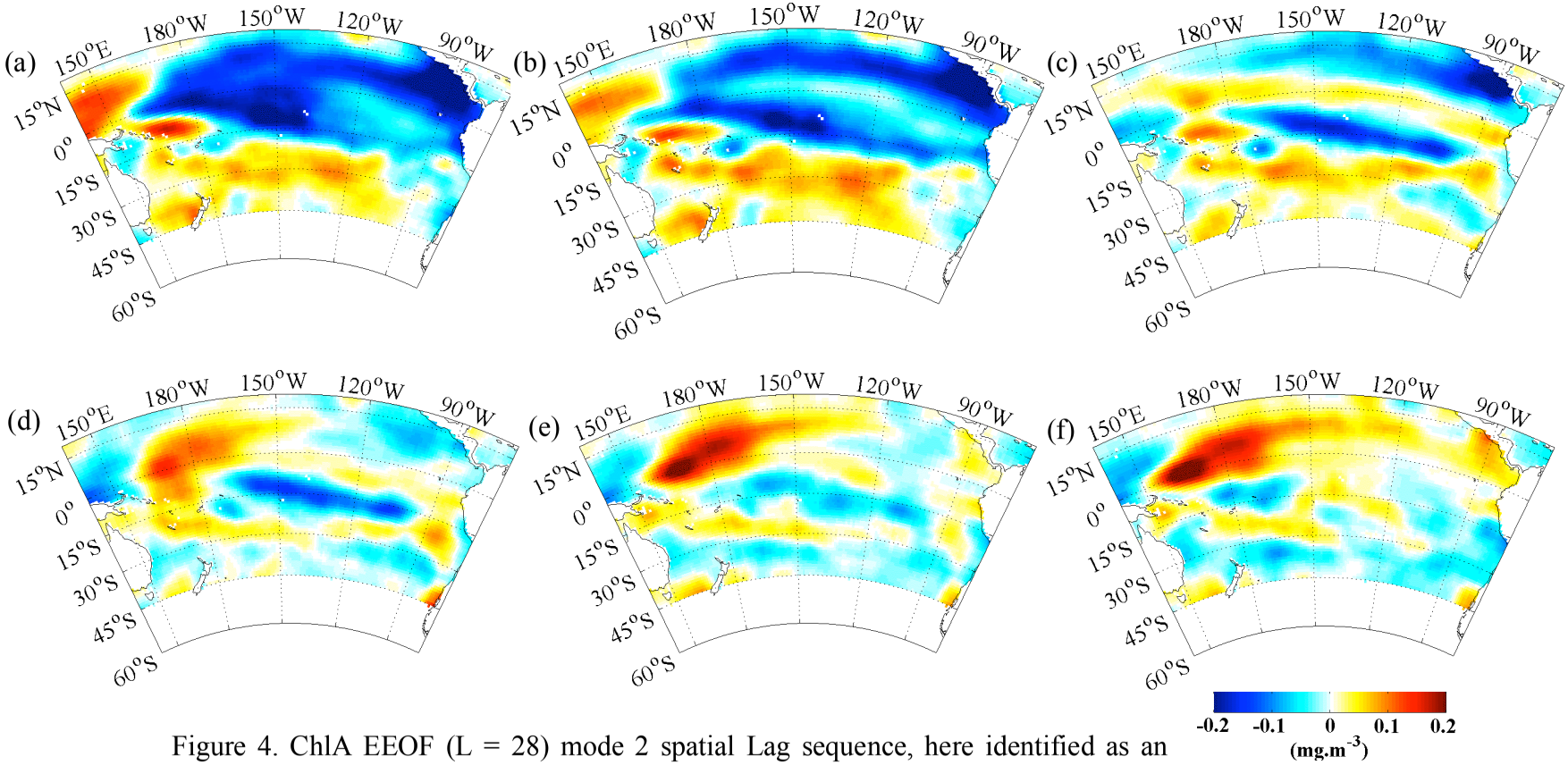

Figure 4. ChlA EEOF (L = 28) mode 2 spatial Lag sequence, here identified as an ENSO transition of phases event (a – f are months 1, 5, 10, 15, 20 and 25, respectively). Figures plotted on a Lambert projection

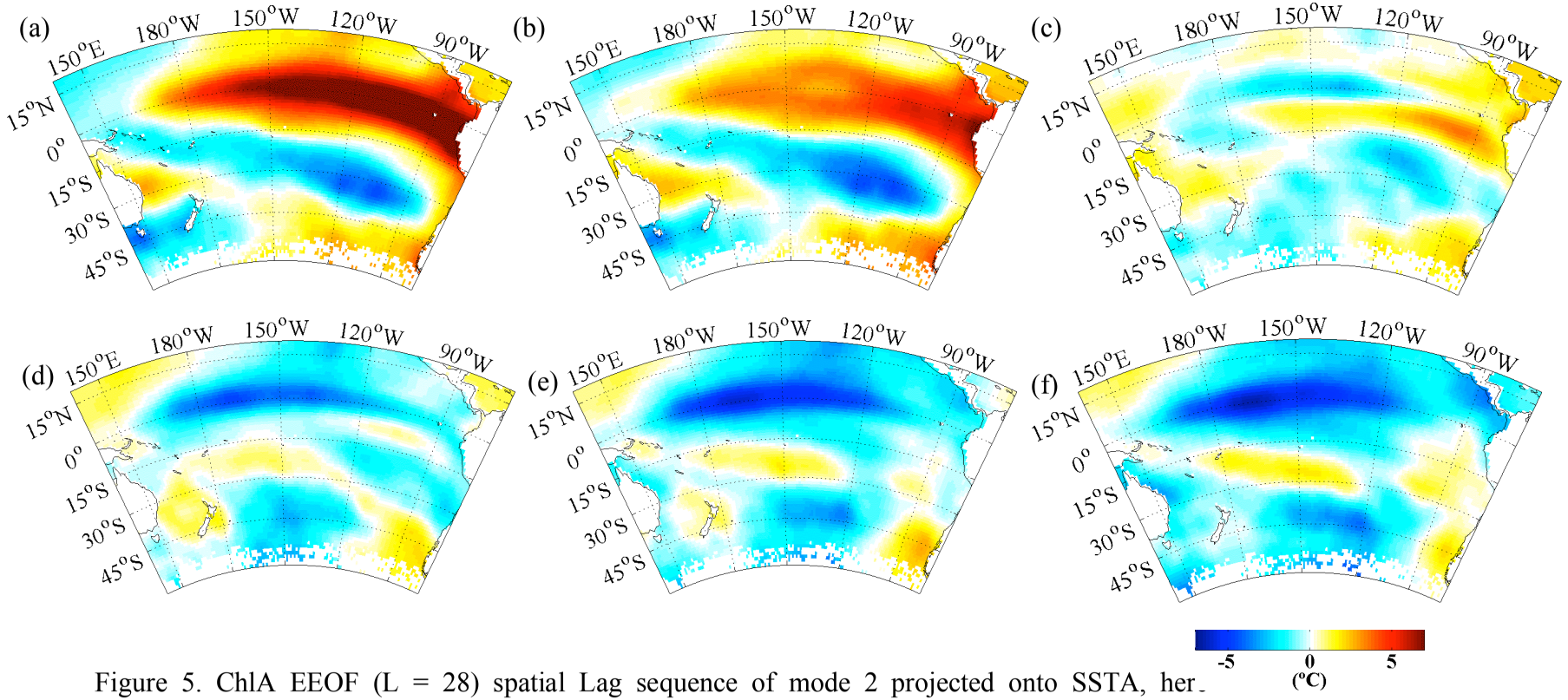

Figure 5. ChlA EEOF (L = 28) spatial Lag sequence of mode 2 projected onto SSTA, her identified as an ENSO transition of phases event (a – f are months 1, 5, 10, 15, 20 and 25, respectively). Figures plotted on a Lambert projection

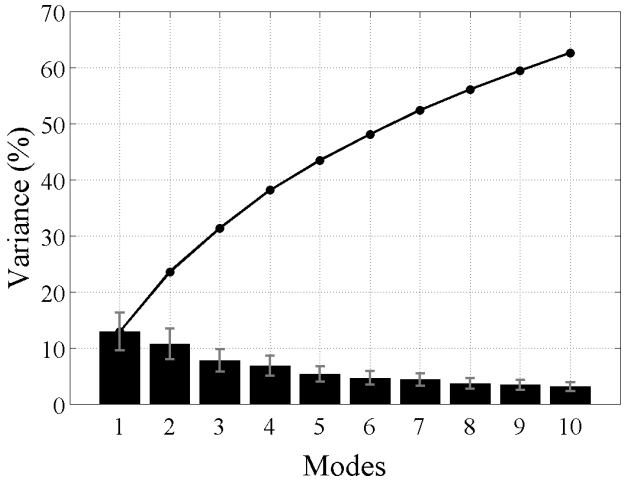

Figure 6. Variance and cumulative variance explained by the 10 leading EEOFs (L = 128-month). EEOF1, which is highly significantly correlated with the El Nino Modoki index (IEMI), explains 13% of the inter-annual ChlA variance. The error bars were calculated according to the North et al. (1982) test for mode independence. We note that there is mode degeneracy according to this test.

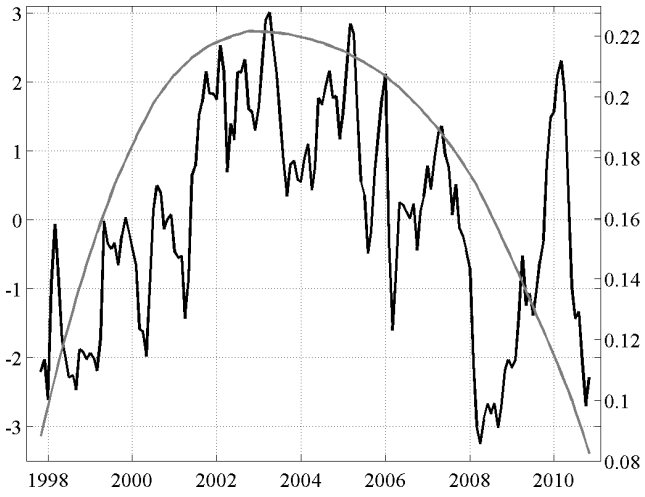

Figure 7. The IEMI time series (black) and EEOF1 (L = 128-month) time series (grey) are shown. These series are highly significantly correlated ($r = 0.60$, $p < 0.01$, accounting for serial correlation according to Davis (1976)).

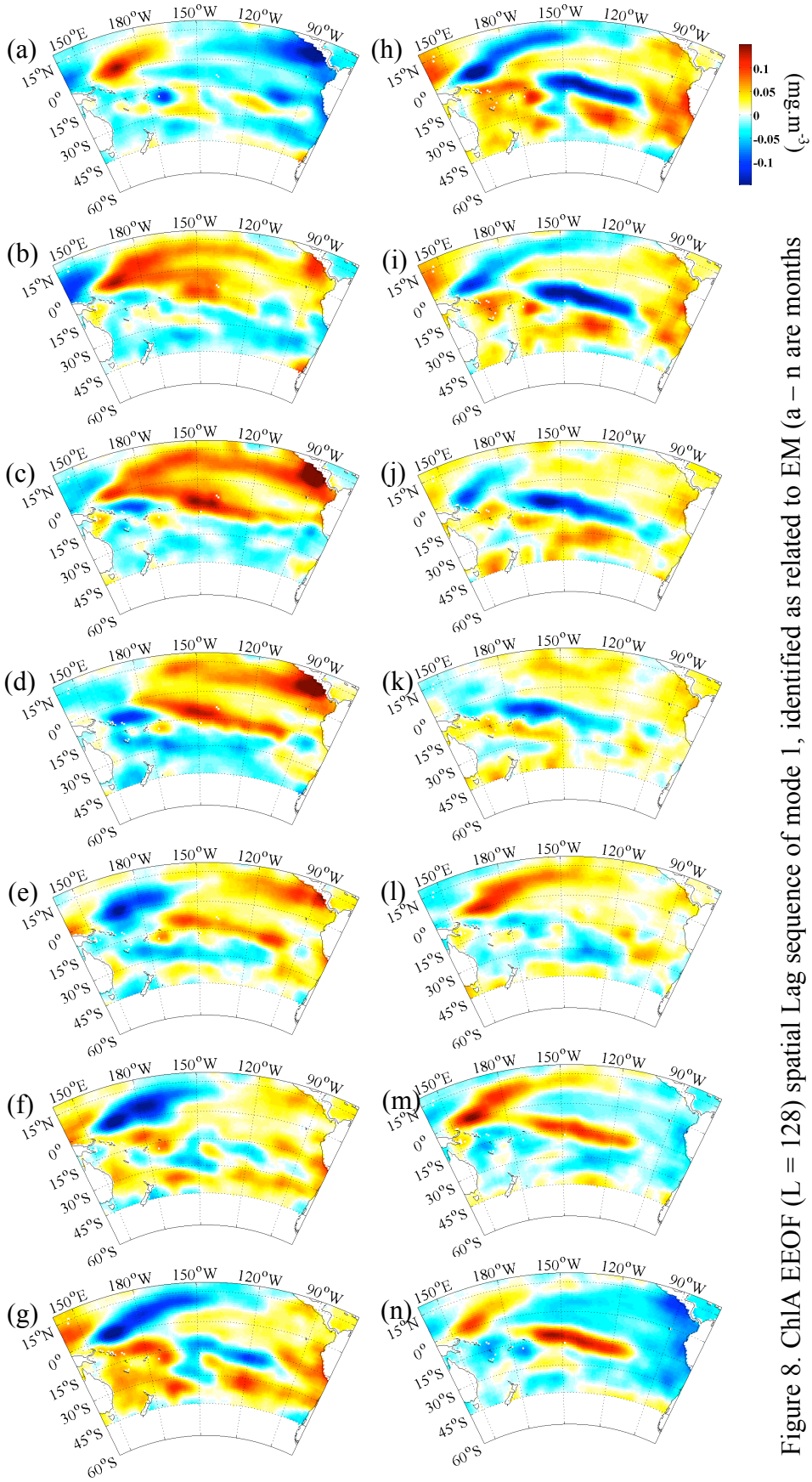

Figure 8. ChlA EEOF (L = 128) spatial Lag sequence of mode 1, identified as related to EM (a – n are months 1 to 128 with increments of 10). Figures plotted on a Lambert projection

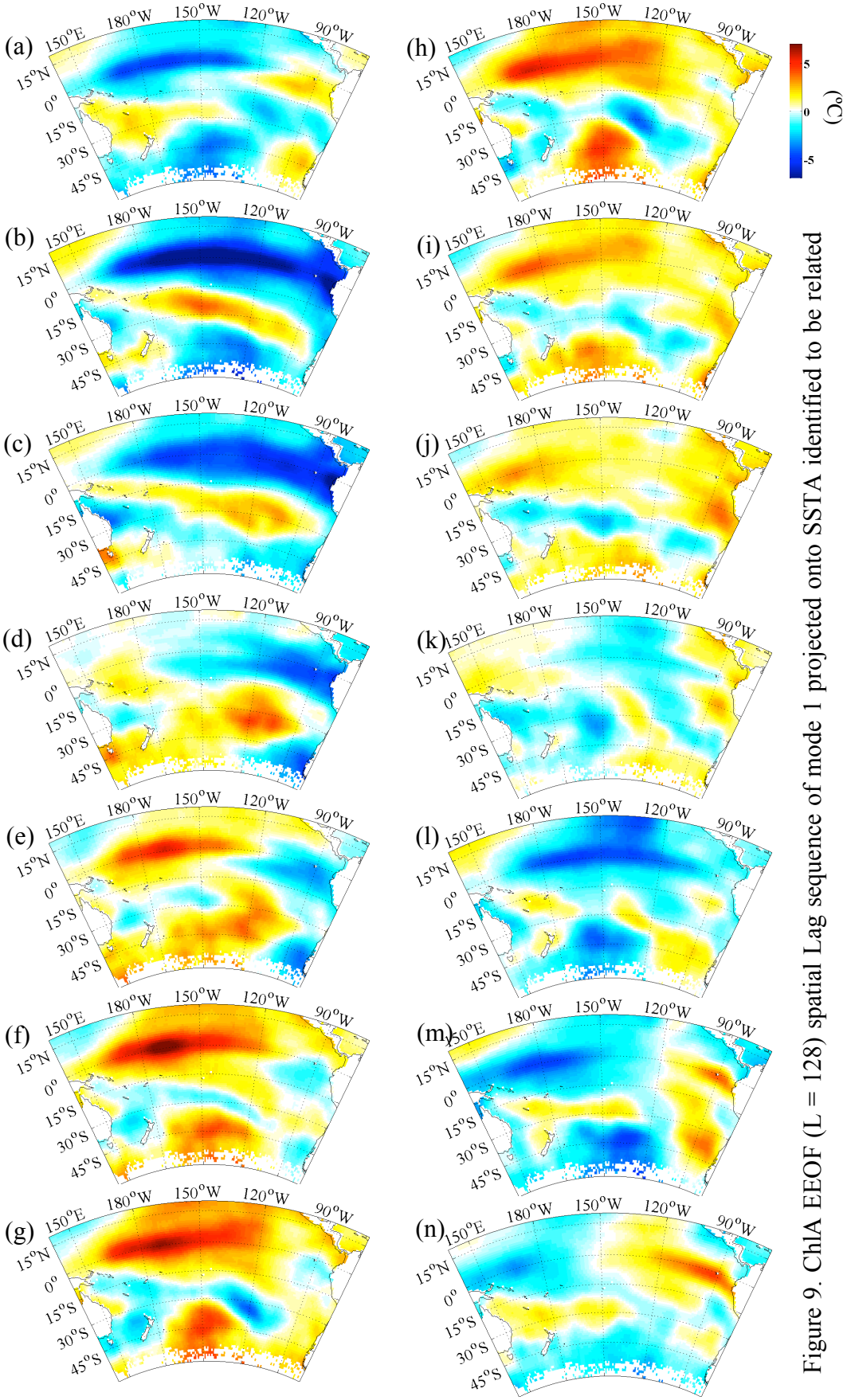

Figure 9. ChlA EEOF (L = 128) spatial Lag sequence of mode 1 projected onto SSTA identified to be related with EM (a – n are months 1 to 128 with increments of 10). Figures plotted on a Lambert projection

7.3 CHAPTER SUMMARY

In this chapter, ENSO and EM maximum spectra, from October 1997 to October 2010, are identified to be at 28 and 128 months, respectively. This period is then used to isolate inter-annual Chl EEOF propagation across the Tropical and South Pacific at exactly these lags, and significantly correlated to time series of indices from both regional climate phenomena. We further project both, ENSO and EM related Chl EEOF modes of variability onto SST, reconstructing the ocean physical variability that characterizes each mode. We note, however, that the ENSO related Chl EEOF mode corresponds to an ENSO phase transition event, which is determined by ENSO high frequencies. In addition, we suggest that the reported trends on phytoplankton over the last decade are connected to EM variability.

CHAPTER 8

Patterns of chlorophyll-*a* variability at the Eastern Australian Current region

8.1 CHAPTER OVERVIEW

This chapter aims to assess phytoplankton patterns of variability regionally at various time scales. For this purpose, the western boundary current of the South Pacific, the Eastern Australian Current (EAC), is selected, and Chl variability patterns of intra-, inter- and multi-annual scales are examined. The impact the southward flowing EAC on phytoplankton distribution at these different time scales is evaluated. Additionally, we assess the Chl patterns during the strong events of two climate modes of variability that are highly influential in this region, the ENSO and the SAM. This chapter addresses the final objective of the thesis.

The main text of this section is a fully drafted paper entitled 'An examination of the seasonal through to inter-annual chlorophyll-*a* variability in the East Australian Current region', intended for submission to the Journal *Deep-Sea Research Part I: Oceanographic Research Papers*, co-authored by A. B. Couto, A. M. Maharaj and N. J. Holbrook.

Candidate's contribution to this paper

I obtained the datasets, wrote the scripts and performed all data analysis. I also produced the figures and drafted the manuscript, which was evaluated by both co-authors. However, input from Dr. Holbrook and Dr. Maharaj was attained regularly during this process.

Seasonal and inter-annual chlorophyll-*a* variability in the Eastern Australian Current region

André B. Couto

Department of Environment and Geography, Macquarie University, Sydney, New South Wales, Australia

Angela M. Maharaj

Department of Environment and Geography, Macquarie University, Sydney, New South Wales, Australia

Neil J. Holbrook

School of Geography, University of Tasmania, Hobart, Tasmania, Australia

Abstract

The EAC forms in low productivity tropical waters, and flow southwards bifurcating around 30ºS. One branch flows eastward throughout the Tasman Front, and another poleward, reaching the southern ocean. During its pathway the low productive EAC waters cross several biogeographical regions. This study provides a comprehensive approach to observe and assess the influence of the EAC on regional to large-scale oceanic satellite derived chlorophyll-*a*. Here we use more than 10 years of surface chlorophyll-*a* satellite observations to evaluate seasonal climatology patterns as well as inter-annual variations of phytoplankton across the EAC. Furthermore, we investigate EAC productivity patterns during different phases of ENSO and SAM. We observe that the injection of poor nutrient EAC waters is mainly

observed in spring in the mid latitudes, and in the summer at higher latitudes; an increase of inter-annual EAC net transport is linked to a decrease in Chl; El Niño events induce a decrease of Chl in the northern region of the EAC and a decrease in the southern region whilst a positive southern annular mode phase may be decreasing Chl in the Subtropical Front region.

Keywords

Western boundary currents, chlorophyll - *a*, satellite sensing, climate, ENSO, SAM

1. Introduction

Climate variability and change appear to play critical roles in South Pacific Ocean circulation, including the East Australian Current (EAC) - with EAC transports apparently affected by El Niño – Southern Oscillation (ENSO), the Southern Annular Mode (SAM), Antarctic ozone depletion and greenhouse warming (e.g., Cai *et al.*, 2005; Holbrook *et al.*, 2005b). Various studies have made connections between, for example, climate and ocean productivity (e.g., Behrenfeld *et al.*, 2006), and mesoscale EAC dynamics and productivity (e.g., Baird *et al.*, 2008). However, the complex inter-relationships between regional to large-scale climate changes, EAC dynamics and ocean productivity are poorly understood.

The EAC is the western boundary current of the South Pacific subtropical gyre, and plays a critical role in transporting heat poleward (Ridgway ,1984). It is also a significant source of mesoscale eddies (Nilsson and Cresswell, 1980; Tilburg *et al.*, 2002; Wilkin and Morrow, 1994) despite of being, on average, relatively weak in intensity compared with most other western boundary currents around the world. The

EAC has a mean net transport of around 10Sv (Ridgway *et al.*, 2008) through the South Coral Sea and Tasman Sea. It is essentially divided into four regions with distinct physical characteristics: (i) the formation region (in the mid Coral Sea, ~17ºS); (ii) the South Coral Sea where the EAC intensifies; (iii) the EAC separation zone, where the main jet separates from the coast turning eastward along the Tasman Front (TF); and (iv) the southward extension to the Subtropical Front (STF), comprising roughly a third of the EAC flow (Ridgway and Dunn, 2003).

Chlorophyll-*a* is a crucial molecule in the photosynthesis process of all photoautotrophs. Through this process, phytoplankton are responsible for 99% of the ocean's primary productivity - an integral component of the planet's biogeochemical cycles of carbon, nitrogen and other major chemical elements (Field *et al.*, 1998). Regionally, phytoplankton primary productivity variability patterns regulate the local marine ecosystems, by providing the base of the food web for the local fauna. The region where the EAC flows across varies quite significantly in terms of oceanic biogeographical regions, depending from the from chosen criteria, regions very quite drastically either in biology either in physical and chemical characteristics (Condie and Dunn, 2006; Longhurst, 1998).

This paper provides a comprehensive assessment of the seasonal variability of chlorophyll-*a* concentration (Chl), as an indicator of phytoplankton biomass, in the EAC region based on satellite remotely sensed observations. Here, we demonstrate that EAC southward flowing warm waters influence regional Chl variability from seasonal to multi-annual scales, despite of the biogeographical environmental characteristics crossed, and investigate the relationship of the regional Chl variability with inter-annual EAC transport variability, and the likely influences of both large scale climate modes of variability, ENSO and SAM, on regional Chl concentrations.

2. Data and Methodology

2.1. Data

Ocean surface Chl concentrations analysed in this study have been obtained from the Sea-viewing Wide Field-of-view Sensor (SeaWiFS) SeaWiFS.r 2010 reprocessing product. Since Chl reflects at specific colour wavelengths, ocean colour measurements obtained using satellite remote sensing instruments provide excellent coverage in space and time of Chl concentrations at near-global scales. Sea surface temperature (SST) data analysed in this study are from the remotely sensed Advanced Very High Resolution Radiometer (AVHRR). Both the Chl concentration and SST datasets were obtained from the Ocean Productivity website hosted by Oregon State University and are composed of matrices containing globally-distributed values, where each matrix corresponds to a monthly mean composite of daily remote sensed observations for the period from October 1997 to December 2007 (n=123). The original Chl maps provide a spatial resolution of 2160 x 4320 pixels, while the SST maps correspondingly comprise of 2048 x 4096 pixels, with both datasets giving full global coverage (i.e., 90ºN-90ºS, 0º-360º). Hence, each pixel represents an area of 9 km^2 and ~10km^2 at the equator, reducing polewards for Chl and SST, respectively.

2.2. Seasonal cycle

From the global maps of both variables, we selected the southwest Pacific subregion defined between 10ºS - 50ºS, 145ºE - 160ºE, in order to focus on the EAC and nearby surrounds. We calculated monthly climatologies, seasonal averages and the seasonal standard deviation (SD) for each three-monthly austral season - they are spring (SON – September, October, November); summer (DJF – December, January,

February); autumn (MAM – March, April, May); and winter (JJA – June, July, August) (Fig 1).

To analyse Chl variability along the EAC pathway, zonal transects across the four EAC regions of formation, intensification, separation, and southward extension were chosen (indicated in Fig 1 bottom right map), corresponding to the latitudes of six Australian cities. These are Bowen (20ºS), where the EAC forms; Brisbane (27ºS) and Coffs Harbour (30ºS), where the EAC intensifies; Sydney (34ºS), just south of the EAC separation zone from the coast; and Merimbula (37ºS) and Hobart (43ºS), in the EAC extension zone where the flow intensity declines. Fig 2 summarizes the seasonal Chl and SST cycles across the six zonal transects extending from the east Australian coast to 160ºE. Cross-correlations were carried out between the Hovmöller patterns of SST and Chl. The aim here is to identify the EAC zone in terms of the Current's Chl/SST signature. To achieve this, each zonal transect for each month, was ranked in their values from lowest Chl (highest SST) to highest Chl (lowest SST) and plotted as a Hovmöller plot (Fig 3).

2.3. Inter-annual variability

To analyse patterns of inter-annual variability, monthly-average values were subtracted from each monthly Chl (or SST) in the distributed time series across the spatial domain, or alternatively seasonal-averages were subtracted from the corresponding three-monthly series at each spatial grid point. Composites of five-year filtered net EAC transports (Ridgway *et al.*, 2008), for three different periods, were calculated. These periods are: (i) October 1997 to December 2000, (ii) January 2001 to December 2002, and (iii) January 2003 to December 2005. Seasonal composites of ENSO and SAM 'strong-event years' were also prepared. We only consider the

ENSO and SAM sources of large-scale climate variability, since the EAC study domain is best described by the influences of these Pacific and Southern Ocean centred climate processes. 'Strong-event years' were identified using the time-series of two climate indices. For ENSO, we used the monthly averaged NINO3.4 SST index (Trenberth, 1997), obtained from the National Center for Atmospheric Research (http://www.cgd.ucar.edu/cas/catalog/climind/Nino_3_3.4_indices.html). For SAM we used the monthly time series observations from the leading empirical orthogonal function analysed on atmospheric geopotential 700 mb hight anomalies polewards of 20ºS, provided from the National Oceanic and Atmospheric Administration website (http://www.cpc.ncep.noaa.gov/products/precip/CWlink/daily_ao_index/aao/aao.shtml). El Niño (EN)-event composites comprise of the 1997 and 2002 years and La Niña (LN)-event composites include 1998 and 1999. SAM-only years were defined when the SAM index surpassed values of 1. Based on this definition, positive SAM phases (SAM+) were composited from the years 1997, 1998, 1999 and 2001. Conversely, the only negative SAM phase (SAM-) identified is for the year 2002. In each case, the summer season corresponding to each event commences in December of the year identified, e.g., for the summer of the EN 1997 event, we examine DJF of the 1997/1998 period.

3. Results

3.1. Chl seasonal cycle at the EAC region

We hypothesise that an inverse relationship between SST and Chl will characterise the EAC. Indeed such a typical inverse relationship between Chl and SST is observed in the climatological monthly values at the meridional transect of the EAC (Fig 1). Broadly, we see low Chl collocated with high SST values in the tropics and

low SST collocated with higher Chl values at higher latitudes. Within our study region, SST values off the east Australian coast are warm in the core of the EAC. The warm EAC path varies in shape with latitude and season. Geographically, the warm EAC waters are observed to be zonally narrower and more intense at lower latitudes (e.g., ~23ºS) and zonally broader and less intense at higher latitudes (e.g., 33ºS), (Fig 1). Seasonally, the warm EAC waters (e.g., across 33^{o}S) are zonally narrower and more intense during summer and autumn than in spring and winter. Evidence of the EAC can be seen in the southward pushing SST contours off Australia's east coast at all latitudes from ~17ºS to the southern tip of Tasmania at almost 44ºS (Fig 1). Geographically, the observed Chl concentration distribution and variability tells a similar story, but instead with low (rather than high) concentrations in the EAC core – i.e., Chl minima corresponding to SST maxima (Fig 1). Seasonally, the Chl concentrations decrease in in spring from ~23ºS to 39ºS and to a lesser extent during the other seasons (Fig 1).

The seasonal cycle is also observed to be quite distinct in the different EAC zones. During SON, Chl concentrations vary from 0.06 - 0.09 mg.m^{-3} in the EAC formation region (~20ºS), and then increases poleward through the Tasman Sea (at latitudes >30ºS) where Chl standard deviation (SD) values are typically >0.06 mg.m^{-3}. However, lower Chl-concentration SDs are observed in the western side of the Tasman Sea (Fig 1). During DJF, high Chl variability occurs mainly in the southern most Tasman Sea region. Variability patterns are low during JJA.

The seasonal cycles of zonally-averaged surface Chl concentrations along the six transects at 20ºS, 27ºS, 30ºS, 34ºS, 37ºS and 43ºS (Fig 2), show three distinct seasonal characteristics. At the lowest latitude (20ºS, off Bowen), a Chl peak of 0.13 mg.m^{-3} is observed during winter. At 27ºS (off Brisbane), Chl values are lowest (<0.1

mg.m^{-3}) during the summer and most of autumn, corresponding to the warmest ocean temperatures in this zone (>25ºC). Conversely, the Chl peak maximum at this latitude occurs during the coldest winter month (August, 0.29 mg.m^{-3}) when SST ~20ºC. At 30ºS (off Coffs Harbour), the maximum Chl value (0.26 mg.m^{-3}) is observed in September, with concentrations increasing from early winter. At 34ºS (off Sydney) and 37ºS (off Merimbula), two annual peaks are observed (in late autumn and early spring), with the absolute maxima occurring in September of 0.34 mg.m^{-3} and 0.45 mg.m^{-3}, at 34ºS and 37ºS respectively. Further south, at 43ºS (off Hobart), an inverse seasonal pattern similar to observations along 27ºS are seen. Here, relatively high concentrations of Chl occur through spring, summer and autumn, and decrease during winter, correlating positively with SST (rather than negatively). Zonally and annually-averaged surface Chl concentrations increase from north to south off the east Australian coast and are calculated as: 0.08 mg.m^{-3} (Bowen); 0.19 mg.m^{-3} (Brisbane); 0.20 mg.m^{-3} (Coffs Harbour); 021 mg.m^{-3} (Sydney); 0.27 mg.m^{-3} (Merimbula); and 0.33 mg.m^{-3} (Hobart).

While the EAC core is readily identifiable by the warm water maxima observed as a southward dip in the isotherms east of Australia throughout the year at all transect latitudes, this relationship is not montonic for corresponding Chl minima. At 27°S and 30ºS (Figs 2B and 2C), the warm SST cores off Brisbane and Coffs Harbour are clearly observed throughout the year. Further, SST seasonal changes are followed closely by the seasonal Chl changes in time and space across the EAC. Further south, at 34ºS (Fig 2D), the SST warm core of the EAC is much less readily identifiable (since it is south of the average separation point from the east Australian coast), and the Chl minima are also more broadly distributed. At 37ºS, a high SST and low Chl pattern persistents through the year from 151ºE-153ºE, less than 100km off the coast

of Merimbula (Fig 2E). Finally, at 43°S, while there is a broad SST seasonal cycle across the zonal section, the EAC core is not at all well defined and is very weak in this 'extension' region. Further, Chl is not anticorrelated with SST in this zone – here other dynamics might have a bigger responsibility for the seasonality in Chl than ocean advection in the EAC as suggested for further north regions (Fig 2F).

Cross-correlation of Chl and SST across all zonal transects yielded a stronger relationship when a longitudinal displacement was considered. For example, at 27°S (off Brisbane), a higher relationship between SST and Chl is observed if the Chl climatological pattern is shifted westward by 33 km; at Sydney this optimum shift occurs at a distance of 23 km, and Merimbula and Hobart, 22 km and 20 km, respectively.

When values are ranked by zonal distribution (Fig 3), we clearly observe the warmest waters near shore at all transects during the entire climatological year, which indicates the presence of the EAC (Ridgway and Godfrey, 1997). However, the Chl zonally minimum does not always necessarily correspond to the warmest zonal SST. Only along the coasts of Sydney (34ºS) and Merimbula (37ºS), do these patterns show synoptically a similar spatio-temporal pattern between the physical and biological variables. Furthermore in Sydney we observe an eastward displacement of both, low Chl and high SST waters, from February to June, then appearing close to shore again form May onwards.

In summary, our results indicate that an increase in SST typically corresponds to a decrease in Chl concentrations through the tropics to mid latitudes. This relationship seems to be strongest during autumn and winter for lower latitudes, and in spring and summer for higher latitudes (Fig 1). Low Chl standard deviations are

also typically associated with warm SST, except during summer and autumn at higher latitudes.

3.2 Inter-annual variability in the EAC region

Based on more than 10 years of observations, annual Chl concentrations are highly variable in the EAC region, with the SON (Fig 4) and DJF (Fig 5) seasons showing the largest variability. In particular, during the SON of 1997, positive anomalies are observed throughout the region. The larger variability is, however, limited to higher latitudes (in the EAC decline region) during the following summer. Large negative anomalies <-0.1 $mg.m^{-3}$ are observed further south, in the STF region. The year following (1998) was characterized by reduced Chl concentrations throughout the EAC intensification, coastal separation, and extension (decline) regions – consistent with a strengthening of the EAC at that time, as reported by Ridgway (2008). Further, positive anomalies were observed to the south of Merimbula. In 1999, positive Chl anomalies were recorded in the EAC formation and decline regions during spring and summer. In 2000, negative Chl anomalies were observed throughout the Tasman Sea. 2001 was a year where positive anomalies were observed throughout the Australian coast during SON, from the formation to the separation regions. This was culminated, in summer, with strong positive anomalies all over the east Australian coast, and strong negative anomalies to the south of the Tasman Sea. These anomalies persist until SON of the following year. However, the summer 2002 was characterized by strong positive anomalies all over the EAC region, which persisted until the summer of 2003/2004. The summer of 2004/2005 comprised of positive anomalies in the Tasman Sea and in the region of the STF.

Further, for the STF region, positive Chl anomalies continued to occur in the summer season for three successive years through to 2006/2007.

Inter-annual zonal transects for SST and Chl values show complex patterns since higher SST were not always systematically observed off the coast to couple with low Chl values. However at some longitudes this coupling is quite visible, as in Brisbane (not shown), Coffs Harbour, Sydney and Merimbula, during SON (Fig 6). Furthermore, low Chl low values seem to move in their zonal axis from year to year.

Informed by multi-annual net EAC transport trends calculated from repeat expendable bathythermograph (XBT) surveys between Sydney and Auckland along the PX34 line (Ridgway *et al.*, 2008), we examined corresponding EAC region changes in Chl concentrations. We found average negative Chl anomalies across the region during the initial period of EAC transport increase (1997-2000); and positive anomalies through the interior subtropical gyre region during the EAC transport slackening and steadying periods (2001-2005), consistent with a relaxation of the gyre intensity and concomitant relaxation of net gyre interior downwelling, as reported by Ridgway (2003) (Fig 7A-C). Furthermore, during the SON season during a period of increased net EAC transport, negative anomalies were present off Merimbula (37^{o}S). Positive anomalies were observed further south in the EAC extension and decline region (Fig 7D).

To further investigate the likely influences of large-scale climate variability on Chl concentrations in the EAC region, surface Chl concentrations were stratified into El Nino, La Nina, SAM+ and SAM- event composites. Inspection and comparison of these Chl composite distributions suggest that both ENSO and SAM might influence Chl across all EAC region, in particular SAM seems to act more in the STF region (Fig 8). We found that positive Chl anomalies are observed during the El Nino event

year composites throughout the EAC region, and specifically at lower latitudes during SON and higher latitudes during DJF – consistent with a reduction in the EAC intensity during the El Nino years. The reverse was observed during La Nina.

SAM+ events correspond to negative Chl anomalies in DJF in the STF region. During the SAM- event (only one during the record), the reverse is indicated, with a broad extent of positive anomalies throughout the EAC region. When comparing to NINO3.4 and SAM index (Fig 9) with the observed inter-annual patterns (Fig 4 and 5), some resemblance is observed between the Chl inter-annual pattern when the respective indices are high and the climate composite patterns (Fig 8). A good example of this is the summer of 1997/98, when a strong EN period is followed by a 3-year LN period. Additionally, inter-annual variability of Chl show patterns that can be related to regional climate signals as, for example, in the 37^{o}S (Merimbula) transect, interannual variability of the summer (DJF) season shows that low Chl concentrations are closer to the coast during La Nina years (Fig 10).

4. Discussion

As described by Jitts (1965), and later confirmed (Condie and Dunn, 2006), the Southwest Pacific can be broken down into subregions that are characterised with distinct physical, chemical and biological profiles. In the present study, we found distinct seasonal distributions of phytoplankton biomass in the EAC region, characteristic of different oceanic regions. From tropics through to midlatitudes, we find: (i) in the tropics to subtropics, a single winter Chl maximum is observed at 20^{o}S (off Bowen) and 30^{o}S (off Coffs Harbour); (ii) in the subtropics to midlatitudes, a large spring Chl bloom is observed seasonally at 34^{o}S (off Sydney) and 37^{o}S (off

Merimbula); and (iii) in the midlatitudes, a large spring bloom and a smaller autumn bloom is observed seasonally at 43°S (off Hobart) (Fig 2).

SST and Chl are typically anti-correlated, with cooler surface waters nested within broader regions of warmer water usually indicating upwelling of deeper waters to the surface and/or vertical mixing, which generally brings nutrient rich waters into the euphotic zone inducing phytoplankton community growth in response. Being a western boundary current, the EAC instead transports warm and nutrient-poor water southward, in a general region of downwelling (rather than upwelling). Since the EAC flows southward year-round, Chl concentrations are typically low in the EAC pathway all through the year.

4.1. EAC formation and intensification region

Our climatological results show that summer (DJF) average Chl concentrations are very low in the EAC formation region (15ºS-22ºS) (Ridgway and Dunn, 2003), with a small standard deviation. While Chl is typically low in summer in this region, At these lower latitudes, summer defines the annual phytoplankton biomass minimum. In the EAC intensification region (22ºS-35ºS) (Ridgway and Dunn, 2003), average summer-time Chl concentrations are similarly low. Additionally, the anticyclonic circulation cells that characterize the region (Ridgway and Dunn, 2003) generally induce upwelling deepening further the thermocline, pushing away nutrients from the euphotic depth. Limiting Chl abundance at the surface even more. However, the larger standard deviations observed in this region during summer are likely to be induced by EAC seasonal intensity maximum (Ridgway and Godfrey, 1997) originating meanders (Ridgway and Dunn, 2003) that will disturb the water column structure, and may induce some nutrient rich deep water towards the surface.

Nevertheless, no enhancement of Chl is observed, suggesting these this flow increase is not strong enough to bring deeper water into the euphotic depth during this season. Overall, there is no clear influence of the EAC on Chl during summer, or throughout the year, in either the formation or intensification regions, except for a subtle decrease of Chl during spring (SON) following the annual Chl maximum as the annual EAC transports begin to intensify.

4.2. EAC separation zone

The main EAC jet separates from the coast at some point between 30ºS and 31.5ºS, where the orientation of the coastline changes. Between 33ºS and 35ºS, the EAC turns sharply to the east (Ridgway and Dunn, 2003). This is a known nutrient enrichment region (Rochford, 1972) that has been well studied (Roughan and Middleton, 2004). This upwelling induced nutrient enrichment occurs as a result of both wind-driven and current-driven processes. Summertime northerly winds, in this region, cause an offshore Ekman transport which brings cool, nutrient rich waters to the surface at the coast, resulting in a regional phytoplankton bloom and, hence, an enhancement of the measured Chl concentrations throughout this EAC region (Baird *et al.*, 2006). Roughan and Middleton (2004) argue that the wind stress forced response is less important than the upwelling caused by encroachment of the EAC across the continental shelf. As the EAC flows southerly the encroachment increases and accelerates the bottom stress on the shelf, enhancing the onshore Ekman pumping at the boundary bottom layer. Our results show that this is observed throughout the year, albeit that the signal is reduced during winter when EAC transports are weaker. The corresponding Chl standard deviations (Fig 1) show the strongest signal in this region during spring (SON), which corresponds in timing with a recurrent regional

algal bloom (Hallegraeff and Jeffery, 1993). At Subtropical latitudes, two distinct low variability patch are observed to occur during SON at the inflow of EAC (Fig 1), one where the main jet of the EAC separates from the coast and turns eastward forming the Tasman Front (~32ºS), and the other follows the southward decline pathway of the EAC extension towards the STF, south of 35ºS (Hamilton, 2006). The Tasman Front is a region characterised by a sharp horizontal gradient of physical and biological properties, where the northern stratified, oligotrophic waters of the Coral Sea meet the vertically well-mixed Tasman Sea with its strong biological activity (Baird *et al.*, 2008). Even though the Tasman Front is a feature with high eddy kinetic energy (Tilburg *et al.*, 2001), it appears to also be a region characterized with little cross-frontal mixing (Baird *et al.*, 2008), consistent with a preference instead for EAC meandering (Hamilton, 1992; Mulhearn, 1987; Stanton, 1981). Thus, the separation of Coral and Tasman Seas in terms of Chl mean values, and high Chl variability throughout the STF dynamical region, mainly during summer, as identified in Fig 1

4.3. The EAC extension (decline region) and Subtropical Front

Following separation from the coast, the EAC bifurcates. The main jet turns sharply eastward (as discussed in the previous subsection), and a weaker jet continues southward, releasing eastward moving eddies until it reaches the STF. Thus in this region, low Chl standard deviations are observed in winter (JJA) and spring (SON), possibly triggered by the more intense EAC during autumn (MAM) (Ridgway and Godfrey, 1997) whereas relatively high Chl variability is observed to the east, which is possibly due to the natural seasonal phytoplankton cycle, plus a higher vertical mixing due to eddy activity. This is well observed at the seasonal transects off Sydney and Merimbula (Fig 2).

The connection between the EAC and the Subtropical Front is commonly described as ambiguous (Ridgway and Dunn, 2003; Stanton and Ridgway, 1988). Following Hamilton (2006), this frontal system has a relatively large mixing area, meridionally through 40-45ºS, where waters from the Tasman Sea meet those from the Subantarctic and mix together. The distribution of Chl concentrations during JJA and SON are similar southwards from ~40ºS. During DJF, however, a zonal increase in Chl occurs down to 45ºS, which is possibly induced by the phytoplankton seasonal cycle caused by the summer-time increase of sunlight, and hence photosynthetically active radiation, combined with the greater water column mixivity due to the high eddy energy present associated with the summer-time intensification of the EAC (Tilburg *et al.*, 2001).

4.4 Inter-annual variability

Based on observations reported by Ridgway et al. (2008), we note that the EAC net transport changed through three phases between October 1997 and December 2005. First, there was an initial increase in transport intensity from 1997-2001. This was followed by a decrease in transport intensity from 2001-2003, and finally the transport became more constant through 2004-2005 (Ridgway et al., 2008). Composite average Chl concentrations calculated for the years defined by these three phases show interesting characteristic changes (Fig 7). An increase in the EAC transport implies a further penetration of low nutrient tropical waters into richer north biogeographical regions. In terms of phytoplankton and Chl variability, this hypothetically would induce lower biological richness and variability. As seen in Fig 7A, during the multi-year EAC transport increase period we observe negative anomalies of Chl, as hypothesized. Hence, a decrease should bring higher Chl

observations, however, this appears to occur only in the north side of the studied region, the South Coral Sea. This might occur due to the strong gradient observed in the Tasman Front, as discussed previously in section 4.1.3, which allow little mixivity between both water masses, the Coral and Tasman Seas. Thus, in a decrease EAC transport period, less tropical nutrient poor waters are brought into the region, which may induce higher concentrations of Chl.

Despite the complex relationship, EAC transport can be related to ENSO variability. Holbrook et al. (2010) showed that ENSO dominated inter-annual to decadal scales is strongly connected to the modulation of the EAC transport, by the action of westward propagating Rossby waves. Composites of ENSO events show that Chl is most impacted on during ENSO variability at the Tasman Sea and STF regions. On the other hand, SAM might have a bigger influence in the southern end of the EAC region, where positive events induce low Chl in convergent STF, as observed by Lovendusky and Gruber (2005). However, a Tasmanian connection with the Southern Hemisphere Supergyre would possibly enhance Chl values in the region. As shown in Fig 7D, during the inter-annual period of increasing EAC net transport, the SON season has strong concentrations of Chl suggesting that high eddy activity may have been present at this time.

5. Conclusions

We have shown that the injection of nutrient poor EAC waters only have a seasonal influence on regional open water Chl concentrations from where the EAC intensifies southward. This influence is mostly observed during the austral spring-time in temperate latitudes and during the austral summer at higher latitudes. Inter-annually, an increase in EAC net transport tends to correspond to a decrease in Chl

concentrations in all four EAC-featured regions, whilst a decrease in EAC transport corresponds with increased Chl concentrations in the Coral Sea. ENSO variability is associated with a decrease (increase) of Chl in the northern (southern) EAC regions, and a decrease (increase) of Chl in the southern region during an El Nino (La Nina) event. We also find that a SAM+ event corresponds with a decrease in Chl, mainly in the region of the Subtropical Front.

References

Baird, M.E., Timko, P.G., Middleton, J.H., Mullaney, T.J., Cox, D.R., Suthers, I.M., 2008. Biological properties across the Tasman Front off southeast Australia. Deep Sea Research Part I: Oceanographic Research Papers 55 (11), 1438-1455.

Baird, M.E., Timko, P.G., Suthers, I.M., Middleton, J.H., 2006. Coupled physical-biological modelling study of the East Australian Current with idealised wind forcing. Part I: Biological model intercomparison. Journal of Marine Systems 59 (3-4), 249-270.

Behrenfeld, M.J., O'Malley, R.T., Siegel, D.A., McClain, C.R., Sarmiento, J.L., Feldman, G.C., Milligan, A.J., Falkowski, P.G., Letelier, R.M., Boss, E.S., 2006. Climate-driven trends in contemporary ocean productivity. Nature 444 (7120), 752-755.

Cai, W., Shi, G., Cowan, T., Bi, D., Ribbe, J., 2005. The response of the Southern Annular Mode, the East Australian Current, and the southern mid-latitude ocean circulation to global warming. Geophys. Res. Lett. 32.

Condie, S.A., Dunn, J.R., 2006. Seasonal characteristics of the surface mixed layer in the Australasian region: implications for primary production regimes and biogeography. Marine and Freshwater Research 57, 569–590.

Field, C.B., Behrenfeld, M.J., Randerson, J.T., Falkowski, P., 1998. Primary production of the biosphere: Integrating terrestrial and oceanic components. Science 281 (5374), 237-240.

Hallegraeff, G.M., Jeffery, S.W., 1993. Annually recurrent diatom blooms in spring along the NSW coast of Australia. Aust. J. Mar. Freshw. Res 44, 325 – 334

Hamilton, L.J., 1992. Surface circulation in the Tasman and Coral Seas: climatological features derived from bathythermograph data. Australian Journal of Marine and Freshwater Research 43, 793-822.

Hamilton, L.J., 2006. Structure of the Subtropical Front in the Tasman Sea. Deep Sea Research Part I: Oceanographic Research Papers 53 (12), 1989-2009.

Holbrook, N.J., Goodwin, I.D., McGregor, S., Molina, E., Power, S.B., 2010. ENSO to multi-decadal time scale changes in East Australian Current transports and Fort Denison sea level: Oceanic Rossby waves as the connecting mechanism. Deep Sea Research Part II: Topical Studies in Oceanography 58 (5), 547-558.

Holbrook, N.J., S-L, C.P., Venegas, S.A., 2005. Oscillatory and propagating modes of temperature variability at the 3–3.5- and 4–4.5-yr time scales in the upper southwest Pacific Ocean. Journal of Climate 18, 719-736.

Holbrook, N.J., S-L, C.P., Venegas, S.A., 2005b. Corrigendum. Journal of Climate 18 (1637-1639).

Jitts, H.R., 1965. The summer characteristics of primary productivity in the Tasman and Coral seas. Australian Journal of Marine and Freshwater Research 16, 151–162.

Longhurst, A.R., 1998. Ecological Geography of the Sea. Academic Press, San Diego.

Lovenduski, N.S., Gruber, N., 2005. Impact of the Southern Annular Mode on Southern Ocean circulation and biology. GEOPHYSICAL RESEARCH LETTERS 32 (11).

Mulhearn, P., 1987. The Tasman Front: a study using satellite infrared imagery. Journal of Physical Oceanography 17, 1148-1155.

Nilsson, C.S., Cresswell, G.R., 1980. The formation and evolution of East Australian current warm-core eddies. Progress in Oceanography 9 (3), 133-183.

Ridgway, K.R., Coleman, R.C., Bailey, R.J., Sutton, P., 2008. Decadal variability of East Australian Current transport inferred from repeated high-density XBT transects, a CTD survey and satellite altimetry. J. Geophys. Res. 113.

Ridgway, K.R., Dunn, J.R., 2003. Mesoscale structure of the mean East Australian Current System and its relationship with topography. Progress in Oceanography 56 (2), 189-222.

Ridgway, K.R., Godfrey, J.S., 1994, Mass and heat budgets in the East Australian current: A direct approach, *J. Geophys. Res.*, *99*(3231–3248).

Ridgway, K.R., Godfrey, J.S., 1997. Seasonal cycle of the East Australian Current. J. Geophys. Res. 102.

Rochford, D.J., 1972. Nutrient enrichment of east Australian coastal waters: I. Evans Head upwelling. Tech. rep., Division of Fisheries and Oceanography, CSIRO, Australia.

Roughan, M., Middleton, J.H., 2004. On the East Australian Current: Variability, encroachment, and upwelling. J. Geophys. Res. 109.

Stanton, B.R., 1981. An oceanographic survey of the Tasman Front. New Zealand Journal of Marine and Freshwater Research 15, 289-297.

Stanton, B.R., Ridgway, N.M., 1988. An oceanographic survey of the subtropical convergence zone in the Tasman Sea. New Zealand Journal of Marine and Freshwater Research 22, 583-593.

Tilburg, C.E., Hurlburt, H.E., O'Brien, J.J., Shriver, J.F., 2001. The dynamics of the East Australian Current system: The Tasman Front, the East Auckland Current and the East Cape Current. J. Phys. Oceanogr. 31 (2917 – 2943).

Tilburg, C.E., Subrahmanyam, B., O'Brien, J.J., 2002. Ocean color variability in the Tasman Sea. Geophys. Res. Lett. 29.

Trenberth, K.E., 1997. The Definition of El Niño. Bulletin of the American Meteorological Society 78 (12), 2771-2777.

Wilkin, J.L., Morrow, R.A., 1994. Eddy kinetic energy and momentum flux in the Southern Ocean: comparison of a global eddy-resolving model with altimeter, drifter, and current-meter data. Journal of Geophysical Research 99 (C4), 7903-7916.

Figures

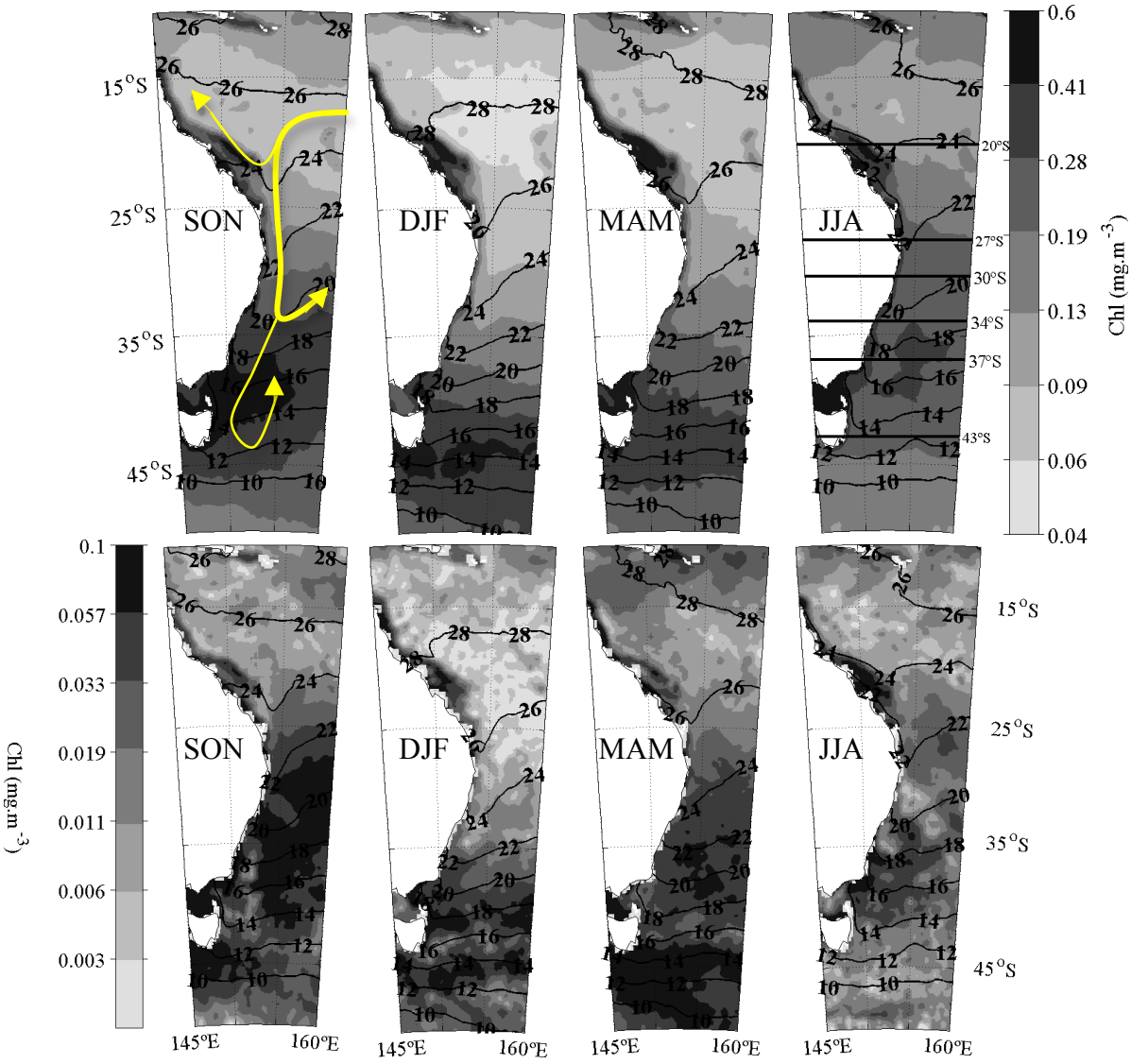

Figure 1. Maps of the Chl concentration seasonal means (top row) and standard deviations (bottom row). Corresponding seasonal SST averages are superimposed by contours in ºC (black solid line). General EAC flow in yellow (adapted from *Hamilton* [2006]). The maps are presented in Lambert projection.

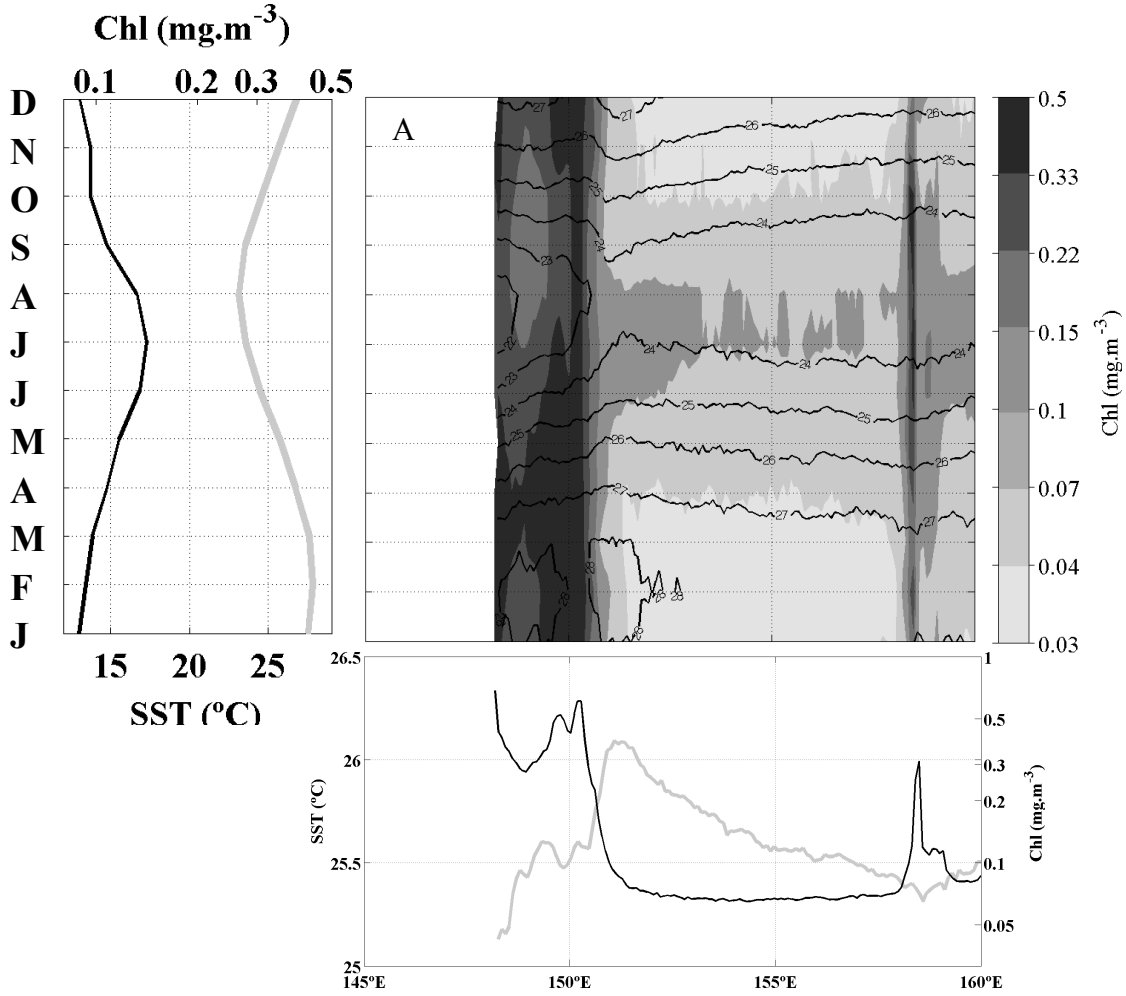

Figure 2(A): Results here correspond to analyses of data along 20°S transect off **Bowen**. Top right: Longitude-time plot of the seasonal (monthly average) cycle of Chl (grey-scale shading) and SST (°C, contours); Top left: Time average of the right panel, demonstrating monthly climatological mean Chl (black line) and SST (grey line). Bottom: Longitudinal average of the top right panel demonstrating annual average Chl concentrations (black line) and SST (grey line).

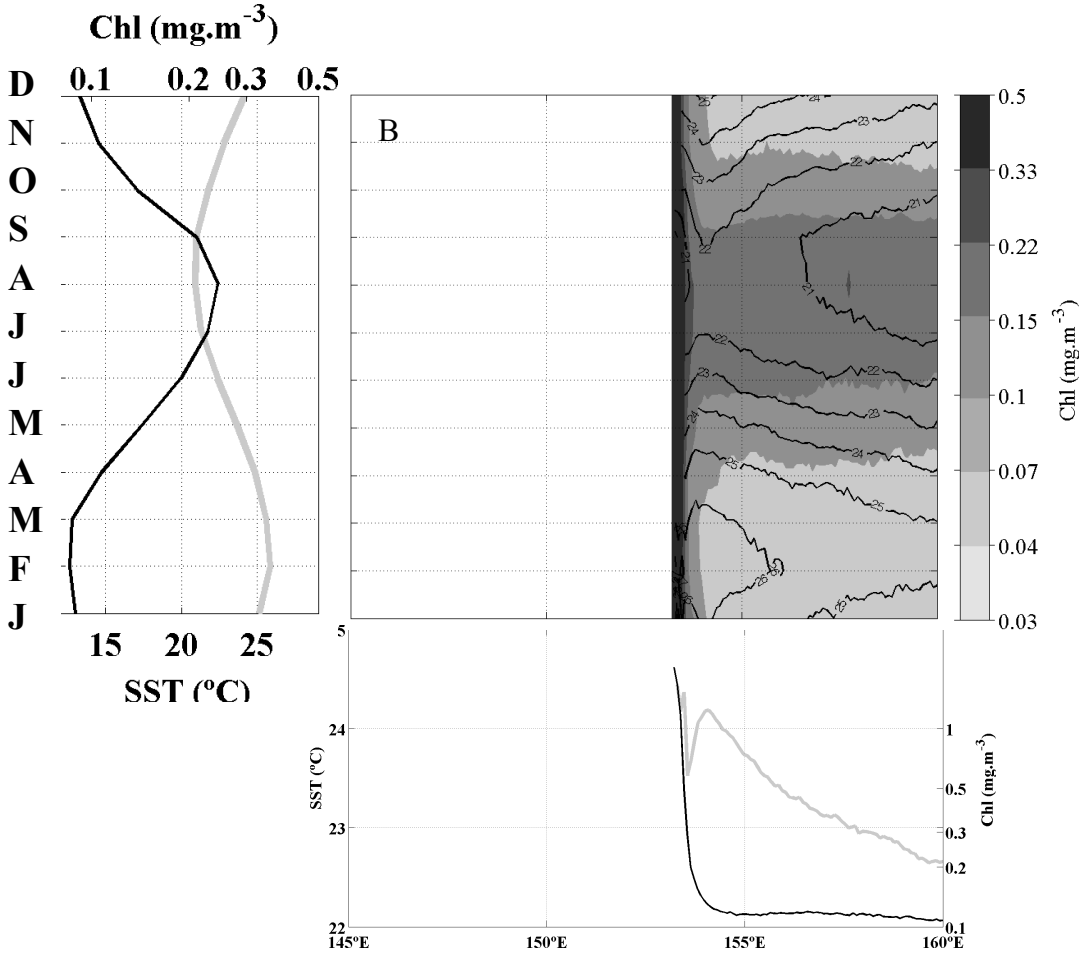

Figure 2(B): As per Fig 2(A), but instead along 27^{o}S off **Brisbane**.

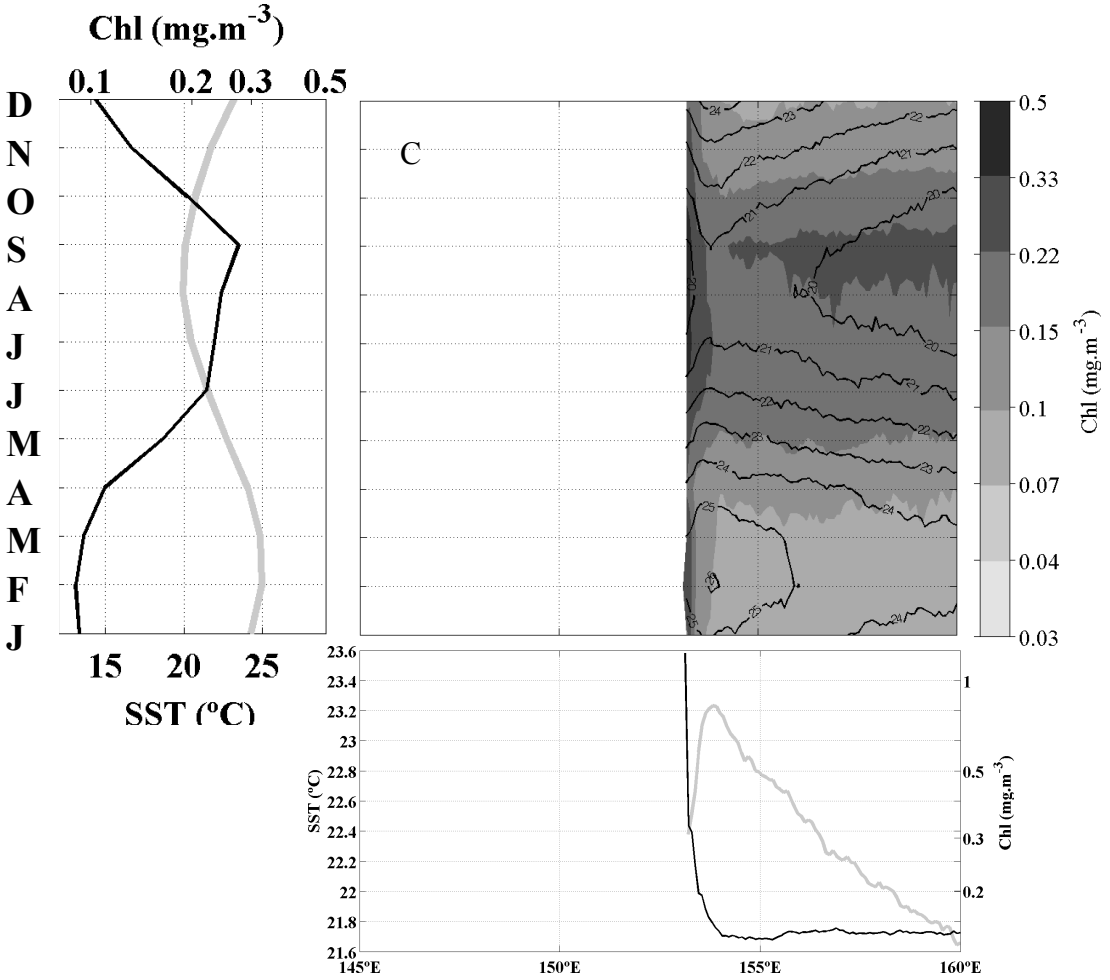

Figure 2(C): As per Fig 2(A), but instead along 30°S off **Coffs Harbour**.

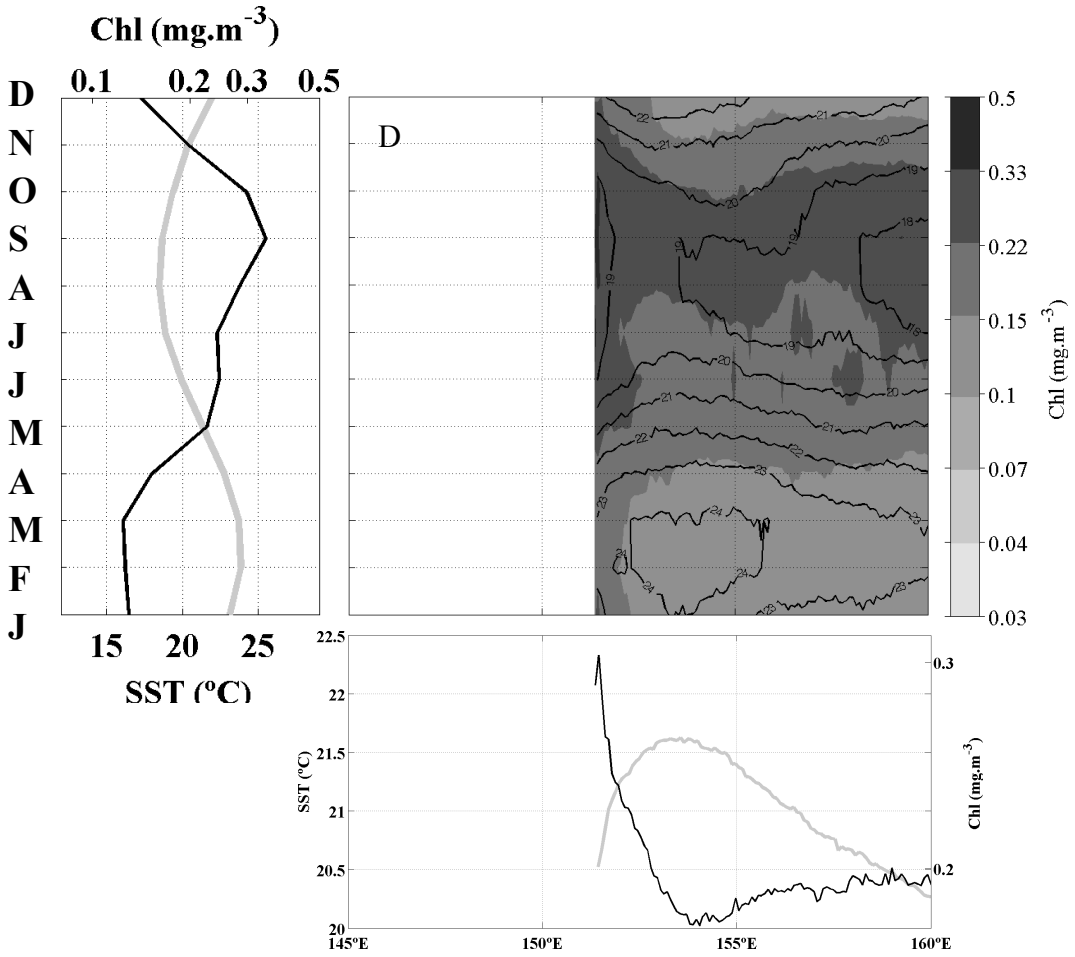

Figure 2(D): As per Fig 2(A), but instead along 34°S off **Sydney**.

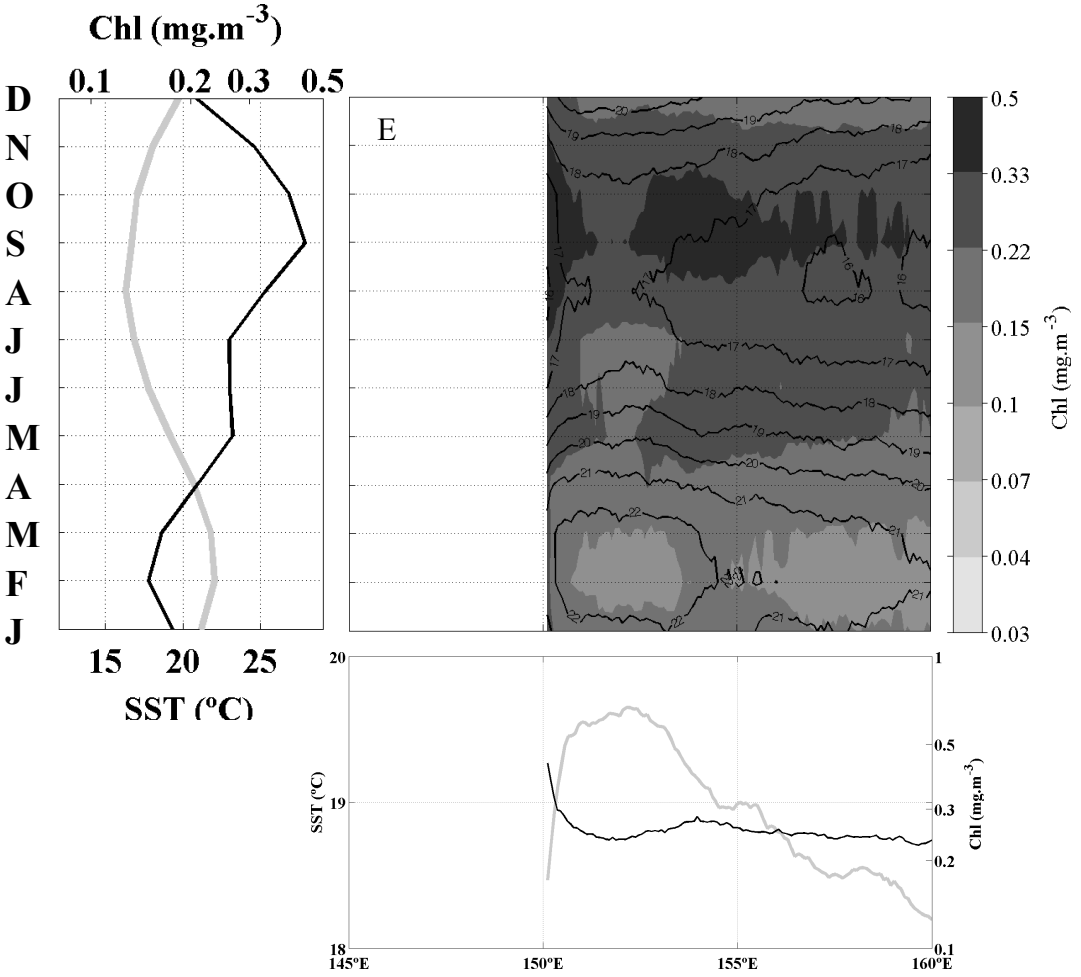

Figure 2(E): As per Fig 2(A), but instead along 37°S off **Merimbula**.

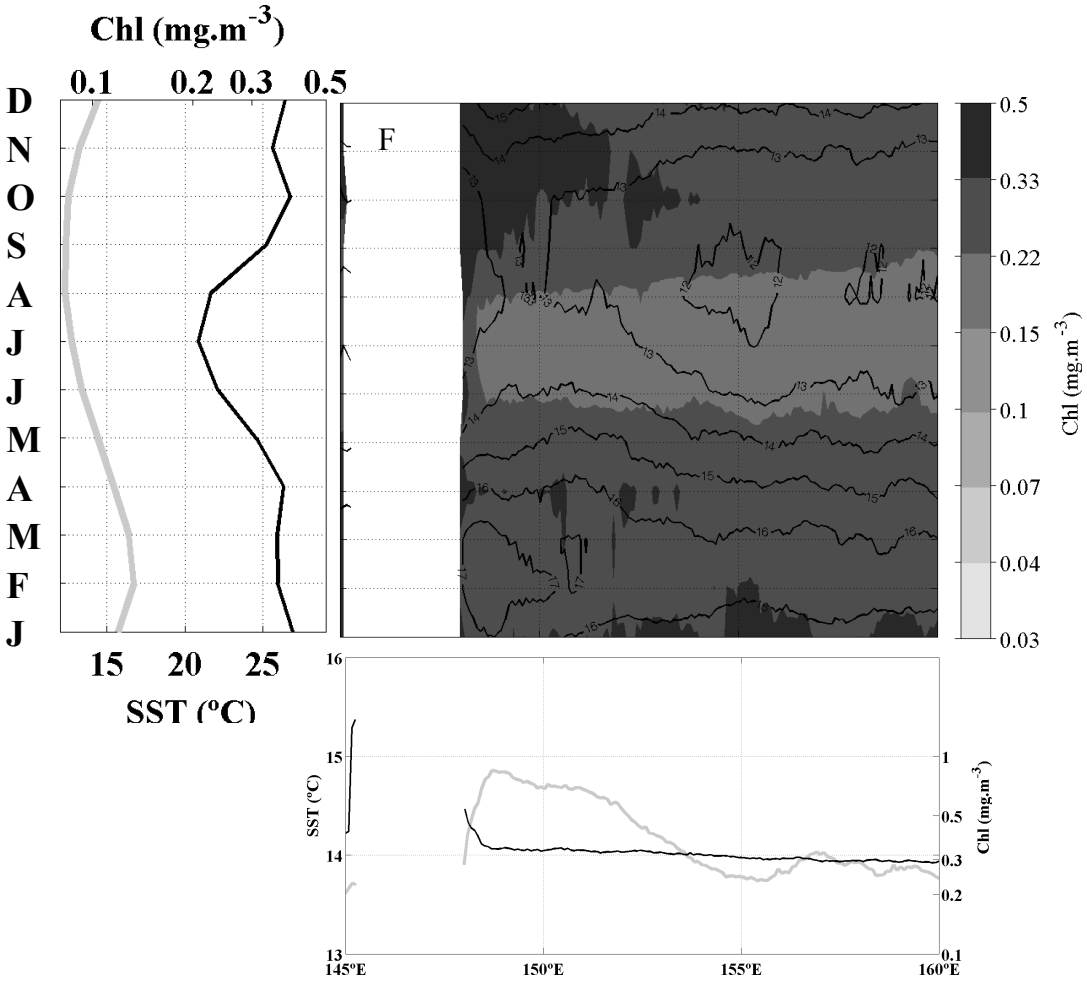

Figure 2(F): As per Fig 2(A), but instead along 43°S off **Hobart**.

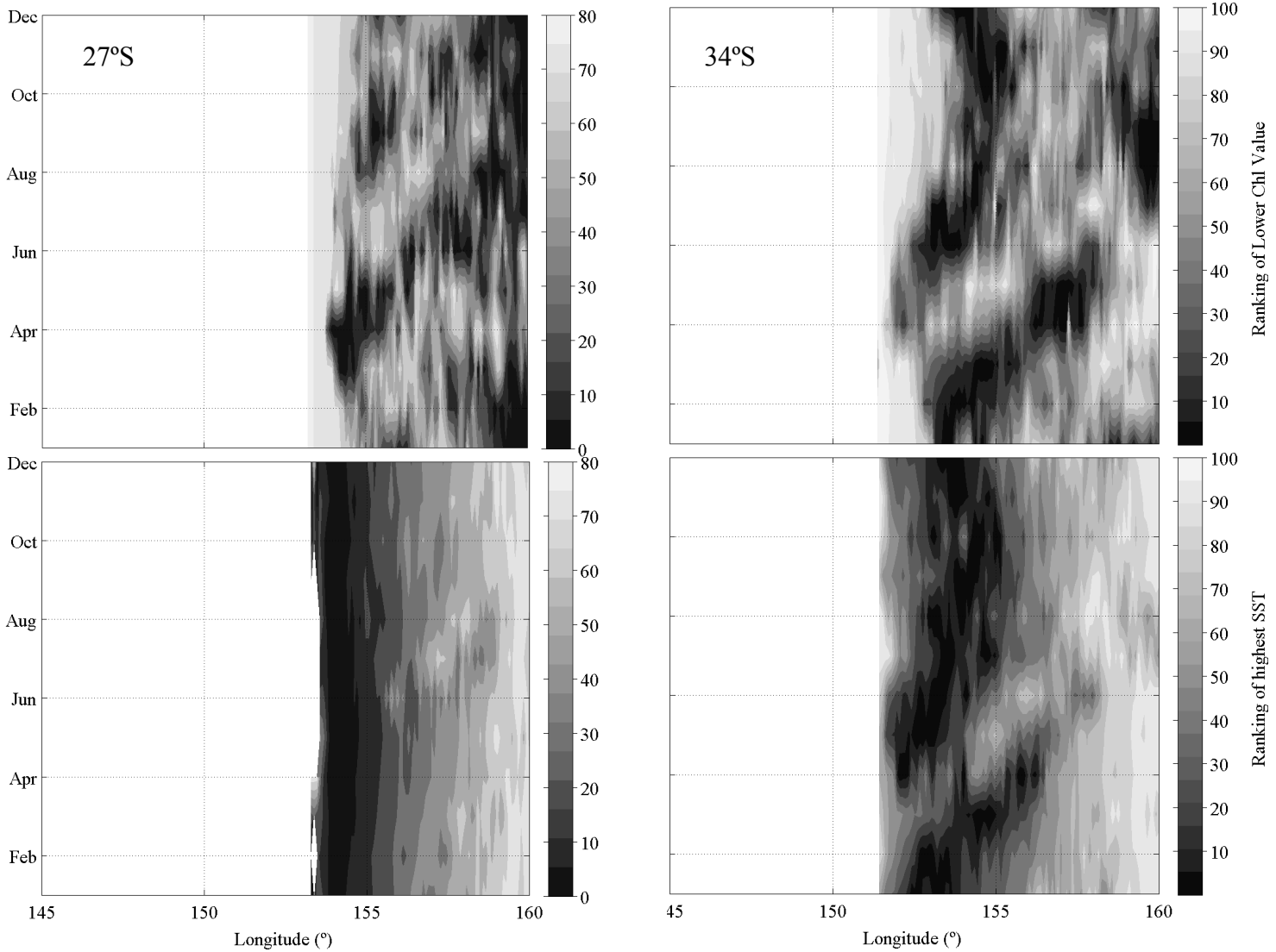

Figure 3. Zonal rank of the Chl concentration minima (top row) and SST maxima (bottom row) along Brisbane (27ºS), Sydney (34ºS), Merimbula (37º) and Hobart (43ºS) transects.

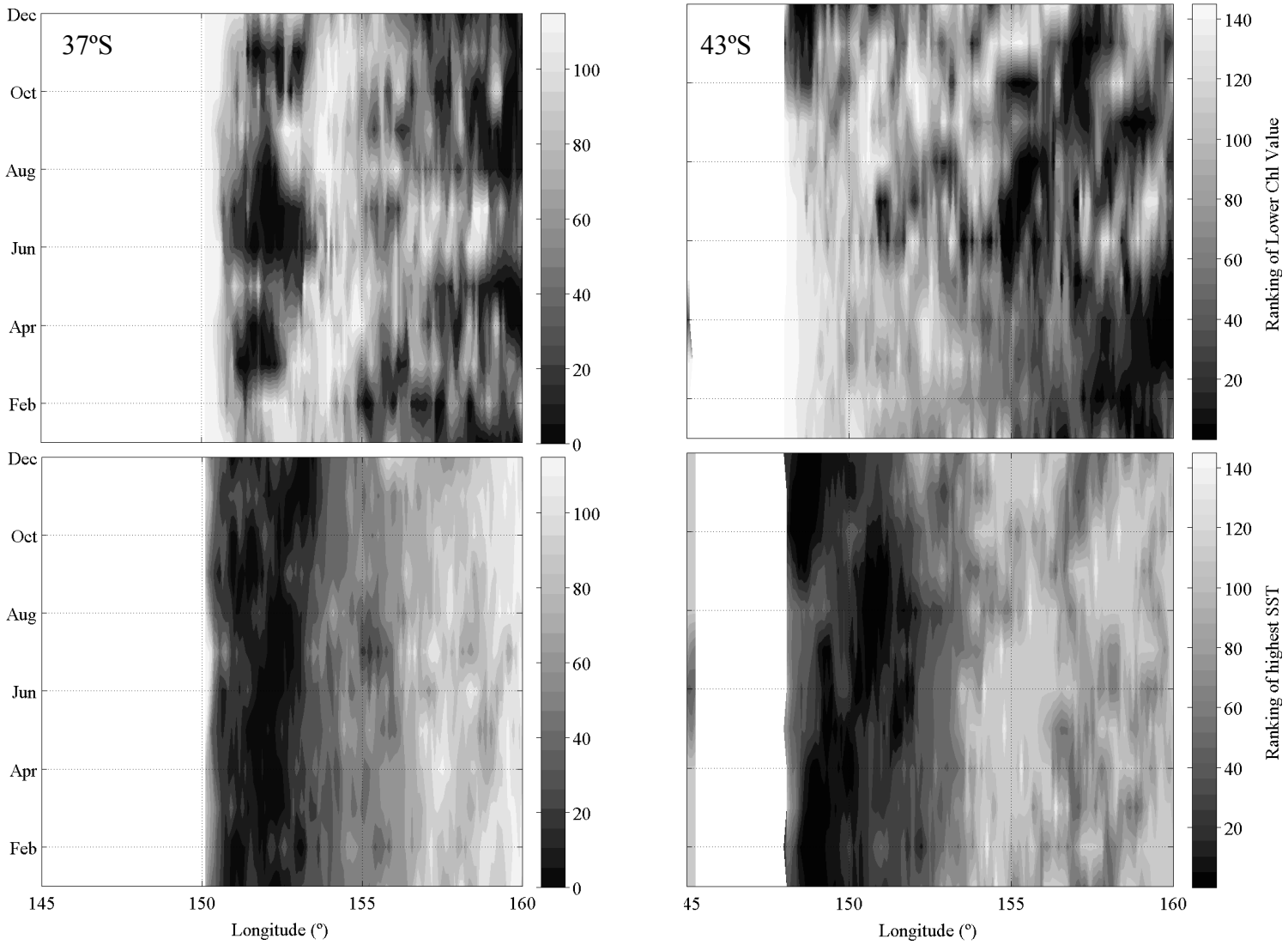

Figure 3. (Continuation).

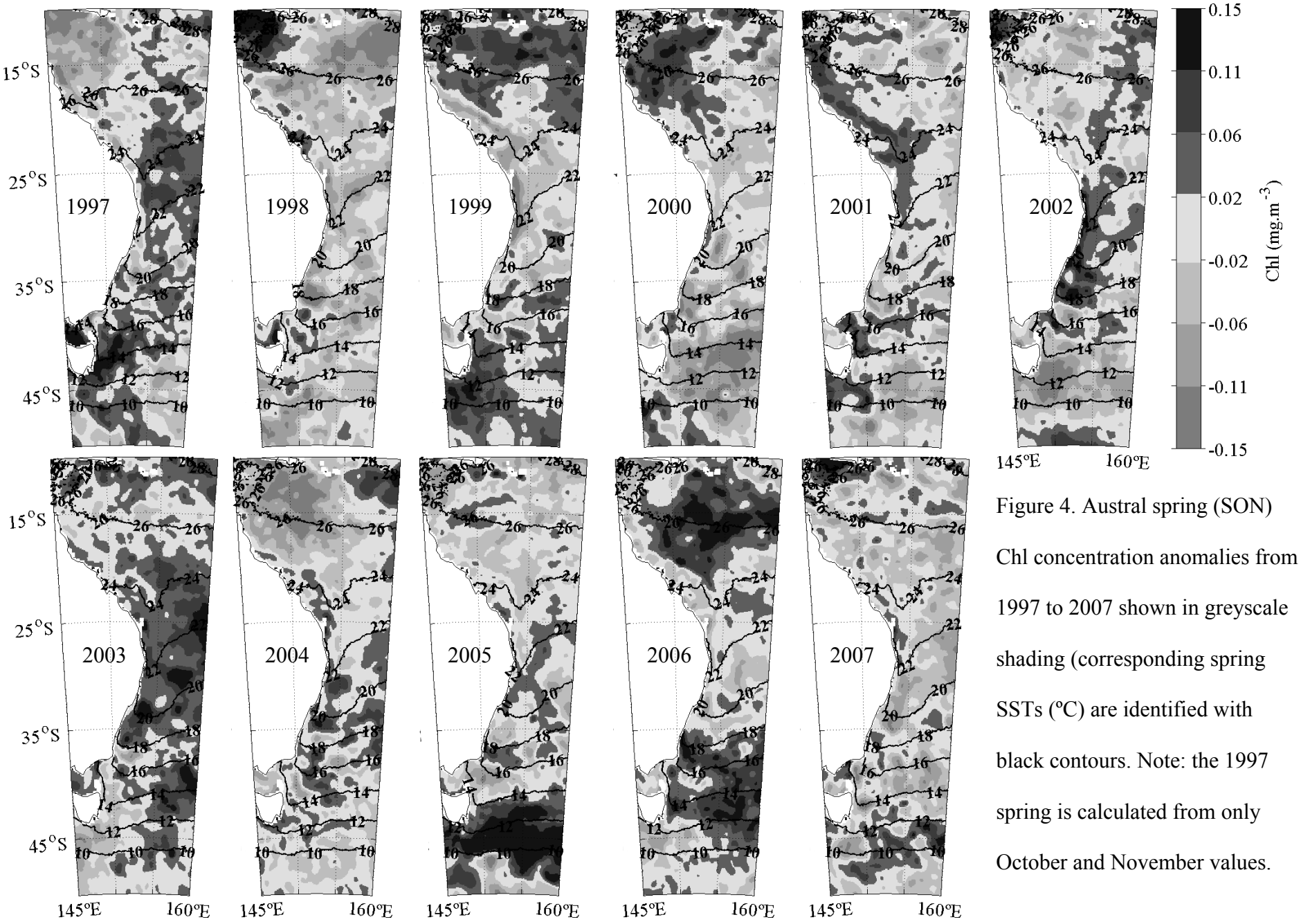

Figure 4. Austral spring (SON) Chl concentration anomalies from 1997 to 2007 shown in greyscale shading (corresponding spring SSTs (ºC) are identified with black contours. Note: the 1997 spring is calculated from only October and November values.

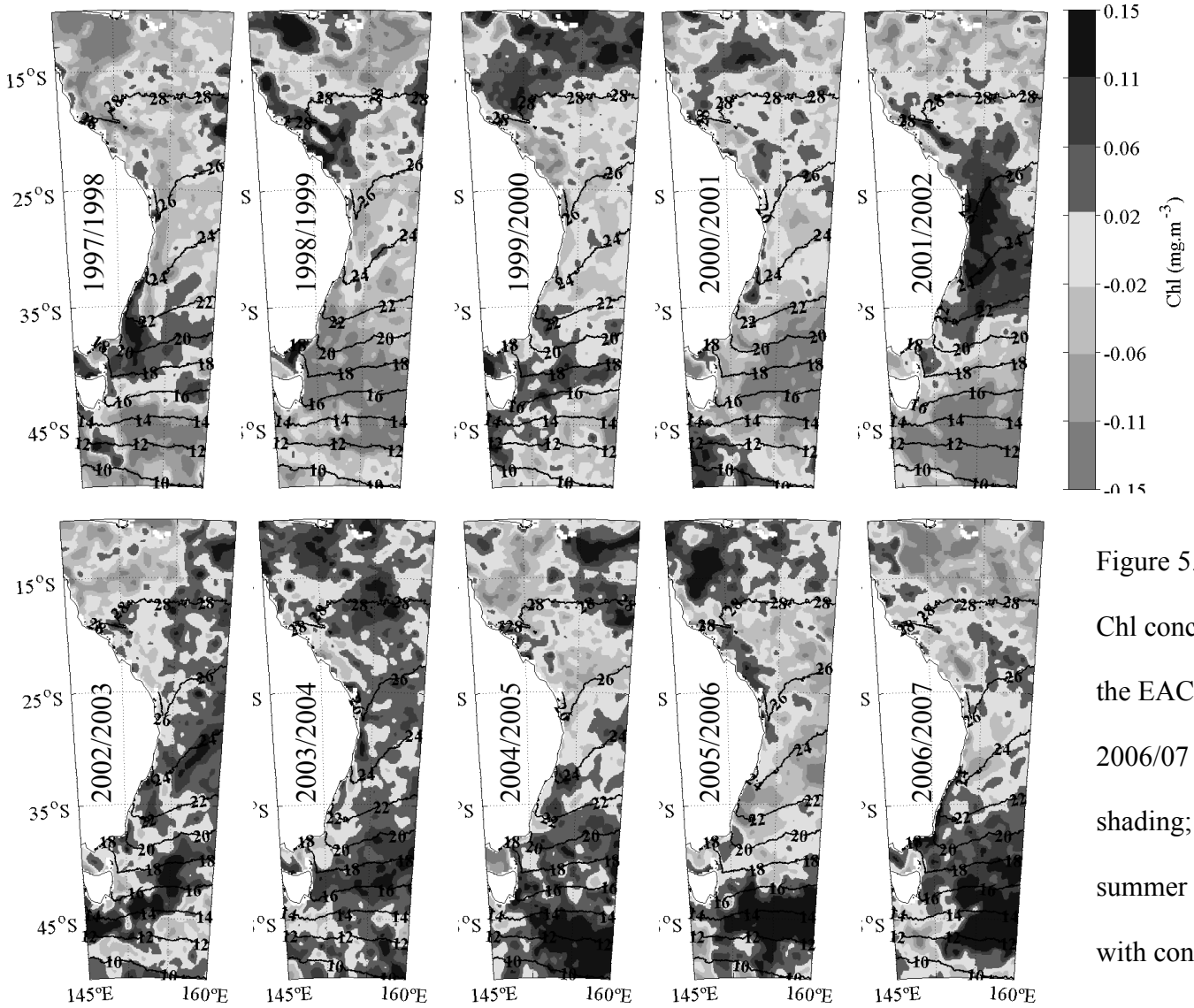

Figure 5. Austral summer (DJF) Chl concentration anomalies in the EAC region from 1997/98 to 2006/07 shown in greyscale shading; The corresponding summer SSTs (ºC) are identified with contour lines.

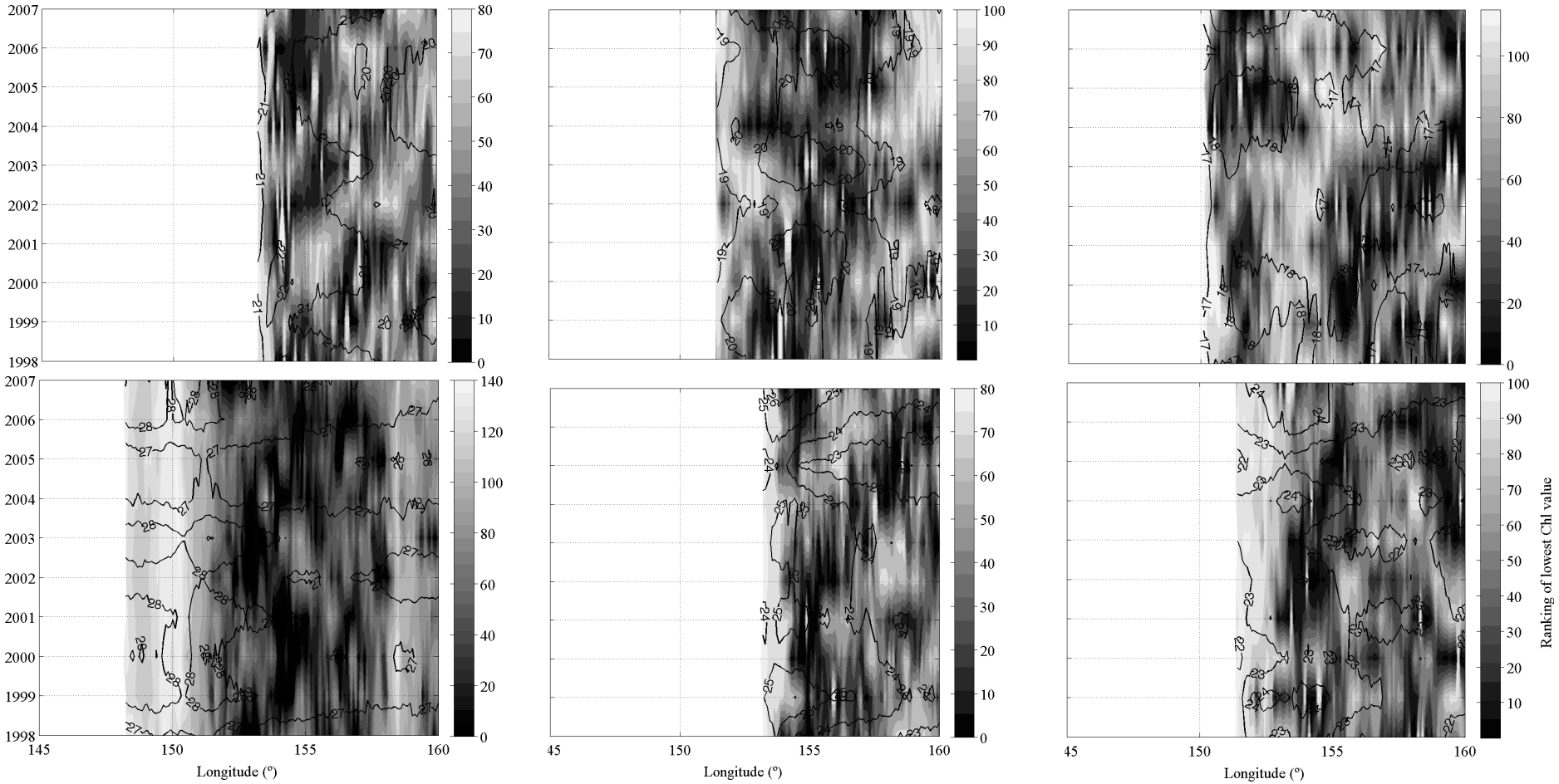

Figure 6. Zonal Ranking of the lowest Chl value during: interannual austral spring (top row) at Coffs Harbor (30ºS, left), Sydney (34ºS, middle) and Merimbula (37ºS, right); inter-annual summer (bottom row) at Bowen (20ºS, left), Coffs Harbor (middle) and Sydney (right), from 1997/98 to 2006/07; with respective SST profiles, in ºC (contour lines).

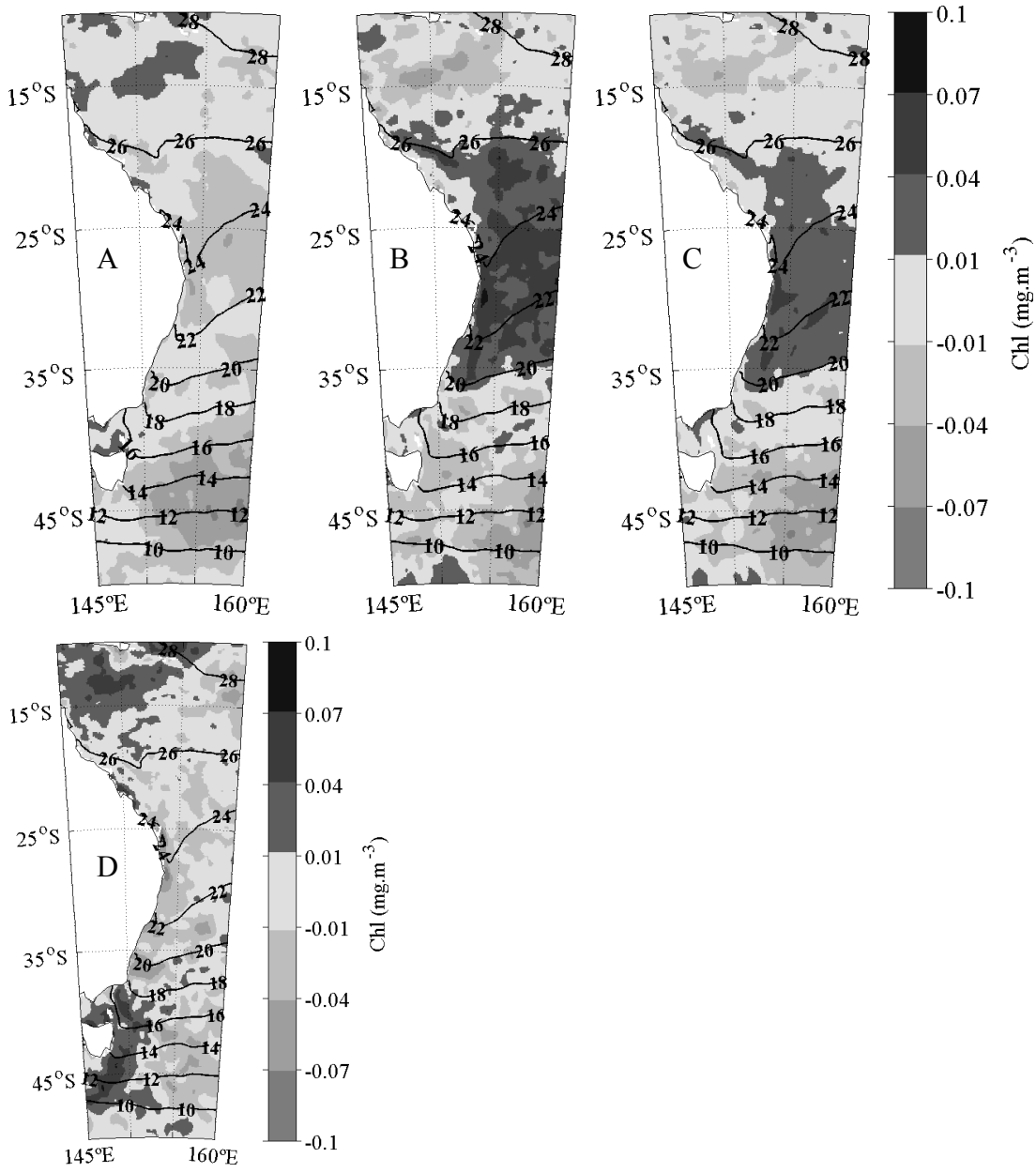

Figure 7. Average Chl concentrations from (A) October 1997 to December 2000, (B) January 2001 to December 2003, (C) January 2004 to December 2005, corresponding to a multi-annual increase (A), decrease (B), and relatively constant (C) net EAC transport based on calculations from repeat XBT surveys along the PX34 line {Ridgway, 2008 #264}. (D) Composite map of the SON Chl concentration anomalies during the EAC increasing transport period from 1997-2000. All maps show the corresponding mean SST (^{o}C) with contour lines.

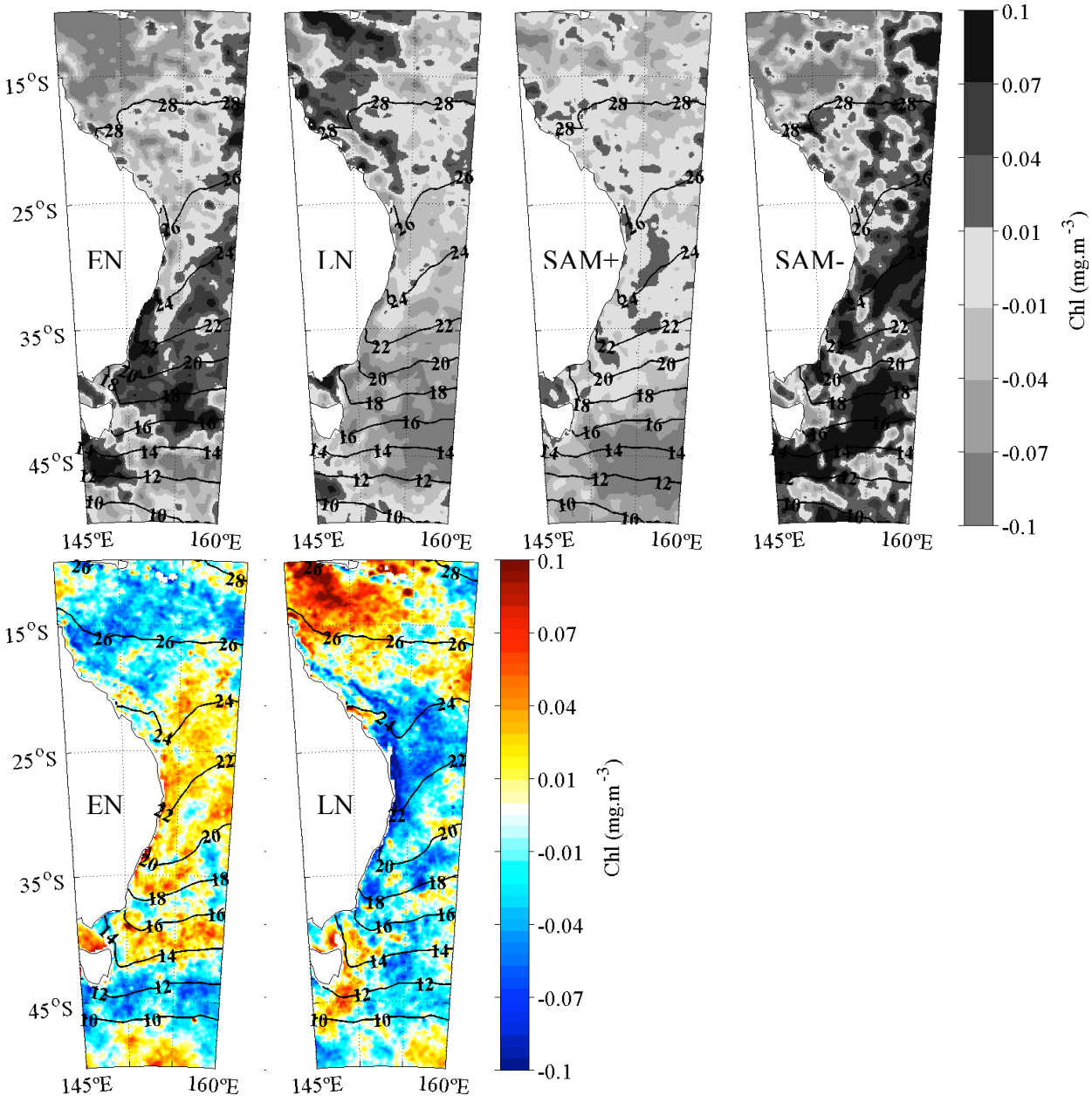

Figure 8. Chl composite anomalies during EN (1997/98 and 2002/03), LN (1998/99, 1999/00, 2000/01), SAM+ (1997/98, 1998/99, 1999/00 and 2001/02) and SAM- (2002/03) events during DJF (top four panels), and EN and LN events during SON (bottom two panels). Corresponding seasonal SST (ºC) is superimposed on each panel with contour lines.

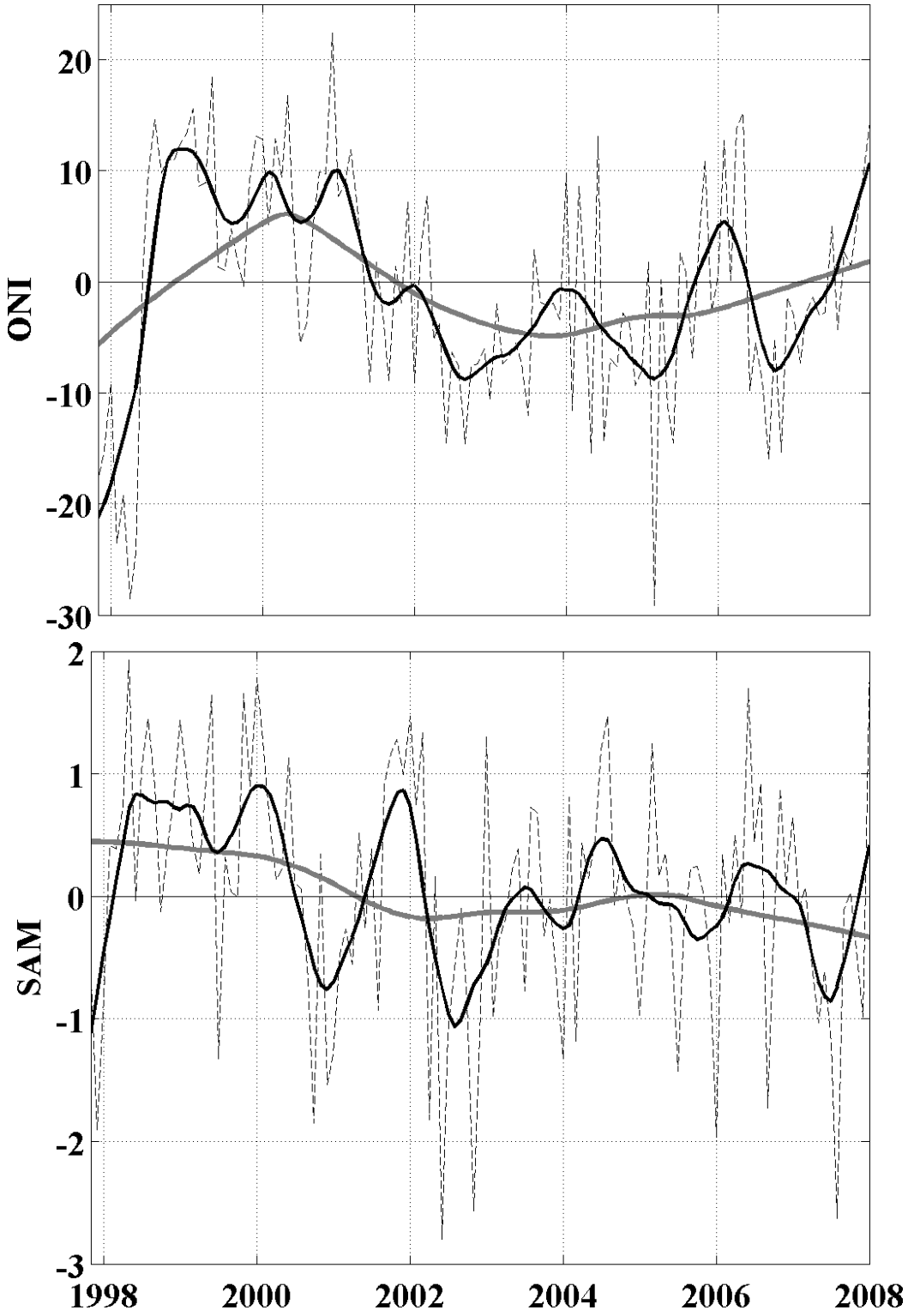

Figure 9. The monthly NINO3.4 (top) and SAM (bottom) index time series (dashed line). Also shown are the corresponding 12-month running mean filtered (black solid line) and 5-year running mean filtered (grey solid line) time series.

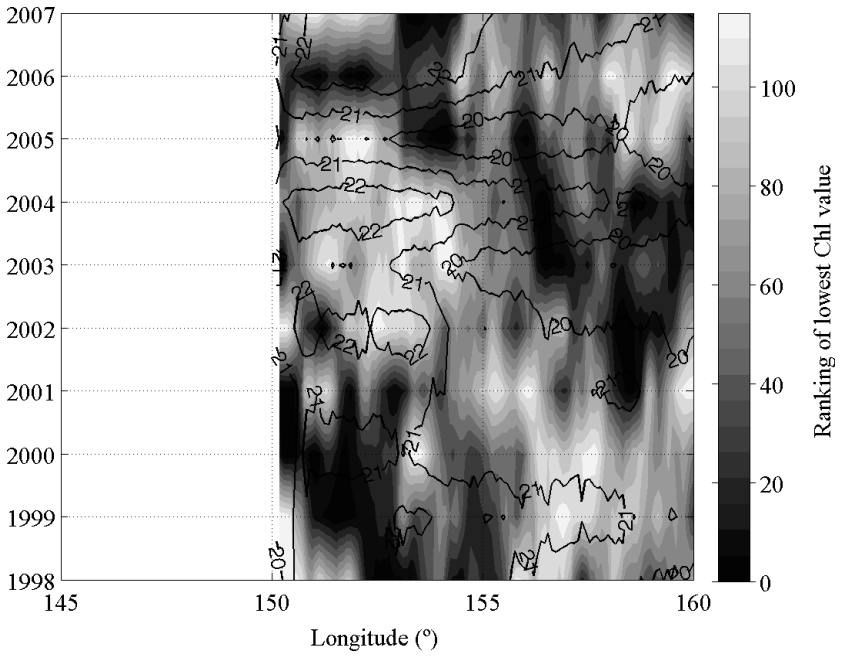

Figure 10. Zonal Ranking of the lowest Chl anomaly value during austral summer composites at Merimbula (37ºS) with respective SST profiles, in ºC (contour lines).

8.3 CHAPTER SUMMARY

In this chapter, we demonstrate that the regional EAC southward influx of poor nutrient waters impacts Chl concentration and variability throughout the South Coral and Tasman Seas. This influence is most conspicuous during spring and summer at higher latitudes. Nevertheless, inter-annual variation of the EAC transport is coupled with Chl variability throughout the region and strong ENSO and SAM events are related to Chl changes of the same amplitude.

CHAPTER 9

GENERAL DISCUSSION AND CONCLUSIONS

The global volume of phytoplankton is dependent on gain and loss processes. Regional environmental conditions may influence growth rate directly (sunlight and nutrient) or indirectly (e.g. wind), whilst advection and grazing may induce a significant regional biomass loss. Environmental climatic factors critically influence phytoplankton net primary productivity (NPP) across several temporal scales. Phytoplankton biomass varies mostly within intra-annual scales. Its global biomass is consumed every 2 to 6 days (Behrenfeld and Falkowski, 1997), and roughly 60% (Yoder and Kennelly, 2003) of its monthly variance is explained during its annual cycle. Inter-annual and multi-annual variability of NPP is predominantly induced by the El Niño – Southern Oscillation (ENSO), whilst decadal patterns are suggested to be linked to the Pacific Decadal Oscillation (Chavez *et al.*, 2011).

Our findings empirically confirm that ENSO is the main driver of NPP inter-annual global variability (chapter 3 and 5), and show that decadal patterns are induced by an ENSO related mode known as El Niño – Modoki (EM). Although, the relationship between EM and ENSO is still unresolved (Takahashi *et al.*, 2011), and the effect of anthropogenic induced climate change on ENSO is highly uncertain (Latif and Keenlyside, 2009), it has been suggested that EM might be derived from the influence of climate change on ENSO (Yeh *et al.*, 2009). Our analysis cannot determine anthropogenic influence on NPP variability mainly due to the small period that the data covers (Henson *et al*., 2009). However, as discussed in the literature the past decadal warming trend is almost certainly due to anthropogenic influence (Barnett *et al.*, 2005; IPCC, 2007; Lyman *et al.*, 2010). Further, our results indicate that the influence of EM on NPP was enhanced in the last decade due to the decadal

trend. And, consequently an additional 18 Pg C was fixed in the ocean via phytoplankton production. The NPP pattern induced by the ENSO mechanism, however, showed no significant difference due to the last decadal trend. The last decade, within the context of a century's timescale, suggests that the trend may be part of a decadal or multi-decadal signal such as the Pacific Decadal Oscillation (Chavez *et al.*, 2011), however, our results show no linkage of the interannual NPP variability with such climate mechanism. Nevertheless, centennial evaluations of NPP patterns are unable to shed further light due to the lack of available data which spans such long temporal scales (Henson *et al.*, 2010; Mackas, 2011; McQuatters-Gollop *et al.*, 2011; Rykaczewski and Dunne, 2011).

In chapter 4, we focused on the main climatic mechanism for inter-annual NPP variability, i.e., ENSO and found that this signal accounted for 9 $Pg.C.yr^{-1}$. We also identified an independent third mode of inter-annual NPP variability, which was strongly linked to this mechanism albeit with lag of 8 months, hence, suggesting that this third mode also represented NPP variability induced by ENSO dynamics.

The evolution of ENSO is arguably well studied (Joseph and Nigam, 2006) and propagating features from ENSO dynamics is known to cross atmospheric and oceanic boundaries (Weare, 2010; White, 1994) though phytoplankton related spatial propagating features are rare to find in the published literature. The novelty of ocean colour satellite observations available during the strong ENSO transition that occurred in 1997/98, provided the unique opportunity to study how such an event impacts global NPP (e.g.Behrenfeld *et al.*, 2001). In chapter 4, we used the extended Empirical Orthogonal Functions (EEOF) technique, thus taking into account propagating features, to evaluate the impact of ENSO on NPP. We discovered that

the ENSO propagating mode now included the previously mentioned independent third mode as the 11th month step of propagation. This result also resembled the synoptic spatial pattern obtained from the difference between the 1997/98 El Niño phase and the 1998/99 La Niña (Behrenfeld *et al.*, 2001). This led us to focus our analysis on the main ENSO region, the Tropical Pacific, which we then extended to the South Pacific to evaluate the impacts of such a phenomenon outside of its main region of influence.

The influence of ENSO on the eastern Tropical Pacific has long been observed (Barber and Chavez, 1983; Pennington *et al.*, 2006). The along-shore component of the trade winds pushes the upper oceanic layer westward through Ekman drift, forcing an intense coastal upwelling, which spreads across the Equatorial Pacific in response to the north/south trade wind Ekman divergence (Amador *et al.*, 2006). This forces the up/downwelling mechanism (Amador *et al.*, 2006), triggering phytoplankton variability observed in the region (Pennington *et al.*, 2006), which occurs more intensively during austral winter up to early spring (Wyrtki *et al.*, 1976). Our results confirmed a seasonal harmony between wind speed (WS) and Chl in this region (chapter 6), whereas the central-east equatorial 'cold tongue' region showed that Chl concentrations followed a seasonal variability according to the pattern of outgoing long-wave radiation (OLR) and sea level pressure (SLP). The results for the latter region suggest that seasonal variability of Chl here is linked to cloudless skies, which occurs when WS also increases. The Western Pacific Warm Pool (WPWP) varies in response to sea surface temperature (SST) and WS forcing (chapter 6). This is a region where warm, nutrient-poor surface waters converge and seasonality in the NECC and SECC transports, enhance water column mixing thus bringing deep

nutrients to the euphotic depth and improving conditions for phytoplankton growth (Messié and Radenac, 2006).

The Inter-Tropical and the South Pacific Convergence Zones (ITCZ and SPCZ, respectively), also appear to affect regional seasonal variability of Chl. As seen in chapter 6, the wet season caused by the seasonal southward emigration of the ITCZ and identified by OLR, signifies less Chl. This relationship, however, is reversed within the southern WPWP region possibly due to the seasonal increase in NECC and SECC transport, which occurs simultaneously with the heavy rain period. This hypothesis can be further extended to the western SPCZ region, where the Chl cycle is otherwise counter-intuitive to what is normally expected from its relationship with SST or WS forcing. Conversely, Chl in the eastern part of the SPCZ shows an impressive seasonal coherence with SST (negatively), WS (positively) and OLR (negatively), hence suggesting that phytoplankton increases in abundance when nutrient rich waters are surfaced (through increase in WS) in the rain season. These Chl 'boundaries' are well illustrated by sea surface height (SSH) seasonality (chapter 6).

At higher latitudes in the South Pacific, Chl seasonality is closely related to either SST or WS variability, which are indirect indicators of either solar radiation or nutrient availability (Longhurst, 1998). SST and WS have a seasonal cycle which is significantly in harmony with Chl over most of the South Pacific except in instability induced oceanic frontal zones such as in the subtropical frontal region.

Nevertheless, it was found that when using SST, photosynthetically available radiation and SSH, almost 60% of the Tropical and South Pacific Chl seasonal variability could be calculated with a high level of confidence, whereas only 40% could be accounted for when solely using SST.

In chapter 7, to verify the signature of the ENSO and EM induced modes on phytoplankton in the Tropical and South Pacific, we used the EEOF technique, as previously used in chapter 4. Although this technique is quite common in the literature being utilized to isolate and compress patterns and link these to known geophysical phenomena, there is an amount of uncertainty that is inherent in this tool which must be considered. Patterns of variability are isolated empirically and by the amount of variance that they explain, without following any specific geophysical coherence. Hence, one can question whether the isolated variability patterns are indeed due to unique natural phenomena, instead of a mixture of somewhat similar processes (Dommenget and Latif, 2002). Nevertheless, the yielded spatial and temporal patterns are strong indicators of what processes might be underpinning such EOF variability modes (Lorenz, 1956), and thus, are considered as such throughout this project.

Our EEOF analysis, which searched for Chl propagating features in the Tropical and South Pacific yielded temporal patterns that significantly matched with ENSO and EM unique modes, even more so than the resemblance found in the spatial patterns (chapter 3 and 4). Whether EM is a unique phenomenon from ENSO or another form of it is still a subject of debate (Li *et al.*, 2010; Takahashi *et al.*, 2011). In fact, both modes have similar spectrum maximums, 2 - 8 years for ENSO (Torrence and Compo, 1998), and, 4 - 10 years for EM (Ashok *et al.*, 2007). Given that these signals also share the same domain, i.e., the Tropical Pacific, a complex and intimate relationship between them is to be expected. Nevertheless, both modes do have unique proprieties and thus are accepted here as different modes. In chapter 7, the propagating Chl inter-annual variability EEOF modes with a cycle of ENSO and

EM maximum spectrum for the last decade is analyzed. Interestingly, the leading mode of the EEOF analysis when L = 28, i.e. targeting ENSO variability, yielded a mode that highly related to EM and explained more variability than the one identified as the ENSO mode. This suggests that EM had more influence on Chl in the past decade than ENSO, contrary to what is commonly suggested by literature (Behrenfeld *et al.*, 2006; Chavez *et al.*, 2011) and indicated in chapter 3 of this report. Nevertheless, each isolated EEOF modes targeted to describe ENSO and EM variability showed features, which corroborated contemporary knowledge of physical mechanisms governing each phenomena. For example, during a transition of ENSO phases, the equatorial Pacific cold tongue warms up from the west to the east, coupled with a similar pattern of decreased Chl (Chavez *et al.*, 2011), while the central Pacific warm water due to an EM event (Ashok *et al.*, 2007) is coupled with a decreased Chl in the western central Equatorial Pacific (for more details see chapter 7).

In the Tropical and South Pacific, the East Australian Current (EAC) reflects ENSO variability (Holbrook *et al.*, 2010), hence, ENSO has a strong influence on the Australian east coast. In chapter 8 of this thesis, we analyzed seasonal and interannual Chl variability patterns in the EAC region along the east coast of Australia and investigated the role of regional climate modes of variability on the Chl.

The EAC crosses several distinct biogeographical regions, where phytoplankton communities face distinct environmental conditions, especially in regards to solar and nutrient availability, and diverse physical mechanisms alter these two parameters (Condie and Dunn, 2006). With respect to the biogeographical variability, our analysis corroborates the literature (chapter 8). Seasonal profiles of Chl throughout the EAC region start in the low latitudes with very poor intra-annual range of values

(<0.03 $mg.m^{-3}$) with a modest peak occurring in winter, to higher latitudes where surface Chl concentrations peak in summer, reaching 0.1 $mg.m^{-3}$ above average. Along most of the EAC pathway, the southward intrusion of warm low nutrient waters reduced Chl volume and variability, at higher latitudes, predominantly where the EAC declines, biological eddy pumping may induce a positive anomaly on Chl concentration.

During the period examined, inter-annual EAC transport varied in three stages (Ridgway *et al.*, 2008), increase (1997-2001), decrease (2001-2003) and a constant transport (2003-2005). These three stages corresponded to distinct patterns of Chl in the region. The initial stage was linked to negative anomalies throughout the region, the second stage to positive Chl anomalies in the South Coral Sea, and a similar Chl pattern for the last period albeit with less amplitude.

Observational studies examining the link between EAC and ENSO variability are sparse in the literature (Suthers *et al.*, 2011). Yet, inter-annual oscillations of SST and of water volume in the region have been observed to be consistent with ENSO dynamics (Holbrook and Maharaj, 2008; Holbrook *et al.*, 2005). More specifically, the EAC transport is strongly modulated by ENSO variability, on inter-annual to decadal scales, by the action of westward propagating Rossby waves (Holbrook *et al.*, 2010). Here we observed that ENSO variability had a greater impact on Chl variability at higher latitudes of the EAC, in the Tasman Sea, and STF regions (chapter 8). Higher latitude regions, on the other hand, have a tight connection with the South Annular Mode (SAM), where inter-annual STF dynamics modulated by SAM strongly impact Chl variability by inducing low values during positive SAM events at the STF (Lovenduski and Gruber, 2005), as observed in chapter 8.

A note on the datasets of phytoplankton indicators used here and some of the mathematical tools. Throughout this project we used remotely sensed Ocean Colour derived datasets, more specifically the Chl and NPP datasets that provide global observations with a relatively high frequency. These two datasets are unique in terms of the insights they provide on phytoplankton distribution but are attached to an uncertain bias impossible to correct with the given spread of *in situ* observations using current technology. As discussed in the methods and data chapter of this thesis report (Chapter 2), the estimated values of either variable have inherent errors that may change the biomass estimates suggested in our findings. There is an urgent need for a high quality observational dataset, which is only possibly if there is an improvement in the frequency and coverage of *in situ* observations for phytoplankton biomass. Variables such as the phytoplankton group composition or ocean biome environmental conditions may change the emitted radiation captured by satellite sensors.These sort of impacts are not assessed in our study. In fact it is beyond the scope of this project to assess these at a global scale. There is an increasing interest in defining regional-specific algorithms which may increase the accuracy of estimates regionally (thus globally), but will introduce a new source of error , which is the regional boundary limits. Nevertheless, regional studies of Chl and NPP validation is a step in the right direction.

NPP estimates through satellite observations are arguably useful, as the NPP variability represented by the available algorithms is roughly 30%. The VGPM algorithm used here is one of the many algorithms that try to reproduce ocean PP, with no more accuracy than the simplest algorithm, such as the Eppley algorithm (which takes no account of the environmental variables, as seen in Chapter 3) or the most complex algorithm. While current remotely sensed ocean colour datasetsare a

unique and valuable tool that provide an unprecedented estimate of global phytoplankton biomass, reducing their inherent and variable bias should be a primary task for the global scientific community.

Mathematical tools are great descriptors, nonetheless, caution should be taken when interpreting the yielded results. Throughout this work, we used a wide range of mathematical tools to analyse spatial-temporal patterns of several fields. These range from simple techniques, such as calculating means, to more complex, such as EOFs. All of these should be taken with caution when interpreting what their outcomes really represent. EOF analyses are a great tool to isolate patterns that explain data variability. While we try to match these patterns to known forcing mechanisms, either spatially and temporally, to prove that a physical relationship exists, some of the patterns produced may well be an artefact of the tool used. Nevertheless, when using such tool the leading modes, which explain most variability and a statistically significant, are usually very convincingly real.

CONCLUSIONS

Throughout this study we observed that atmosphere and ocean physical and chemical characteristics are tightly connected to phytoplankton seasonal variability, but, inter-annual anomaly patterns can be explained through regional climate modes. Using Chl and NPP satellite derived estimates, we confirm that ENSO is the main mechanism of global through to regional phytoplankton inter-annual variability. To our knowledge, this is the first study to identify and examine the EM mode as a main forcing mechanism of inter-annual Chl/NPP variability. This mode explains a majority of the Chl/NPP decadal variability, even though its relationship with ENSO is yet to be clarified. Irrespective of the complex impact of the EAC on regional

phytoplankton distribution, ENSO influence seems to induce a clear pattern, which interacts with another regional climate mode (SAM) further south in the EAC extension.

We suggest that even though the main mechanisms that influence NPP throughout the global ocean are identified with temporally limited data, we have gained valuable insight into the main climatic processes that induce inter-annual NPP variability (ENSO and EM), via both atmosphere and/or ocean dynamics fields. Further work isessential to remove the great uncertainties that still exist regarding NPP distribution patterns at a regional to global perspective and on intra- to multi-annual scales. We note however, that available datasets may not be ideal to assess phytoplankton biomass patterns since they intrinsically contain estimation errors. Nevertheless, the introduction of satellite observational sensors has marked a new era in the advancement of earth systemscience, over several temporal and spatial scales.

Further, in order to evaluate the connections between climate modes and Chl/NPP found in this work empirically, modelling the proposed mechanisms would be an ideal exercise. We suggest the use of biogeochemical models to assess possible connections between large-scale climate mechanisms, either in a global and/or regional perspective. Additionally, we recommend the use of modelling techniques to evaluate possible scenarios of anthropogenically forced climate change to understand its implications on phytoplankton distribution, and the consequent impacts on our global biogeochemical system.

References

Amador, J. A., et al. (2006), Atmospheric forcing of the eastern tropical Pacific: A review, *Progress In Oceanography*, *69*(2-4), 101-142.

Antoine, D., et al. (1996), Oceanic primary production 2. Estimation at global scale from satellite (coastal zone color scanner) chlorophyll, *Global Biogeochemical Cycles*, *10*(1), 57-69.

Ashok, K., et al. (2007), El Niño Modoki and its possible teleconnection, *Journal of Geophysical Research C: Oceans*, *112*(11).

Atlas, R., et al. (1996), A multiyear global surface wind velocity data set using SSM/I wind observations, *Bull. Amer. Meteor. Soc.*, *77*, 869–882.

Barber, R. T., and F. P. Chavez (1983), Biological consequences of El Niño, *Science*, *222*(4629), 1203-1210.

Barnett, T. P., et al. (2005), Penetration of Human-Induced Warming into the World's Oceans, *Science*, *309*(5732), 284-287.

Behrenfeld, M. J., and P. G. Falkowski (1997), Photosynthetic rates derived from satellite-based chlorophyll concentration, *Limnology and Oceanography*, *42*(1), 1-20.

Behrenfeld, M. J., et al. (2001), Biospheric primary production during an ENSO transition, *Science*, *291*(5513), 2594-2597.

Behrenfeld, M. J., et al. (2006), Climate-driven trends in contemporary ocean productivity, *Nature*, *444*(7120), 752-755.

Bjornsson, H., and S. A. Venegas (1997), A manual for EOF and SVD analyses of climate data, 52 pp, McGill University, Montréal, Québec.

Cai, W., et al. (2011), Interactions of ENSO, the IOD, and the SAM in CMIP3 Models, *Journal of Climate*, *24*(6), 1688-1704.

Carr, M. E., et al. (2006), A comparison of global estimates of marine primary production from ocean color, *Deep-Sea Research Part II: Topical Studies in Oceanography*, *53*(5-7), 741-770.

Chavez, F. P., and R. T. Barber (1987), An estimate of new production in the equatorial Pacific, *Deep Sea Research Part A. Oceanographic Research Papers*, *34*(7), 1229-1243.

Chavez, F. P., et al. (1999), Biological and chemical response of the equatorial Pacific Ocean to the 1997-98 El Nino, *Science*, *286*(5447), 2126-2131.

Chavez, F. P., et al. (2011), Marine Primary Production in Relation to Climate Variability and Change, *Annual Review of Marine Science*, *3*(1), 227-260.

Chiswell, S. M., and R. Lukas (1990), The Hawaii Ocean Time-series (HOT), *EOS, Transactions of the American Geophysical Union*, *71*.

Condie, S. A., and J. R. Dunn (2006), Seasonal characteristics of the surface mixed layer in the Australasian region: implications for primary production regimes and biogeography, *Marine and Freshwater Research*, *57*, 569–590.

Davis, R. E. (1976), Predictability of Sea Surface Temperature and Sea Level Pressure Anomalies over the North Pacific Ocean, *Journal of Physical Oceanography*, *6*(3), 249-266.

Demarcq, H. (2009), Trends in primary production, sea surface temperature and wind in upwelling systems (1998-2007), *Progress in Oceanography*, *83*(1-4), 376-385.

deYoung, B., et al. (2004), Challenges of Modeling Ocean Basin Ecosystems, *Science*, *304*(5676), 1463-1466.

Di Lorenzo, E., et al. (2008), North Pacific Gyre Oscillation links ocean climate and ecosystem change, *Geophys. Res. Lett.*, *35*(8), L08607.

Di Lorenzo, E., et al. (2010), Central Pacific El Nino and decadal climate change in the North Pacific Ocean, *Nature Geosci*, *3*(11), 762-765.

Dommenget, D., and M. Latif (2002), A cautionary note on the interpretation of EOFs, *Journal of Climate*, *15*(2), 216-225.

Dommenget, D., and M. Jansen (2009), Predictions of Indian Ocean SST Indices with a Simple Statistical Model: A Null Hypothesis, *Journal of Climate*, *22*(18), 4930-4938.

Eppley, R. W., et al. (1985), Estimating ocean primary production from satellite chlorophyll. Introduction to regional diffrences and statistics for the Southern California Bight, *Journal of Plankton Research*, *7*(1), 14.

Field, C. B., et al. (1998), Primary production of the biosphere: Integrating terrestrial and oceanic components, *Science*, *281*(5374), 237-240.

Fine, R. A., et al. (1994), The western equatorial Pacific: A water mass crossroads, *J. Geophys. Res.*, *99*(C12), 25063-25080.

Friedrichs, M. A. M., et al. (2008), Assessing the uncertainties of model estimates of primary productivity in the tropical Pacific Ocean, *J. Mar. Syst.*

Garcia, H. E., et al. (2010), World Ocean Atlas 2009. Vol. 4, Nutrients (phosphate, nitrate, silicate), 398 pp, National Oceanic and Atmospheric Administration, Washington, D.C.

Garcìa-Garcìa, D., et al. (2011), Australian water mass variations from GRACE data linked to Indo-Pacific climate variability, *Remote Sensing of Environment*, *In Press, Corrected Proof*.

Hamilton, L. J. (2006), Structure of the Subtropical Front in the Tasman Sea, *Deep Sea Research Part I: Oceanographic Research Papers*, *53*(12), 1989-2009.

Henson, S. A., et al. (2009), Is global warming already changing ocean productivity?, *Biogeosciences Discussions*, *6*(6), 10311-10354.

Henson, S. A., et al. (2010), Detection of anthropogenic climate change in satellite records of ocean chlorophyll and productivity, *Biogeosciences*, *7*(2), 621-640.

Holbrook, N. J., et al. (2005), Oscillatory and propagating modes of temperature variability at the 3–3.5- and 4–4.5-yr time scales in the upper southwest Pacific Ocean, *Journal of climate*, *18*, 719-736.

Holbrook, N. J., and A. M. Maharaj (2008), Southwest Pacific subtropical mode water: A climatology, *Progress In Oceanography*, *77*(4), 298-315.

Holbrook, N. J., et al. (2010), ENSO to multi-decadal time scale changes in East Australian Current transports and Fort Denison sea level: Oceanic Rossby waves as the connecting mechanism, *Deep Sea Research Part II: Topical Studies in Oceanography*, *58*(5), 547-558.

IPCC (2007), Climate change 2007: The physical science basis. Contribution of working group I to the fourth assessment report of the intergovernmental panel on climate change (IPCC), 996 pp, Cambridge University Press, Cambridge, United Kingdom, New York, NY, USA.

Joseph, R., and S. Nigam (2006), ENSO Evolution and Teleconnections in IPCC's Twentieth-Century Climate Simulations: Realistic Representation?, *Journal of Climate*, *19*(17), 4360-4377.

Kalnay, E., et al. (1996), The NCEP/NCAR 40-Year Reanalysis Project, *Bulletin of the American Meteorological Society*, *77*(3), 437-471.

Kessler, W. S. (2002), Mean Three-Dimensional Circulation in the Northeast Tropical Pacific*, *Journal of Physical Oceanography*, *32*(9), 2457-2471.

Kiladis, G. N., et al. (1989), Origin of the South Pacific Convergence Zone, *Journal of Climate*, *2*(10), 1185-1195.

Kim, J.-M., et al. (2011), Shifts in biogenic carbon flow from particulate to dissolved forms under high carbon dioxide and warm ocean conditions, *Geophys. Res. Lett.*, *38*(8), L08612.

Larkin, N. K., and D. E. Harrison (2005), On the definition of El Niño and associated seasonal average U.S. weather anomalies, *Geophys. Res. Lett.*, *32*(13), L13705.

Latif, M., and N. S. Keenlyside (2009), El Niño/Southern Oscillation response to global warming, *Proceedings of the National Academy of Sciences of the United States of America*, *106*(49), 20578-20583.

Le Traon, P. Y., et al. (2003), Can we merge GEOSAT follow-on with TOPEX/Poseidon and ERS-2 for an improved description of the ocean circulation?, *Journal of Atmospheric and Oceanic Technology*, *20*(6), 889-895.

Li, G., et al. (2010), Indices of El Niño and El Niño Modoki: An improved El Niño Modoki index, *Advances in Atmospheric Sciences*, *27*(5), 1210-1220.

Longhurst, A., et al. (1995), An estimate of global primary production in the ocean from satellite radiometer data, *Journal of Plankton Research*, *17*(6), 1245-1271.

Longhurst, A. R. (1998), *Ecological Geography of the Sea*, Academic Press, San Diego.

Lorenz, E. N. (1956), Empirical orthogonal functions and statistical weather prediction. , 49 pp, Department of Meteorology, Massachusetts Institute of Technology.

Lovenduski, N. S., and N. Gruber (2005), Impact of the Southern Annular Mode on Southern Ocean circulation and biology, *Geophysical Research Letters*, *32*(11).

Lyman, J. M., et al. (2010), Robust warming of the global upper ocean, *Nature*, *465*(7296), 334-337.

Mackas, D. L. (2011), Does blending of chlorophyll data bias temporal trend?, *Nature*, *472*(7342), E4-E5.

McClain, C., et al. (2004), *An overview of the SeaWiFS project and strategies for producing a climate research quality global ocean bio-optical time series*, 38 pp., Elsevier, Kidlington, ROYAUME-UNI.

McQuatters-Gollop, A., et al. (2011), Is there a decline in marine phytoplankton?, *Nature*, *472*(7342), E6-E7.

Messié, M., and M.-H. Radenac (2006), Seasonal variability of the surface chlorophyll in the western tropical Pacific from SeaWiFS data, *Deep Sea Research Part I: Oceanographic Research Papers*, *53*(10), 1581-1600.

Meyers, G., et al. (2007), The Years of El Niño, La Niña, and Interactions with the Tropical Indian Ocean, *Journal of Climate*, *20*(13), 2872-2880.

Michaels, A. F. (1995), Ocean time-series research near Bermuda: The hydrostation S time-series and the Bermuda Atlantic Time-series Study (BATS) program, in *Ecological Time Series*, edited by T. M. Powell and J. H. Steele, pp. 181-208, Chapman & Hall Publishing, New York.

Murtugudde, R., et al. (2002), Effects of penetrative radiation of the upper tropical ocean circulation, *Journal of Climate*, *15*(5), 470-486.

Murtugudde, R. G., et al. (1999), Ocean color variability of the tropical Indo-Pacific basin observed by SeaWiFS during 1997-1998, *Journal of Geophysical Research C: Oceans*, *104*(C8), 18351-18366.

Nealson, K. H., and P. G. Conrad (1999), Life: Past, present and future, *Philosophical Transactions of the Royal Society B: Biological Sciences*, *354*(1392), 1923-1939.

O'Reilly, J. E., et al. (2000), Ocean color chlorophyll a algorithms for SeaWiFS, OC2, and OC4: Version 4. In: SeaWiFS Postlaunch Technical Report Series, in *SeaWiFS Postlaunch Calibration and Validation Analyses, Part 3*, edited by S. B. Hooker and E. R. Firestone, pp. 9-23, NASA, Goddard Space Flight Center, Greenbelt Maryland.

Pennington, J. T., et al. (2006), Primary production in the eastern tropical Pacific: A review, *Progress in Oceanography*, *69*(2-4), 285-317.

Power, S., et al. (2006), *The predictability of interdecadal changes in ENSO activity and ENSO teleconnections*, 17 pp., American Meteorological Society, Boston, MA, ETATS-UNIS.

Qu, T., et al. (2008), Semiannual variation in the western tropical Pacific Ocean, *Geophys. Res. Lett.*, *35*(16), L16602.

Rayner, N. A., et al. (2003), Global analyses of sea surface temperature, sea ice, and night marine air temperature since the late nineteenth century, *J. Geophys. Res.*, *108*.

Richoux, N. B., and P. W. Froneman (2009), Plankton trophodynamics at the subtropical convergence, Southern Ocean, *Journal of Plankton Research*, *31*(9), 1059-1073.

Ridgway, K. R., and J. R. Dunn (2003), Mesoscale structure of the mean East Australian Current System and its relationship with topography, *Progress In Oceanography*, *56*(2), 189-222.

Ridgway, K. R., et al. (2008), Decadal variability of East Australian Current transport inferred from repeated high-density XBT transects, a CTD survey and satellite altimetry, *J. Geophys. Res.*, *113*.

Rykaczewski, R. R., and J. P. Dunne (2011), A measured look at ocean chlorophyll trends, *Nature*, *472*(7342), E5-E6.

Sabine, C. L., et al. (2004), The Oceanic Sink for Anthropogenic CO2, *Science*, *305*(5682), 367-371.

Siegel, D. A., et al. (1995), Solar radiation, phytoplankton pigments and the radiant heating of the equatorial Pacific warm pool, *J. Geophys. Res.*, *100*(C3), 4885-4891.

Suthers, I. M., et al. (2011), The strengthening East Australian Current, its eddies and biological effects – an introduction and overview, *Deep Sea Research Part II: Topical Studies in Oceanography*, *58*(5), 538-546.

Takahashi, K., et al. (2011), ENSO regimes: Reinterpreting the canonical and Modoki El Niño, *Geophys. Res. Lett.*, *38*(10), L10704.

Thomalla, S. J., et al. (2011), Regional scale characteristics of the seasonal cycle of chlorophyll in the Southern Ocean, *Biogeosciences Discuss.*, *8*(3), 4763-4804.

Torrence, C., and G. P. Compo (1998), A Practical Guide to Wavelet Analysis, *Bulletin of the American Meteorological Society*, *79*(1), 61-78.

Trenberth, K. E. (2010), Global change: The ocean is warming, isn't it?, *Nature*, *465*(7296), 304-304.

Vimont, D. J. (2005), The Contribution of the Interannual ENSO Cycle to the Spatial Pattern of Decadal ENSO-Like Variability*, *Journal of Climate*, *18*(12), 2080-2092.

Vincent, E., et al. (2009), Interannual variability of the South Pacific Convergence Zone and implications for tropical cyclone genesis, *Climate Dynamics*, *36*(9), 1881-1896.

Weare, B. C. (2010), Tropospheric-stratospheric wave propagation during El Niño-Southern Oscillation, *J. Geophys. Res.*, *115*(D18), D18122.

White, W. B. (1994), Slow El NiÒo-Southern Oscillation boundary waves, *J. Geophys. Res.*, *99*(C11), 22737-22751.

Willis, J. K., et al. (2008), Assessing the globally averaged sea level budget on seasonal to interannual timescales, *J. Geophys. Res.*, *113*(C6), C06015.

Wyrtki, K., et al. (1976), Eddy energy in the oceans, *J. geophys. Res*, *81*(15), 2641-2646.

Wyrtki, K., and G. Meyers (1976), The Trade Wind Field Over the Pacific Ocean, *Journal of Applied Meteorology*, *15*(7), 698-704.

Yeh, S.-W., et al. (2009), El Niño in a changing climate, *Nature*, *462*(7273), 674-674.

Yoder, J. A., and M. A. Kennelly (2003), Seasonal and ENSO variability in global ocean phytoplankton chlorophyll derived from 4 years of SeaWiFS measurements, *Global Biogeochemical Cycles*, *17*(4), 23-21.

REFERENCES

Ahrens, M.A., Peters, R.H., 1991. Patterns and Limitations in Limnoplankton Size Spectra. Canadian Journal of Fisheries and Aquatic Sciences 48 (10), 1967-1978.

Amador, J.A., Alfaro, E.J., Lizano, O.G., Magaña, V.O., 2006. Atmospheric forcing of the eastern tropical Pacific: A review. Progress in Oceanography 69 (2-4), 101-142.

Antoine, D., Andre, J.M., Morel, A., 1996. Oceanic primary production 2. Estimation at global scale from satellite (coastal zone color scanner) chlorophyll. Global Biogeochemical Cycles 10 (1), 57-69.

Ashok, K., Behera, S.K., Rao, S.A., Weng, H., Yamagata, T., 2007. El Niño Modoki and its possible teleconnection. Journal of Geophysical Research C: Oceans 112 (11).

Atlas, R., Hoffman, R.N., Bloom, S.C., Jusem, J.C., Ardizzone, J., 1996. A multiyear global surface wind velocity data set using SSM/I wind observations. Bull. Amer. Meteor. Soc. 77, 869–882.

Baird, M.E., Timko, P.G., Middleton, J.H., Mullaney, T.J., Cox, D.R., Suthers, I.M., 2008. Biological properties across the Tasman Front off southeast Australia. Deep Sea Research Part I: Oceanographic Research Papers 55 (11), 1438-1455.

Baird, M.E., Timko, P.G., Suthers, I.M., Middleton, J.H., 2006. Coupled physical-biological modelling study of the East Australian Current with idealised wind forcing. Part I: Biological model intercomparison. Journal of Marine Systems 59 (3-4), 249-270.

Barber, R.T., Chavez, F.P., 1983. Biological consequences of El Niño. Science 222 (4629), 1203-1210.

Barnett, T.P., Pierce, D.W., AchutaRao, K.M., Gleckler, P.J., Santer, B.D., Gregory, J.M., Washington, W.M., 2005. Penetration of Human-Induced Warming into the World's Oceans. Science 309 (5732), 284-287.

Behrenfeld, M.J., Falkowski, P.G., 1997. Photosynthetic rates derived from satellite-based chlorophyll concentration. Limnology and Oceanography 42 (1), 1-20.

Behrenfeld, M.J., O'Malley, R.T., Siegel, D.A., McClain, C.R., Sarmiento, J.L., Feldman, G.C., Milligan, A.J., Falkowski, P.G., Letelier, R.M., Boss, E.S., 2006a. Climate-driven trends in contemporary ocean productivity. Nature 444 (7120), 752-755.

Behrenfeld, M.J., Randerson, J.T., McClain, C.R., Feldman, G.C., Los, S.O., Tucker, C.J., Falkowski, P.G., Field, C.B., Frouin, R., Esaias, W.E., Kolber, D.D., Pollack, N.H., 2001. Biospheric primary production during an ENSO transition. Science 291 (5513), 2594-2597.

Behrenfeld, M.J., Worthington, K., Sherrell, R.M., Chavez, F.P., Strutton, P., McPhaden, M., Shea, D.M., 2006b. Controls on tropical Pacific Ocean productivity revealed through nutrient stress diagnostics. Nature 442 (7106), 1025-1028.

Bjerknes, J., 1969. Atmospheric teleconnections from the Equatorial Pacific. Monthly Weather Review 97 (3), 163-172.

Bjornsson, H., Venegas, S.A., 1997. A manual for EOF and SVD analyses of climate data. CCGCR Report McGill University, Montréal, Québec, p. 52.

Cai, W., Shi, G., Cowan, T., Bi, D., Ribbe, J., 2005. The response of the Southern Annular Mode, the East Australian Current, and the southern mid-latitude ocean circulation to global warming. Geophys. Res. Lett. 32.

Cai, W., Sullivan, A., Cowan, T., 2011. Interactions of ENSO, the IOD, and the SAM in CMIP3 Models. Journal of Climate 24 (6), 1688-1704.

Campbell, J.W., 1995. The lognormal distribution as a model for bio-optical variability in the sea. J. Geophys. Res. 100 (C7), 13237-13254.

Carr, M.E., Friedrichs, M.A.M., Schmeltz, M., Noguchi Aita, M., Antoine, D., Arrigo, K.R., Asanuma, I., Aumont, O., Barber, R., Behrenfeld, M., Bidigare, R., Buitenhuis, E.T., Campbell, J., Ciotti, A., Dierssen, H., Dowell, M., Dunne, J., Esaias, W., Gentili, B., Gregg, W., Groom, S., Hoepffner, N., Ishizaka, J., Kameda, T., Le Que?re, C., Lohrenz, S., Marra, J., Me?lin, F., Moore, K., Morel, A., Reddy, T.E., Ryan, J., Scardi, M., Smyth, T., Turpie, K., Tilstone, G., Waters, K., Yamanaka, Y., 2006. A comparison of global estimates of marine primary production from ocean color. Deep-Sea Research Part II: Topical Studies in Oceanography 53 (5-7), 741-770.

Chavez, F.P., Barber, R.T., 1987. An estimate of new production in the equatorial Pacific. Deep Sea Research Part A. Oceanographic Research Papers 34 (7), 1229-1243.

Chavez, F.P., Messié, M., Pennington, J.T., 2011. Marine Primary Production in Relation to Climate Variability and Change. Annual Review of Marine Science 3 (1), 227-260.

Chavez, F.P., Strutton, P.G., Friederich, G.E., Feely, R.A., Feldman, G.C., Foley, D.G., McPhaden, M.J., 1999. Biological and chemical response of the equatorial Pacific Ocean to the 1997-98 El Nino. Science 286 (5447), 2126-2131.

Chiswell, S.M., Lukas, R., 1990. The Hawaii Ocean Time-series (HOT). EOS, Transactions of the American Geophysical Union 71.

Chu, P., 2011. Global upper ocean heat content and climate variability. Ocean Dynamics, 1-16.

Cimatoribus, A.A., Drijfhout, S.S., Dijkstra, H.A., 2011. A global hybrid coupled model based on atmosphere-SST feedbacks. Climate Dynamics, 1-16.

Condie, S.A., Dunn, J.R., 2006. Seasonal characteristics of the surface mixed layer in the Australasian region: implications for primary production regimes and biogeography. Marine and Freshwater Research 57, 569–590.

Cunningham, A., Carrie, I.D., Korb, R.E., 2011. Two-component modeling of the optical properties of a diatom bloom in the Southern Ocean. Remote Sensing of Environment 115 (6), 1434-1442.

Davis, R.E., 1976. Predictability of Sea Surface Temperature and Sea Level Pressure Anomalies over the North Pacific Ocean. Journal of Physical Oceanography 6 (3), 249-266.

Demarcq, H., 2009. Trends in primary production, sea surface temperature and wind in upwelling systems (1998-2007). Progress in Oceanography 83 (1-4), 376-385.

deYoung, B., Heath, M., Werner, F., Chai, F., Megrey, B., Monfray, P., 2004. Challenges of Modeling Ocean Basin Ecosystems. Science 304 (5676), 1463-1466.

Di Lorenzo, E., Cobb, K.M., Furtado, J.C., Schneider, N., Anderson, B.T., Bracco, A., Alexander, M.A., Vimont, D.J., 2010. Central Pacific El Nino and decadal climate change in the North Pacific Ocean. Nature Geosci 3 (11), 762-765.

Dommenget, D., Jansen, M., 2009. Predictions of Indian Ocean SST Indices with a Simple Statistical Model: A Null Hypothesis. Journal of Climate 22 (18), 4930-4938.

Dommenget, D., Latif, M., 2002. A cautionary note on the interpretation of EOFs. Journal of Climate 15 (2), 216-225.

Eppley, R.W., 1972. Temperature and phytoplankton growth in the sea. Fishery Bulletin 70, 1063-1085.

Eppley, R.W., Stewart, E., Abbott, M.R., U., H., 1985. Estimating ocean primary production from satellite chlorophyll. Introduction to regional diffrences and statistics for the Southern California Bight. Journal of Plankton Research 7 (1), 14.

Field, C.B., Behrenfeld, M.J., Randerson, J.T., Falkowski, P., 1998. Primary production of the biosphere: Integrating terrestrial and oceanic components. Science 281 (5374), 237-240.

Fine, R.A., Lukas, R., Bingham, F.M., Warner, M.J., Gammon, R.H., 1994. The western equatorial Pacific: A water mass crossroads. J. Geophys. Res. 99 (C12), 25063-25080.

Friedrichs, M.A.M., Carr, M.E., Barber, R.T., Scardi, M., Antoine, D., Armstrong, R.A., Asanuma, I., Behrenfeld, M.J., Buitenhuis, E.T., Chai, F., Christian, J.R., Ciotti, A.M., Doney, S.C., Dowell, M., Dunne, J., Gentili, B., Gregg, W., Hoepffner, N., Ishizaka, J., Kameda, T., Lima, I., Marra, J., Me?lin, F., Moore, J.K., Morel, A., O'Malley, R.T., O'Reilly, J., Saba, V.S., Schmeltz, M., Smyth, T.J., Tjiputra, J., Waters, K., Westberry, T.K., Winguth, A., 2008. Assessing the uncertainties of model estimates of primary productivity in the tropical Pacific Ocean. Journal of Marine Systems.

Frigo, M., Johnson, S.G., 1998. FFTW: An Adaptive Software Architecture for the FFT. Proceedings of the International Conference on Acoustics, Speech, and Signal Processing 3, 1381-1384.

Garcia, H.E., Locarnini, R.A., Boyer, T.P., Antonov, J.I., Zweng, M.M., Baranova, O.K., Johnson, D.R., 2010. World Ocean Atlas 2009. Vol. 4, Nutrients (phosphate, nitrate, silicate). In: Levitus, S. (Ed.). National Oceanic and Atmospheric Administration, Washington, D.C., p. 398.

Gladan, Ž.N., Marasović, I., Grbec, B., Skejić, S., Bužančić, M., Kušpilić, G., Matijević, S., Matić, F., 2009. Inter-decadal Variability in Phytoplankton Community in the Middle Adriatic (Kaštela Bay) in Relation to the North Atlantic Oscillation. Springer, Heidelberg, ALLEMAGNE.

Hallegraeff, G.M., Jeffery, S.W., 1993. Annually recurrent diatom blooms in spring along the NSW coast of Australia. Aust. J. Mar. Freshw. Res 44, 325 – 334

Hamilton, L.J., 1992. Surface circulation in the Tasman and Coral Seas: climatological features derived from bathythermograph data. Australian Journal of Marine and Freshwater Research 43, 793-822.

Hamilton, L.J., 2006. Structure of the Subtropical Front in the Tasman Sea. Deep Sea Research Part I: Oceanographic Research Papers 53 (12), 1989-2009.

Henson, S.A., Sarmiento, J.L., Dunne, J.P., Bopp, L., Lima, I., Doney, S.C., John, J., Beaulieu, C., 2009. Is global warming already changing ocean productivity? Biogeosciences Discussions 6 (6), 10311-10354.

Henson, S.A., Sarmiento, J.L., Dunne, J.P., Bopp, L., Lima, I., Doney, S.C., John, J., Beaulieu, C., 2010. Detection of anthropogenic climate change in satellite records of ocean chlorophyll and productivity. Biogeosciences 7 (2), 621-640.

Holbrook, N.J., Goodwin, I.D., McGregor, S., Molina, E., Power, S.B., 2010. ENSO to multi-decadal time scale changes in East Australian Current transports and Fort Denison sea level: Oceanic Rossby waves as the connecting mechanism. Deep Sea Research Part II: Topical Studies in Oceanography 58 (5), 547-558.

Holbrook, N.J., Maharaj, A.M., 2008. Southwest Pacific subtropical mode water: A climatology. Progress in Oceanography 77 (4), 298-315.

Holbrook, N.J., S-L, C.P., Venegas, S.A., 2005a. Corrigendum. Journal of Climate 18 (1637-1639).

Holbrook, N.J., S-L, C.P., Venegas, S.A., 2005b. Oscillatory and propagating modes of temperature variability at the 3–3.5- and 4–4.5-yr time scales in the upper southwest Pacific Ocean. Journal of Climate 18, 719-736.

Holton, J.R., 2004. Chapter 6 Synoptic-scale motions I: Quasi-Geostrophic analysis. International Geophysics. Academic Press, pp. 139-181.

Huang, Z., Morimoto, H., 2008. Wavelet based fractal analysis of El Niño/La Niña episodes. Hydrological Research Letters 2, 70-74.

IPCC, 2007. Climate change 2007: The physical science basis. Contribution of working group I to the fourth assessment report of the intergovernmental panel on climate change (IPCC). In: Solomon, S., Qin, D., Manning, M., Chen, Z., Marquis, M., Averyt, K.B., Tignor, M.M.B., Henry LeRoy Miller, J. (Eds.). Cambridge University Press, Cambridge, United Kingdom, New York, NY, USA, p. 996.

Jitts, H.R., 1965. The summer characteristics of primary productivity in the Tasman and Coral seas. Australian Journal of Marine and Freshwater Research 16, 151–162.

Joseph, R., Nigam, S., 2006. ENSO Evolution and Teleconnections in IPCC's Twentieth-Century Climate Simulations: Realistic Representation? Journal of Climate 19 (17), 4360-4377.

Kahru, M., Gille, S.T., Murtugudde, R., Strutton, P.G., Manzano-Sarabia, M., Wang, H., Mitchell, B.G., 2010. Global correlations between winds and ocean chlorophyll. J. Geophys. Res. 115 (C12), C12040.

Kalnay, E., Kanamitsu, M., Kistler, R., Collins, W., Deaven, D., Gandin, L., Iredell, M., Saha, S., White, G., Woollen, J., Zhu, Y., Leetmaa, A., Reynolds, R., Chelliah, M., Ebisuzaki, W., Higgins, W., Janowiak, J., Mo, K.C., Ropelewski, C., Wang, J., Jenne, R., Joseph, D., 1996. The NCEP/NCAR 40-Year Reanalysis Project. Bulletin of the American Meteorological Society 77 (3), 437-471.

Kessler, W.S., 2002. Mean Three-Dimensional Circulation in the Northeast Tropical Pacific*. Journal of Physical Oceanography 32 (9), 2457-2471.

Kiladis, G.N., von Storch, H., Loon, H., 1989. Origin of the South Pacific Convergence Zone. Journal of Climate 2 (10), 1185-1195.

Kim, J.-M., Lee, K., Shin, K., Yang, E.J., Engel, A., Karl, D.M., Kim, H.-C., 2011. Shifts in biogenic carbon flow from particulate to dissolved forms under high carbon dioxide and warm ocean conditions. Geophys. Res. Lett. 38 (8), L08612.

Larkin, N.K., Harrison, D.E., 2005. On the definition of El Niño and associated seasonal average U.S. weather anomalies. Geophys. Res. Lett. 32 (13), L13705.

Latif, M., Keenlyside, N.S., 2009. El Niño/Southern Oscillation response to global warming. Proceedings of the National Academy of Sciences of the United States of America 106 (49), 20578-20583.

Le Traon, P.Y., Faugère, Y., Hernandez, F., Dorandeu, J., Mertz, F., Ablain, M., 2003. Can we merge GEOSAT follow-on with TOPEX/Poseidon and ERS-2 for an improved description of the ocean circulation? Journal of Atmospheric and Oceanic Technology 20 (6), 889-895.

Li, G., Ren, B., Yang, C., Zheng, J., 2010. Indices of El Niño and El Niño Modoki: An improved El Niño Modoki index. Advances in Atmospheric Sciences 27 (5), 1210-1220.

Longhurst, A., Sathyendranath, S., Platt, T., Caverhill, C., 1995. An estimate of global primary production in the ocean from satellite radiometer data. Journal of Plankton Research 17 (6), 1245-1271.

Longhurst, A.R., 1998. Ecological Geography of the Sea. Academic Press, San Diego.

Lorenz, E.N., 1956. Empirical orthogonal functions and statistical weather prediction. . In: Lorenz, E.N. (Ed.), Statistical Forecasting Project Tech. Rep. Department of Meteorology, Massachusetts Institute of

Technology, p. 49.

Lovenduski, N.S., Gruber, N., 2005. Impact of the Southern Annular Mode on Southern Ocean circulation and biology. GEOPHYSICAL RESEARCH LETTERS 32 (11).

Lyman, J.M., Good, S.A., Gouretski, V.V., Ishii, M., Johnson, G.C., Palmer, M.D., Smith, D.M., Willis, J.K., 2010. Robust warming of the global upper ocean. Nature 465 (7296), 334-337.

Mackas, D.L., 2011. Does blending of chlorophyll data bias temporal trend? Nature 472 (7342), E4-E5.

Martinez, E., Antoine, D., D‚ÄôOrtenzio, F., Gentili, B., 2009. Climate-Driven Basin-Scale Decadal Oscillations of Oceanic Phytoplankton. Science 326 (5957), 1253-1256.

Masotti, I., Moulin, C., Alvain, S., Bopp, L., Tagliabue, A., Antoine, D., 2011. Large-scale shifts in phytoplankton groups in the Equatorial Pacific during ENSO cycles. Biogeosciences 8 (3), 539-550.

McClain, C., Charles, R., Feldman, Gene, C., Hooker, Stanford, B., 2004. An overview of the SeaWiFS project and strategies for producing a climate research quality global ocean bio-optical time series. Elsevier, Kidlington, ROYAUME-UNI.

McQuatters-Gollop, A., Reid, P.C., Edwards, M., Burkill, P.H., Castellani, C., Batten, S., Gieskes, W., Beare, D., Bidigare, R.R., Head, E., Johnson, R., Kahru, M., Koslow, J.A., Pena, A., 2011. Is there a decline in marine phytoplankton? Nature 472 (7342), E6-E7.

Messié, M., Radenac, M.-H., 2006. Seasonal variability of the surface chlorophyll in the western tropical Pacific from SeaWiFS data. Deep Sea Research Part I: Oceanographic Research Papers 53 (10), 1581-1600.

Meyers, G., McIntosh, P., Pigot, L., Pook, M., 2007. The Years of El Niño, La Niña, and Interactions with the Tropical Indian Ocean. Journal of Climate 20 (13), 2872-2880.

Michaels, A.F., 1995. Ocean time-series research near Bermuda: The hydrostation S time-series and the Bermuda Atlantic Time-series Study (BATS) program. In: Powell, T.M., Steele, J.H. (Eds.), Ecological Time Series. Chapman & Hall Publishing, New York, pp. 181-208.

Morel, A., Berthon, J.F., 1989. Surface pigments, algal biomass profiles, and potential production of the euphotic layer: relationships reinvestigated in view of remote-sensing applications. Limnology & Oceanography 34 (8), 1545-1562.

Mulhearn, P., 1987. The Tasman Front: a study using satellite infrared imagery. Journal of Physical Oceanography 17, 1148-1155.

Murtugudde, R., Beauchamp, J., McClain, C.R., Lewis, M., Busalacchi, A.J., 2002. Effects of penetrative radiation of the upper tropical ocean circulation. Journal of Climate 15 (5), 470-486.

Murtugudde, R.G., Signorini, S.R., Christian, J.R., Busalacchi, A.J., McClain, C.R., Picaut, J., 1999. Ocean color variability of the tropical Indo-Pacific basin observed by SeaWiFS during 1997-1998. Journal of Geophysical Research C: Oceans 104 (C8), 18351-18366.

Nealson, K.H., Conrad, P.G., 1999. Life: Past, present and future. Philosophical Transactions of the Royal Society B: Biological Sciences 354 (1392), 1923-1939.

Nilsson, C.S., Cresswell, G.R., 1980. The formation and evolution of East Australian current warm-core eddies. Progress in Oceanography 9 (3), 133-183.

North, G.R., Bell, T.L., Cahalan, R.F., Moeng, F.J., 1982. Sampling Errors in the Estimation of Empirical Orthogonal Functions. Monthly Weather Review 110 (7), 699-706.

O'Reilly, J.E., Maritorena, S., Siegel, D., O'Brien, M.C., Toole, D., Mitchell, B.G., Kahru, M., Chavez, F.P., Strutton, P., Cota, G., Hooker, S.B., McClain, C.R., Carder, K.L., Muller-Karger, F., Harding, L., Magnuson, A., Phinney, D., Moore, G.F., Aiken, J., Arrigo, K.R., Letelier, R., Culver, M., 2000. Ocean color chlorophyll a algorithms for SeaWiFS, OC2, and OC4: Version 4. In: SeaWiFS Postlaunch Technical Report Series. In: Hooker, S.B., Firestone, E.R. (Eds.), SeaWiFS Postlaunch Calibration and Validation Analyses, Part 3. NASA, Goddard Space Flight Center, Greenbelt Maryland., pp. 9-23.

Pennington, J.T., Mahoney, K.L., Kuwahara, V.S., Kolber, D.D., Calienes, R., Chavez, F.P., 2006. Primary production in the eastern tropical Pacific: A review. Progress in Oceanography 69 (2-4), 285-317.

Qu, T., Gan, J., Ishida, A., Kashino, Y., Tozuka, T., 2008. Semiannual variation in the western tropical Pacific Ocean. Geophys. Res. Lett. 35 (16), L16602.

Raven, P.H., Evert, R.F., Eichhorn, S.E., 2005. Photosynthesis, Light, and Life. Biology of Plants. Freeman, W. H. , pp. 119–127.

Rayner, N.A., Parker, D.E., Horton, E.B., Folland, C.K., Alexander, L.V., Rowell, D.P., Kent, E.C., Kaplan, A., 2003. Global analyses of sea surface temperature, sea ice, and night marine air temperature since the late nineteenth century. J. Geophys. Res. 108.

Richoux, N.B., Froneman, P.W., 2009. Plankton trophodynamics at the subtropical convergence, Southern Ocean. Journal of Plankton Research 31 (9), 1059-1073.

Ridgway, K.R., Coleman, R.C., Bailey, R.J., Sutton, P., 2008. Decadal variability of East Australian Current transport inferred from repeated high-density XBT transects, a CTD survey and satellite altimetry. J. Geophys. Res. 113.

Ridgway, K.R., Dunn, J.R., 2003. Mesoscale structure of the mean East Australian Current System and its relationship with topography. Progress in Oceanography 56 (2), 189-222.

Ridgway, K.R., Godfrey, J.S., 1997. Seasonal cycle of the East Australian Current. J. Geophys. Res. 102.

Rochford, D.J., 1972. Nutrient enrichment of east Australian coastal waters: I. Evans Head upwelling. Tech. rep., Division of Fisheries and Oceanography, CSIRO, Australia.

Roughan, M., Middleton, J.H., 2004. On the East Australian Current: Variability, encroachment, and upwelling. J. Geophys. Res. 109.

Rykaczewski, R.R., Dunne, J.P., 2011. A measured look at ocean chlorophyll trends. Nature 472 (7342), E5-E6.

Sabine, C.L., Feely, R.A., Gruber, N., Key, R.M., Lee, K., Bullister, J.L., Wanninkhof, R., Wong, C.S., Wallace, D.W.R., Tilbrook, B., Millero, F.J., Peng, T.-H., Kozyr, A., Ono, T., Rios, A.F., 2004. The Oceanic Sink for Anthropogenic CO2. Science 305 (5682), 367-371.

Saji, N.H., Goswami, B.N., Vinayachandran, P.N., Yamagata, T., 1999. A dipole mode in the tropical Indian Ocean. Nature 401 (6751), 360-363.

Siegel, D.A., Ohlmann, J.C., Washburn, L., Bidigare, R.R., Nosse, C.T., Fields, E., Zhou, Y., 1995. Solar radiation, phytoplankton pigments and the radiant heating of the equatorial Pacific warm pool. J. Geophys. Res. 100 (C3), 4885-4891.

Smith, T.M., Reynolds, R.W., Livezey, R.E., Stokes, D.C., 1996. Reconstruction of Historical Sea Surface Temperatures Using Empirical Orthogonal Functions. Journal of Climate 9 (6), 1403-1420.

Stanton, B.R., 1981. An oceanographic survey of the Tasman Front. New Zealand Journal of Marine and Freshwater Research 15, 289-297.

Stanton, B.R., Ridgway, N.M., 1988. An oceanographic survey of the subtropical convergence zone in the Tasman Sea. New Zealand Journal of Marine and Freshwater Research 22, 583-593.

Strutz, T., 2010. Data Fitting and Uncertainty: A practical introduction to weighted least squares and beyond. Vieweg+Teubner, Wiesbaden.

Suthers, I.M., Young, J.W., Baird, M.E., Roughan, M., Everett, J.D., Brassington, G.B., Byrne, M., Condie, S.A., Hartog, J.R., Hassler, C.S., Hobday, A.J., Holbrook, N.J., Malcolm, H.A., Oke, P.R., Thompson, P.A., Ridgway, K., 2011. The strengthening East Australian Current, its eddies and biological effects – an introduction and overview. Deep Sea Research Part II: Topical Studies in Oceanography 58 (5), 538-546.

Takahashi, K., Montecinos, A., Goubanova, K., Dewitte, B., 2011. ENSO regimes: Reinterpreting the canonical and Modoki El Niño. Geophys. Res. Lett. 38 (10), L10704.

Tett, P., 1973. The use of log-normal statistics to describe phytoplankton populations from the Firth of Lorne area. Journal of Experimental Marine Biology and Ecology 11 (2), 121-136.

Thomalla, S.J., Fauchereau, N., Swart, S., Monteiro, P.M.S., 2011. Regional scale characteristics of the seasonal cycle of chlorophyll in the Southern Ocean. Biogeosciences Discuss. 8 (3), 4763-4804.

Tilburg, C.E., Hurlburt, H.E., O'Brien, J.J., Shriver, J.F., 2001. The dynamics of the East Australian Current system: The Tasman Front, the East Auckland Current and the East Cape Current. J. Phys. Oceanogr. 31 (2917 – 2943).

Tilburg, C.E., Subrahmanyam, B., O'Brien, J.J., 2002. Ocean color variability in the Tasman Sea. Geophys. Res. Lett. 29.

Torrence, C., Compo, G.P., 1998. A Practical Guide to Wavelet Analysis. Bulletin of the American Meteorological Society 79 (1), 61-78.

Trenberth, K.E., 1997. The Definition of El Niño. Bulletin of the American Meteorological Society 78 (12), 2771-2777.

Trenberth, K.E., 2010. Global change: The ocean is warming, isn't it? Nature 465 (7296), 304-304.

Trenberth, K.E., Hurrell, J.W., 1994. Decadal atmosphere-ocean variations in the Pacific. Climate Dynamics 9 (6), 303-319.

Venegas, S.A., 2001. Statistical methods for signal detection in climate. DCESS report. Danish Centre for Earth System Science, Niels Bohr Institute for Astronomy, Physics and Geophysics, University of Copenhagen, Denmark.

Vincent, E., Lengaigne, M., Menkes, C., Jourdain, N., Marchesiello, P., Madec, G., 2009. Interannual variability of the South Pacific Convergence Zone and implications for tropical cyclone genesis. Climate Dynamics 36 (9), 1881-1896.

Weare, B.C., 2010. Tropospheric-stratospheric wave propagation during El Niño-Southern Oscillation. J. Geophys. Res. 115 (D18), D18122.

White, W.B., 1994. Slow El Niño-Southern Oscillation boundary waves. J. Geophys. Res. 99 (C11), 22737-22751.

White, W.B., Peterson, R.G., 1996. An Antarctic circumpolar wave in surface pressure, wind, temperature and sea-ice extent. Nature 380 (6576), 699-702.

Wilkin, J.L., Morrow, R.A., 1994. Eddy kinetic energy and momentum flux in the Southern Ocean: comparison of a global eddy-resolving model with altimeter, drifter, and current-meter data. Journal of Geophysical Research 99 (C4), 7903-7916.

Willis, J.K., Chambers, D.P., Nerem, R.S., 2008. Assessing the globally averaged sea level budget on seasonal to interannual timescales. J. Geophys. Res. 113 (C6), C06015.

Wolter, K., Timlin, M.S., 1993. Monitoring ENSO in COADS with a seasonally adjusted principal component index., Proc. of the 17th Climate Diagnostics Workshop, Norman, OK, NOAA/NMC/CAC, NSSL, Oklahoma Clim. Survey, CIMMS and the School of Meteor., Univ. of Oklahoma, pp. 52-57.

Wyrtki, K., Magaard, L., Hager, J., 1976. Eddy energy in the oceans. J. geophys. Res 81 (15), 2641-2646.

Wyrtki, K., Meyers, G., 1976. The Trade Wind Field Over the Pacific Ocean. Journal of Applied Meteorology 15 (7), 698-704.

Yeh, S.-W., Kug, J.-S., Dewitte, B., Kwon, M.-H., Kirtman, B.P., Jin, F.-F., 2009. El Niño in a changing climate. Nature 462 (7273), 674-674.

Yoder, J.A., Kennelly, M.A., 2003. Seasonal and ENSO variability in global ocean phytoplankton chlorophyll derived from 4 years of SeaWiFS measurements. Global Biogeochemical Cycles 17 (4), 23-21.

Yu, J.-Y., Kim, S.T., 2011. Relationships between Extratropical Sea Level Pressure Variations and the Central Pacific and Eastern Pacific Types of ENSO. Journal of Climate 24 (3), 708-720.